doi : 10.17596/0003798

JAMSTEC *Chikyu* SCORE Expedition 912 Leg 1

Preliminary Cruise Report

Enigmatic recurrence pattern of Tokai earthquake in Nankai Trough, southwest Japan: The link between great earthquakes and ridge subduction

Toshiya Kanamatsu (JAMSTEC), Ken Ikehara (AIST), Kan-Hsi Hsiung (JAMSTEC),
Io Miura (U. Tokyo), Natsumi Okutsu (JAMSTEC), Kan Aoike (JAMSTEC)

Acknowledgements

Expedition 912 shipboard scientists thank all MQJ ship crews and drilling staffs, MWJ laboratory technical staffs, MarE3 Operation Superintendent and his staffs, expedition managers for their efforts on programs. This cruise was implemented as Chikyu Shallow Core Program (SCORE) program of Japan Drilling Earth Science Consortium (J-DESC)

Contents

1. Cruise Information *5*

2. Expedition 912 Leg. 1 Shipboard Scientists *5*

3. Shipboard Log *6*

4. Scientific objectives *8*

4.1 Proposed site 9

5. Shipboard core analysis flow *12*

6. Operation *16*

7. Method *17*

7.1 Visual core descriptions 17

7.2 Smear slides 18

7.3. Physical property 18

7.4. X-ray computed tomography and MSCL 20

7.5 Paleomagnetism 22

8. Preliminary Results *24*

8.1 Lithostratigraphy 24

8.2 Smear slides 26

8.3 Physical property measurements 26

8.4 X-ray CT scanning and MSCL 29

8.5 Paleomagnetism 32

9. Post-cruise research plan ***35***

10. References ***36***

APPENDIX

1. X-CT image and Split core images ***A1***

2. VCD ***A17***

1. Cruise Information

Cruise ID: CK20-S01, Exp. 912
Name of vessel: D/V Chikyu
Proposal representative: Toshiya Kanamatsu (IMG, JAMSTEC)
Cruise period: Jan. 5th, 2020 - Jan. 15th, 2020
Leg period: Jan. 5th, 2020 – Jan. 8th, 2020
Ports of departure / arrival: Shimizu / Sasebo
Coring area: Enshu-nada, Tokai, Nankai Trough.

2. Expedition 912 Leg. 1 Shipboard Scientists

Toshiya Kanamatsu (Chief Scientist, Lead Proponent)
Subduction Dynamics Research Center (SDR), Research Institute for Marine Geodynamics (IMG)
Japan Agency for Marine-Earth Science and Technology (JAMSTEC)
2-15, Natsushima-cho, Yokosuka-city, Kanagawa, 237-0061, Japan

Ken Ikehara (Sedimentologist, Proponent)
The Research Institute of Geology and Geoinformation (IGG), Geological Survey of Japan (GSJ)
National Institute of Advanced Industrial Science and Technology (AIST)
AIST Tsukuba Central 7, 1-1-1 Higashi, Tsukuba, Ibaraki, 305-8567, Japan

Kan-Hsi Hsiung (Sedimentologist, Proponent)
Subduction Dynamics Research Center (SDR), Research Institute for Marine Geodynamics (IMG)
Japan Agency for Marine-Earth Science and Technology (JAMSTEC)
2-15, Natsushima-cho, Yokosuka-city, Kanagawa, 237-0061, Japan

Io Miura (Physical Property)
Atmosphere and Ocean Research Institute (AORI)
The University of Tokyo
5-1-5, Kashiwanoha, Kashiwa-shi, Chiba 277-8564 Japan

Natsumi Okutsu (Expedition Project Manager)
Institute for Marine-Earth Exploration and Engineering (MarE3) Japan
Agency for Marine-Earth Science and Technology (JAMSTEC) 2-15,
Natsushima-cho, Yokosuka-city, Kanagawa, 237-0061, Japan

Kan Aoike (Expedition Project Manager)
Institute for Marine-Earth Exploration and Engineering (MarE3)
Japan Agency for Marine-Earth Science and Technology (JAMSTEC)
2-15, Natsushima-cho, Yokosuka-city, Kanagawa, 237-0061, Japan

3. Shipboard Log

Date	Area	Plan
5th Jan	10:00 Depart Shimizu port 13:00-14:00 Pre spud meeting 19:30 Arrive Site	Leave port Transit
6th Jan	08:10 Core 1H inner barrel Landing 08:13 Shoot Core 1H w/17.8 MPa SPP 08:13-08:19 Release Core 1H w/CLW and DW (1m) 08:19-08:48 Retrieve Core 1H 08:48 Core 1H on deck No getting mud line, move to new hole (Hole B) 11:37 Shoot Core 1H w/17.2MPa SPP @2437.0 mBRT 11:38 Release Core 1H w/CLW of **41.8kN** 1:38-12:15 Retrieve Core 1H 12:18 Core 1H of Hole B on deck 14:12 Core 2H inner barrel Landing 14:14 Shoot Core 2H w/17.7MPa SPP @2446.5 mBRT 14:20 Release Core 2H w/CLW and **DW (30kN)** 14:43 Core 2H on deck 15:38 Core 3H inner barrel landing 15:41 Shoot Core 3H w/16.8MPa SPP @2456 mBRT 15:48 Release Core 3H w/CLW and **DW (60KN)** 16:23 Core 3H on deck 17:40 Core 4H inner barrel Landing 17:44 Shoot Core 4H w/16.8MPa SPP @2465.5 mBRT 17:54 Release Core 4H w/CLW and **DW (130kN)** 18:26 Core 4H on deck 22:18 Core 5H inner barrel Landing 22:20 Shoot Core 5H w/17.1MPa SPP @2475.0 mBRT 22:26 Release Core 5H w/CLW and **DW (80kN)** 22:55 Core 5H on deck 23:40 6H inner barrel Landing 23:41 Shoot Core 6H w/16.6MPa SPP @2484.5mBRT, Partial, Bleed off pressure 23:51 Release Core 6H **w/DW (240kN)** 23:51-24:00 Retrieve Core 6H	HPCS operation

7th Jan	00:23 Core 6H on deck 01:41 Core 7H inner barrel (3 shear pins) Landing 01:44 Shoot Core 7H w/28.9MPa SPP @2492.5 mBRT 01:53 Release Core 7H **w/DW (240kN)** 02:22 Core 7H on deck 05:22 Core 8H inner barrel (3 shear pins) Landing 05:27 Shoot Core 8H w/24.3MPa SPP @2499.0 mBRT 05:37 Release Core 8H **w/DW (108kN)** 06:00 Core 8H on deck 07:06 Core 9H inner barrel (3 shear pins) Landing 07:10 Shoot Core 9H w/25.9MPa SPP, Bleed off @2506.5 mBRT 07:10 Release Core 9H **w/DW (125kN)** 07:52 Core 9H on deck 09:13 Run Core 10F inner barrel (3 shear pins) 1st Landing 09:17 1st Shoot Core 10F -> Failed, No shear 09:20 2nd Shoot Core 10F-> Failed, No shear 09:29 2nd Landing 09:31 3rd Shoot Core 10F w/27.9MPa SPP, Bleed off @2510.0 mBRT 09:37 Release Core 10F **w/DW (130kN)** 10:01 Core 10F on deck 10:15 Run and then drill down 11:06 Core 11F inner barrel (3 shear pins) Landing 11:46 Shoot Core 11F (3rd) w/34.8MPa SPP, Bleed off @2514.5 mBRT 11:49 Release Core 11F **w/DW (215kN)** 12:28 Core 11F on deck 13:20 Run and then drill down 14:07 Core 12H inner barrel (2 shear pins) Landing 14:09 Shoot Core 12H w/25.8MPa SPP, Bleed off @2519 mBRT 14:18 Release Core 12H **w/DW (170kN)** 14:52 Core 12H on deck	HPCS operation
8th Jan	02:00 end of Leg1 and move to Kikai site: Strat of Leg 2	Transit
10th Jan	Leg 2 (Kikai caldera)	Transit/HPCS
11th Jan	Leg 2 (Kikai caldera)	HPCS
12th Jan	Leg 2 (Kikai caldera)	HPCS
13th Jan	Leg 2 (Kikai caldera)/Transit	HPCS
14th Jan	Transit	HPCS
15th Jan	Sasebo 12:30 disembarkation	End of cruise

4. Scientific objectives

One of approaches to elucidate the nature of earthquake occurrence in a seismogenic zone is to understand its spatio-temporal recurrence pattern in the past. This has been mainly investigated through historical literature studies and tsunami deposit studies ashore. Additionally, recent works have revealed that marine sediments also contain important information on the past earthquake occurrence. However, such verification in Nankai Trough, southeast Japan has not yet been sufficiently studied so far. We propose to study a continuous sedimentary sequence at a local tectonic basin to investigate the unique recurrence pattern of Tokai segment, Nankai Trough. It is considered that the historical earthquake occurrence of Tokai segment is deviated from those of other segments due to a ridge subduction. We plan to validate its hypothesis by observing the earthquake recurrence intervals in geologic time. Hydraulic Piston Coring System (HPCS) of the ocean drilling vessel (D/V) *Chikyu* can provide an opportunity to obtain an excellent long and continuous sedimentary record to unravel the earthquake recurrence pattern of Tokai segment.

Earthquakes along the Nankai Trough (hereinafter referred to as "Nankai Trough Earthquake"), have occurred repeatedly and the next occurrence is expected to be imminent because more than 70-years have passed since the last Nankai Trough Earthquake in 1946. Despise large amount of knowledge accumulation and developments of observatories to monitor earthquake activities in the Nankai Trough, it is still difficult to estimate its future occurrence. Now "Earthquake Research Committee (2013)" consider that Nankai Trough Earthquake has occurred with more diverse and complicated manners in time and space rather than regular occurrence. On the other hand, reconstruction of past-earthquake is still essential for understanding their occurrence properties, especially because information before AD 1361 is still incomplete (Satake, 2015). Documentation of past-Nankai Trough Earthquake has been investigated mainly using historical document and shore geological records. Additionally, it is indicated that deep-sea sediments also contain important information on earthquake occurrence. For example, marine geological surveys in the Japan Trench have revealed that turbidites corresponding to historical huge earthquakes have been preserved in deep-sea basins (Ikehara et al., 2016). Such verification in the Nankai Trough area has not yet been sufficiently studied so far.

The megathrust in the Nankai Trough is separated to several segments based on the rupture patterns of historical earthquakes (e.g. Ando,1975). The eastmost segment: Tokai segment reveals enigmatic recurrence interval in the historical record. The last occurrence in the Tokai segment was proposed to be in AD 1854 (Ansei-Tonankai). Because the rupture of Tonanaki earthquake in AD 1944 might not propagate to the Tokai segment (e.g. Ando, 1975), it is believed that the stress has been accumulated in the Tokai segment since AD 1854 and is still laid up there. What has controlled such unique occurrence in Nankai Trough Earthquake? As one of potential control factors, effects of subducting oceanic architectures such as ridge and seamount on the earthquake rupturing have been discussed (e.g. Kodaira et al., 2002, 2003, Yokota et al., 2015). Off Tokai, Zenisu Ridge, which is a seamount chain formed during spreading episodes of the Shikoku Basin (Ishizuka et al., 2003), aligns parallel to the Nankai Trough (Figure 4.1). Kodaira et al. (2003), and Park et al. (2003) revealed that similar to the Zenisu Ridge but older ridges are subducting beneath the continental wedge and considered that the ridges controlled the rupture propagation in AD 1944 earthquake. Kodaira et al. (2003) concluded that the location of "Deeper Paleo Zenisu" (Figure 4.1), which is sited beneath the area of strong coupling between the plates, is evidential for "subducted seamount = strongly locked" hypothesis. Those studies suggest that the ridge subduction in the Tokai segment has affected on the earthquake occurrence by blocking rupture propagation of earthquakes. Another idea on effect of seamount

subduction is that a subducting seamount causes creeping in a plate boundary, which will result in weak interplate coupling (e. g. Wang and Bilek, 2014). In both cases, the Tokai earthquake recurrence interval is expected to be longer than those of the other segments. Such record should be observed in the earthquake recurrence pattern in Tokai segment. However, records form historical literature and geological shore studies are not enough longer to confirm the recurrence intervals of Tokai segment, especially records for the time before 14th century (Satake, 2015). In order to verify this hypothesis, we propose to unravel the earthquake recurrence times of the Tokai segment using a long marine sediment record. A primary objective is to determine whether "enigmatic recurrence" observed in the historical record is found in the geological record.

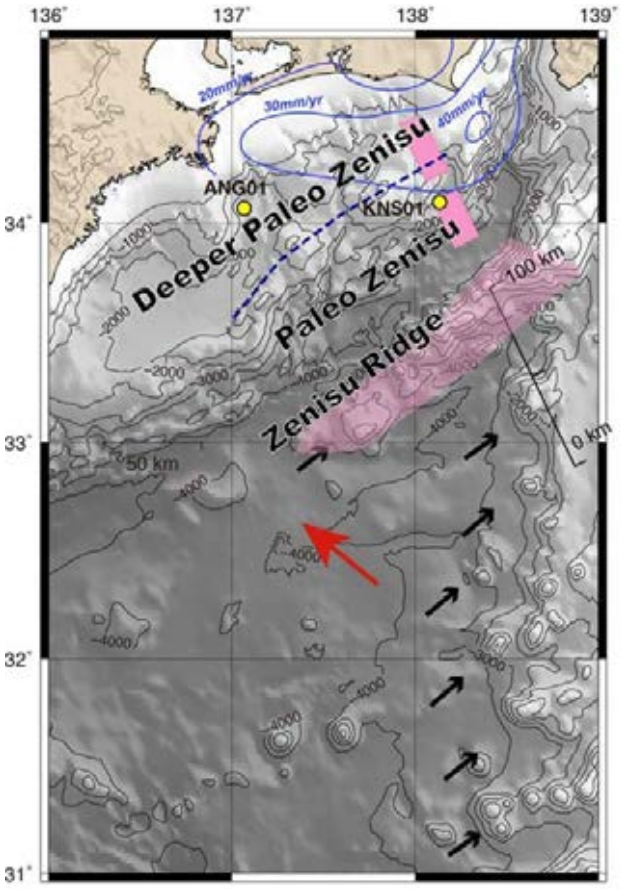

Figure 4.1 Cyclic ridge subduction modified from Kodaiea et al., (2003). Locations of the subducted deeper and the Paleo-Zenisu ridges are shown by thick pink boxes. Blue dotted line: the seaward end of the back stop (Nakanishi et al., 2002). Blue line contour: the back-slip distribution. Black arrows indicate sub-parallel volcanic ridges on the incoming plate. Red arrow indicates the plate motion of the Philippine Sea Plate. Yellow circles are proposed sites.

4.1 Proposed site

It becomes obvious that historical or instrumental records are too short and not always sufficient to estimate "earthquake recurrence time" (e. g. Goldfinger et al., 2013). Thus, a long record is proper to characterize the complex and multiscale earthquake recurrence intervals. A long continuous sedimentation off Tokai area is observed in proposed sites (Figure 4.2). Several active fault systems develop on the landward slope in parallel to the Nankai Trough. Arai et al. (2006) divided sedimentary sequences into four stratigraphic groups in this area. Kanasunose Group is defined as a well stratified strata in Kanasunose Trough (Figure 4.3). We propose to make coring at KNS01 site in Kanasunose Trough, which is located in the footwall side of Tokai thrust (e.g. Ashi, 1997, The Research group for active submarine faults off Tokai, 1999, Mazzotti, et al., 2002). In the KNS01, the surface sediment core GH97-311 (2.7 m) was studied and 13 turbidite layers have been recognized up to 3,000 years ago (Ikehara, 2001). Turbidite depositional age determined by radiocarbon ages of planktonic foraminifera in hemipelagic mud suggest that their occurrence interval are 70-600 years, which are expected to have been induced by earthquakes. This study demonstrates that KNS01 site is excellent for detailed stratigraphy of seismo-turbidite. A sequence above 3.30 seconds (ca. 75 m) consists of subhorizontally distinct reflectors with several tens-m interval (Figure 4.3). We focus on this sequence for our investigation, because it is interpreted from the acoustic facies that the excellent turbidite deposition has continued from 75m to the present time under the same condition. That is suitable to investigate whether "enigmatic recurrence" observed in the historical record is recognized also in the geological record in long term. The long record is necessary to validate the stability of "enigmatic recurrence" of this sequence. The proposed sequence, therefore, is ideal to achieve the objective. We

estimate the thickness of this interval as 75 m, and the age of target depth as 75 ka, if the sedimentation rate of core GH97-311 is adopted.

In addition, we would like to recover the sediment below the 3.30 seconds (TWT), because the discontinuity presumably represents indication of conversion of subduction framework around the area, and the lower sequence may show the different earthquake record from the interval above 75 m. We propose to confirm a stratigraphy of the event and to study the recurrence in the lower interval by additional 20 m coring to reach one of reflectors of the underlying strata.

ANG01a, an alternate site, is located in the west of "Anoriguchi Canyon" (Figure 4.3). Well stratified reflectors parallel to the seafloor in this area is defined as "Hamamatsu-oki Group" by Arai (2008). From the reflector image (Figure 4.4), we expect a similar depositional environment to that of KNS01. A sub-horizontal reflective interval (60 m) is our primary target. The underlying landward declining strata (~20 m) is an additional target to understand timing of a local tectonic event in this area like KN01.

It is considered that the upper sequences at KNS01 and ANG01a have a potential to involve earthquake recurrence record affected by the ridge subduction for the following reasons. (1) Both sites are located around "strong coupling zone" (Figure 4.1), which is interpreted to be related to the subduction of "Deeper Paleo Zenisu". (2) The landward slopes are heavily deformed by large fault systems parallel to the trough (Figure 4.2) and uplift of outer ridges (e.g. Park et al., 2003). Those observations suggest that the morphotectonics in the study area is largely controlled by the ridge subduction. Therefore, we consider the sedimentary records in both sites are substantially sufficient for achieving our objective.

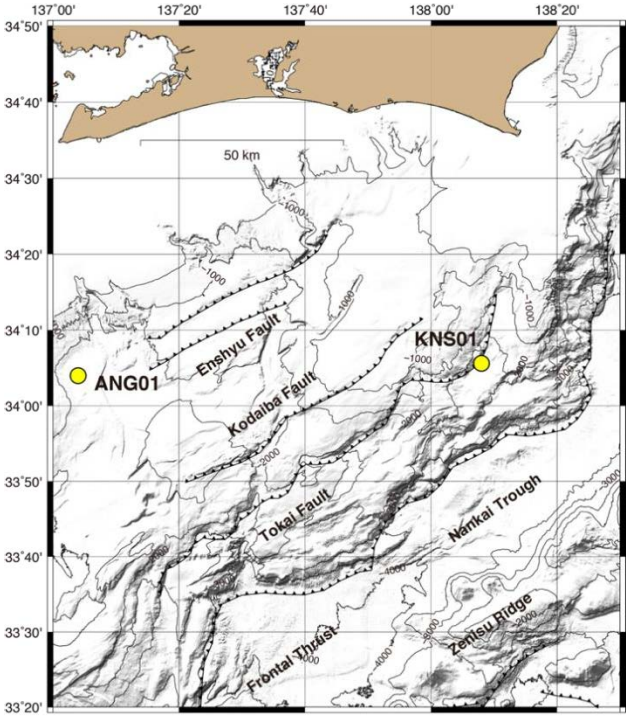

Figure 4.2 Seafloor topography off Tokai, locations of proposed sites are shown in yellow circles. Structural summary map from Arai et al., (2006).

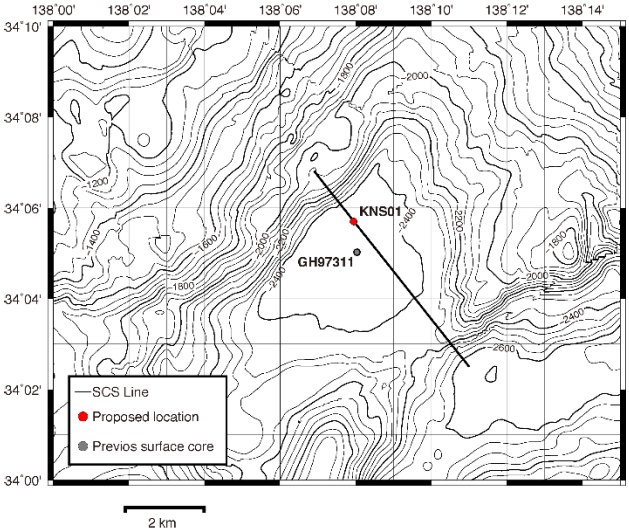

Figure 4.3 Red solid circle shows the location of KNS01(Primary site). Gray solid circle shows the location of GH97-311 (Ikehara, 2001). Black solid line shows SCS survey line (https://gbank.gsj.jp/marineseisdb/Tokai/index_Tokai.html). A seismic image of this line is presented in Figure 4.4. This figure was prepared using GMT5.4.4, Generic Mapping Tools; Wessel and Smith (1991).

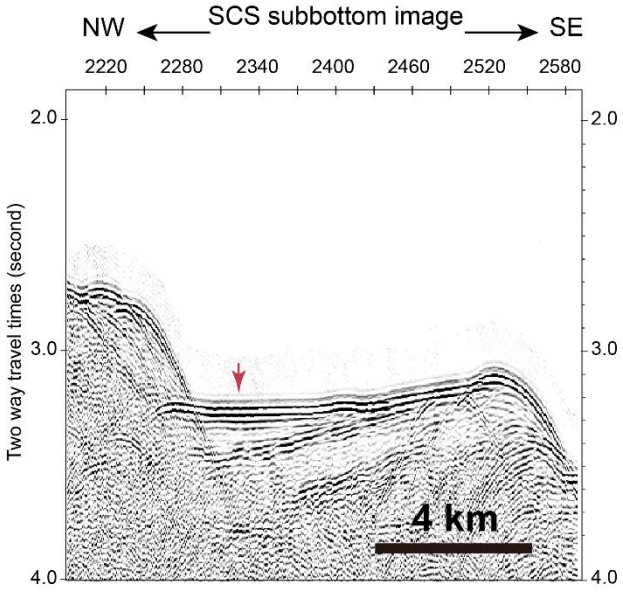

Figure 4.4 Sub-bottom image around KNS01. Primary target interval is the subhorizontal layer. Red arrow is the proposed position. The sub-seafloor depth is estimated using a velocity of 1500m/s. Additional 20-m coring (light green) is planned to understand the timing of local tectonic event.

5. Shipboard core analysis flow

Two holes were drilled for coring at Site C9035 (Tables 5.1 - 5.3). All cores were taken by the Hydraulic Piston Coring System (HPCS) and the short-HPCS (S-HPCS) of Chikyu. The HPCS is designed to take a 9.5-m long core while the S-HPCS is a tool modified from the HPCS to take a shorter core of 4.5 m, 3 m or 1.5 m long. In this expedition, the 4.5-m type S-HPCS was used. Cores were then used for shipboard sampling and analysis. General core analysis flow is shown in Figure 5.1, and detailed protocol is described in 7. Method.

Cores retrieved on the deck were delivered to the Core Cutting Area generally about 30 minutes later after the retrieval. The recovered core length excluding lengths of obvious void spaces were then measured and the Drilling Operations team determined the penetration length (= advance) based on the drilling parameters, the recovered core length and the core condition. A core was cut into 1.4-m long sections and each section length was entered into the J-CORES database, along with core identification information, drilling advance and depth information. Then each core sections were examined with the X-ray Computed Tomography (X-CT) scanner. After the X-CT scanning, core sections were examined by the whole-round multisensory core logger (MSCL-W) for gamma ray attenuation (GRA) density, magnetic susceptibility (MS), and natural gamma radiation (NGR), P-wave velocity, electrical resistivity. Measurement intervals are described in 7.4. X-ray computed tomography and MSCL.

After the MSCL-W scanning, the core section was split lengthwise along the lines delimiting the archive and working halves. Archive-half sections were processed in the following way: digital images were taken with the photo image logger (MSCL-I) prior to visual core description (VCD) by shipboard scientists. Minuscule samples (approximately the amount that could easily be picked up on the end of a toothpick) were taken from the archive half in areas of lithologic interest for smear slide analysis. After the VCD was completed, paleomagnetic measurement was conducted using the superconducting rock magnetometer (SRM) before the archive halves were prepared for storage.

For working-half sections, shipboard analysis of physical properties was conducted; penetrometer for half-round core, and discrete samples were taken for moisture and density measurements (MAD). All half-round core sections were vacuum sealed and transferred to cold storage. After expedition, all cores were transported under a cold condition (4°C) to the Kochi Core Center (KCC) in Kochi, Japan. The personal sampling party of each leg is planned at the KCC sometime after the core transportation.

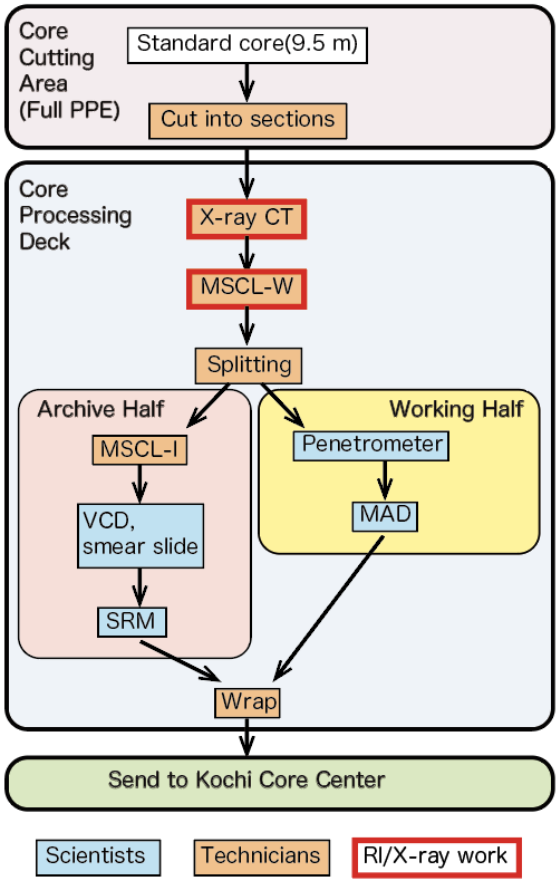

Figure 5.1 Schematic illustration of shipboard core analysis flow.

Table 5.1 Hole summary of C9035.

Site	Hole	Location	Water depth (mbsl)	Number of cores	Total cored interval (m)	Initial core recovery (%)
C9035	A	34°5.7000'N, 138°8.0300'E	2413.5	1	9.5	105.3
	B	34°5. 6962'N, 138°8.0346'E	2414.0	12	80.0	104.7

Table 5.2 Section summary of cores retrieved from Hole C9035A

Section	Curated length (m)	Top depth [m CSF-A]	Bottom depth [m CSF-A]	Top depth [m CSF-B]	Bottom depth [m CSF-B]
C9035A-1H-1	1.40	0	1.40	0	1.397
C9035A-1H-2	1.41	1.40	2.81	1.397	2.804
C9035A-1H-3	1.41	2.81	4.22	2.804	4.212
C9035A-1H-4	1.41	4.22	5.63	4.212	5.619
C9035A-1H-5	1.40	5.63	7.03	5.619	7.016
C9035A-1H-6	1.41	7.03	8.44	7.016	8.423
C9035A-1H-7	1.285	8.44	9.725	8.423	9.706
C9035A-1H-CC	0.295	9.725	10.02	9.706	10.000

Table 5.3 Section summary of cores retrieved from Hole C9035B

Section	Curated length (m)	Top depth [m CSF-A]	Bottom depth [m CSF-A]	Top depth [m CSF-B]	Bottom depth [m CSF-B]
C9035B-1H-1	1.4	0	1.4	0	1.4
C9035B-1H-2	1.405	1.4	2.805	1.4	2.805
C9035B-1H-3	0.82	2.805	3.625	2.805	3.625
C9035B-1H-CC	0.285	3.625	3.91	3.625	3.91
C9035B-2H-1	1.4	4	5.4	4	5.332
C9035B-2H-2	1.4	5.4	6.8	5.332	6.664
C9035B-2H-3	1.4	6.8	8.2	6.664	7.996
C9035B-2H-4	1.415	8.2	9.615	7.996	9.342
C9035B-2H-5	1.405	9.615	11.02	9.342	10.679
C9035B-2H-6	1.41	11.02	12.43	10.679	12.021
C9035B-2H-7	1.305	12.43	13.735	12.021	13.262
C9035B-2H-CC	0.25	13.735	13.985	13.262	13.5
C9035B-3H-1	1.4	13.5	14.9	13.5	14.823
C9035B-3H-2	1.405	14.9	16.305	14.823	16.152
C9035B-3H-3	1.405	16.305	17.71	16.152	17.48
C9035B-3H-4	1.405	17.71	19.115	17.48	18.808
C9035B-3H-5	1.405	19.115	20.52	18.808	20.136
C9035B-3H-6	1.435	20.52	21.955	20.136	21.492
C9035B-3H-7	1.29	21.955	23.245	21.492	22.712
C9035B-3H-CC	0.305	23.245	23.55	22.712	23
C9035B-4H-1	0.12	23	23.12	23	23.112
C9035B-4H-2	1.405	23.12	24.525	23.112	24.426
C9035B-4H-3	1.405	24.525	25.93	24.426	25.74
C9035B-4H-4	1.4	25.93	27.33	25.74	27.049
C9035B-4H-5	1.405	27.33	28.735	27.049	28.363
C9035B-4H-6	1.405	28.735	30.14	28.363	29.676
C9035B-4H-7	1.405	30.14	31.545	29.676	30.99
C9035B-4H-8	1.22	31.545	32.765	30.99	32.131
C9035B-4H-CC	0.395	32.765	33.16	32.131	32.5
C9035B-5H-1	1.4	32.5	33.9	32.5	33.822
C9035B-5H-2	1.405	33.9	35.305	33.822	35.149
C9035B-5H-3	1.405	35.305	36.71	35.149	36.476
C9035B-5H-4	1.405	36.71	38.115	36.476	37.802
C9035B-5H-5	1.405	38.115	39.52	37.802	39.129
C9035B-5H-6	1.405	39.52	40.925	39.129	40.456
C9035B-5H-7	1.28	40.925	42.205	40.456	41.665
C9035B-5H-CC	0.355	42.205	42.56	41.665	42

(**Table 5.3** continued)

Section	Curated length (m)	Top depth [m CSF-A]	Bottom depth [m CSF-A]	Top depth [m CSF-B]	Bottom depth [m CSF-B]
C9035B-6H-1	1.4	42	43.4	42	43.312
C9035B-6H-2	1.4	43.4	44.8	43.312	44.625
C9035B-6H-3	1.43	44.8	46.23	44.625	45.965
C9035B-6H-4	1.44	46.23	47.67	45.965	47.315
C9035B-6H-5	1.4	47.67	49.07	47.315	48.627
C9035B-6H-6	1.165	49.07	50.235	48.627	49.719
C9035B-6H-CC	0.3	50.235	50.535	49.719	50
C9035B-7H-1	1.4	50	51.4	50	51.314
C9035B-7H-2	1.415	51.4	52.815	51.314	52.642
C9035B-7H-3	1.225	52.815	54.04	52.642	53.792
C9035B-7H-4	1.22	54.04	55.26	53.792	54.937
C9035B-7H-5	1.255	55.26	56.515	54.937	56.115
C9035B-7H-CC	0.41	56.515	56.925	56.115	56.5
C9035B-8H-1	0.73	56.5	57.23	56.5	57.2
C9035B-8H-2	1.4	57.23	58.63	57.2	58.542
C9035B-8H-3	1.49	58.63	60.12	58.542	59.97
C9035B-8H-4	1.48	60.12	61.6	59.97	61.388
C9035B-8H-5	1.435	61.6	63.035	61.388	62.764
C9035B-8H-6	0.94	63.035	63.975	62.764	63.665
C9035B-8H-CC	0.35	63.975	64.325	63.665	64
C9035B-9H-1	1.295	64	65.295	64	65.228
C9035B-9H-2	1.305	65.295	66.6	65.228	66.466
C9035B-9H-3	0.725	66.6	67.325	66.466	67.154
C9035B-9H-CC	0.365	67.325	67.69	67.154	67.5
C9035B-10F-1	0.42	67.5	67.92	67.5	67.886
C9035B-10F-2	1.405	67.92	69.325	67.886	69.178
C9035B-10F-3	1.465	69.325	70.79	69.178	70.525
C9035B-10F-4	1.315	70.79	72.105	70.525	71.733
C9035B-10F-CC	0.29	72.105	72.395	71.733	72
C9035B-11F-1	1.48	72	73.48	72	73.339
C9035B-11F-2	1.465	73.48	74.945	73.339	74.664
C9035B-11F-3	1.39	74.945	76.335	74.664	75.921
C9035B-11F-4	0.38	76.335	76.715	75.921	76.265
C9035B-11F-CC	0.26	76.715	76.975	76.265	76.5
C9035B-12H-1	0.875	76.5	77.375	76.5	77.375
C9035B-12H-2	1.005	77.375	78.38	77.375	78.38
C9035B-12H-3	1.005	78.38	79.385	78.38	79.385
C9035B-12H-CC	0.805	79.385	80.19	79.385	80.19

6. Operation

Chikyu SCORE Expedition 912 Leg.1 began on 4th January 2020 when the D/V Chikyu left the port of Shimizu. The specific operation timetable for this expedition is described in 3. Shipboard Log. The vessel arrived at the proposed site on 19:30 on 5th January. On the same day, we started making up and running the HPCS assembly without Guide Horn after confirming the low sea current. Spud-in occurred at C9035A at 8:13 on 6th January. However, since the mudline cannot be observed in Core 1H, we moved the vessel to C9035B, 10 m southeast of C9035A. At C9035B, we first retrieved Core 1H and observed the mud line. The water depth turned out to be 2414.0 mbsl. Six cores including 1H were retrieved by the end of the day.

On 7th January, we continued coring and retrieved Cores 6H~12H. Since advance of the core was getting decrease from Core 6H and became 3.5m at Core 9H, we changed the coring system to S-HPCS. Apparent recovery of subsequent two cores, 10F and 11F, was over 100%, we then switched to HPCS for the next core. Each core's depth, advance and recovery were shown in Table 6.1.

Because a severe weather had been forecasted, we ended the operations at this site after retrieving the last core, 12H. This core, however, was stuck in the inner barrel due to expansion of the core and probably buckling of the core liner inside the inner barrel. A hydraulic piston pump was used along with burner heating and hummer banging to take out the stuck core. After 3 hours, all pieces of the core were taken out. The total depth of C9035B was 80.0 mbsf. The vessel departed the drilling site on 8th January and arrived at the site of Leg.2 on 10th, January. After the Leg.2 operations were completed, we arrived at the Port of Sasebo on 15th, January and the expedition terminated.

Table 6.1 Summary of each core's advance and recovery. Recovery of Cores 8H, 10F and 11F includes a flow-in part, 3.8 m, 1.1 m and 2.0 m in length, respectively.

Hole	Core	Below Seafloor (mbsf)		Advance (m)	Recovery (m)	Recovery (%)
		Top of core	Bottom of core			
A	1H	0.0	9.5	9.5	10.0	105.3
B	1H	0.0	4.0	4.0	3.9	97.5
B	2 H	4.0	13.5	9.5	9.9	104.5
B	3 H	13.5	23.0	9.5	10.0	105.1
B	4 H	23.0	32.5	9.5	10.1	106.2
B	5 H	32.5	42.0	9.5	10.1	105.8
B	6 H	42.0	50.0	8.0	8.4	105.5
B	7 H	50.0	56.5	6.5	6.7	103.1
B	8 H	56.5	64.0	7.5	7.6	101.6
B	9 H	64.0	67.5	3.5	3.7	104.9
B	10F	67.5	72.0	4.5	4.8	106.7
B	11F	72.0	76.5	4.5	4.9	108.2
B	12H	76.5	80.0	3.5	3.7	105.7

7. Method

7.1 Visual core descriptions

Visual core description (VCD) sheets provide a summary of the data obtained during shipboard analysis of each core. Detailed observations of each section were initially recorded by hand on paper, adjacent to the printed scanned image of that section. Copies of these original descriptions will be scanned and converted to PDF files and be included in "Supplementary material". Site, hole, core, section and depth (in centimeters core depth below seafloor) are given at the right top of the VCD sheet. Columns on the VCD sheets include the graphic representation, drilling (coring) disturbance (type and intensity), sedimentary structures, shipboard samples and color. These columns are discussed in more detail below.

Graphic lithology

Lithologies of the core intervals recovered are represented on the VCD sheets by graphics in the Graphic Representation column. A maximum of two different lithologies (for interbedded sediments) can be represented within the same core interval. The major lithology and some distinctive secondary lithologies, such as tephra layers, are included graphically in the Graphic Representation column. Because most of the obtained sediments were fine-grained, it was difficult to determine the exact lithological name. Smear slide observation will provide the exact lithological name.

Sediment (core) disturbance

Core disturbance from the drilling process can impact the integrity of the stratigraphic sequence. Drilling disturbances, if any, are documented for both soft and firm sediments using the following classification scheme:

- Slightly disturbed: bedding contacts are slightly bent or bowed in a concave-downward appearance.
- Moderately disturbed: bedding is moderately deformed but probably still in the correct stratigraphic sequence.
- Heavily disturbed: sediment is completely deformed and may show no traces of original bedding or structure.

In addition to this first-order assessment of disturbance, a number of other terms may appear on the VCD to characterize drilling disturbances. Some of the more common types observed are summarized below:

- Flow-in: soupy, displaced sediment pulled into the core liner during HPC coring.
- Fall-in: downhole contamination resulting from the falling of loose material from the drill hole walls into the top of the core. The uppermost 10-15 cm of each core was inspected during description for potential "fall-in."
- Soupy or mousse-like: intervals are water saturated and have lost all aspects of original bedding.
- Cracked or fractured: firm sediments are broken but not displaced or rotated significantly, and soft sediments are cracked due to gas expansion and so on.

Stratification and sedimentary structures

The locations and types of stratification and sedimentary structures visible on the prepared surfaces of the split cores are shown in the Structures column of the VCD sheet or are written in section description column in word. In the written description, layers and bedding thickness were further described and classified basically following terminology based on Stow (2005):

- Thin lamination = <3 mm thick.
- Medium lamination = 0.3–0.6 cm thick.
- Thick lamination = 0.6–1 cm thick.
- Very thin bed = 1–3 cm thick.
- Thin bed = 3–10 cm thick.

- Medium bed = 10–30 cm thick.
- Thick bed = 30–100 cm thick.
- Very thick bed = >100 cm thick.

Descriptive terms for bed boundaries such as sharp, erosive, gradual, irregular, bioturbated and burrowed are used.

Shipboard samples

Sample material taken for shipboard sedimentological analyses consisted of smear slides and samples for physical properties (moisture and density).

Sediment Color

On Expedition 912 Leg. 1, the dominant sediment colors for each core are recorded in section description on the VCD sheets using color codes (the corresponding hue and chroma) and names in Revised Standard Soil Color Charts.

7.2 Smear slides

One or more smear slide samples of the main lithology were collected from the working half of each core catcher. Additional samples were collected from areas of interest (e.g., turbidite layers, ash layers, mottles, etc.). A small amount of sediment was taken with a wooden toothpick and put on a 2.5 cm × 7.5 cm glass slide. The sediment sample was homogenized with a drop of deionized water and evenly spread across the slide to create a very thin (about <50 μm) uniform layer of sediment grains for quantification. The glass with dispersed sample was dried on a hot plate. A drop of optical adhesive was added as a mounting medium to a coverslip, which was carefully placed on the dried sample to prevent air bubbles from being trapped in the adhesive. Then the glass of smear slide was fixed in an ultraviolet light box. Smear slides were examined with a transmitted-light petrographic microscope equipped with a standard eyepiece micrometer.

The texture of siliciclastic grains (relative abundance of sand-, silt-, and clay-sized grains) and the proportions and presence of biogenic and mineral components were recorded on a smear slide sample sheet. Mineral and biogenic components and their percentage abundances were identified and estimated using Rothwell (1989). Smear slides analyses could estimate sand-sized and larger grains. The mineralogy of clay-sized grains will not be determined from smear slides. The quantitative grain size measurements of C9035 will be conducted in post-cruise researches.

7.3. Physical property

Moisture and density (MAD) measurements

Index properties, including bulk density, dry density, grain density, water content, and porosity, were derived from wet and dry mass and dry volume, measured on discrete samples from core section working halves. One or two samples were taken from every working half core section, each with an approximate volume of 10 cm^3, by a plastic syringe (20 mm in diameter). Each discrete sample for MAD were collected from semi-pelagic mud beneath the turbidite layer after measurement unconfined compressive strength (UCS).

Wet and dry masses were measured using a paired electronic balance system, which is designed to compensate for ship heave. A standard mass of similar value to the sample was placed on the reference balance to increase accuracy. The sample mass was determined to a precision of ±0.005 g. The balance system was calibrated at least once per 12 h.

To minimize desiccation, MAD sample collection was immediately followed by measurement of wet sediment mass (M_{wet}). After M_{wet} measurements, samples were dried in a convection oven at 105° ± 5°C for 24 h. Dry samples were placed in a desiccator for at least 1 h to equilibrate to room temperature (~24°C), and then dry sediment mass (M_{dry}) and dry sediment volume (V_{dry}) were measured. A five-chamber Quantachrome pentapycnometer was used to measure V_{dry} with a helium-displacement technique providing precision of ± 0.04 cm. The five-chamber system allowed the measurement of four sample volumes and one calibration sphere. Each measured volume is the

average of five measurement. The calibration sphere was rotated between all measurement chambers to monitor for errors in each chamber. The pycnometer was calibrated at least once per 24 h.

Water content

Water content (W_c) is the ratio of pore fluid mass to dry sediment mass (W_c[dry]). Corrections are required for salt when measuring the water content of marine samples. In addition to the water content calculation in W_c[dry], we calculated the ratio of pore fluid mass to total sample mass (W_c[wet]). The equations for water content are

$$W_c(dry) = (M_{wet} - M_d)/(M_d - sM_{wet})$$

and

$$W_c(wet) = \frac{M_{wet} - M_d}{M_{wet}(1-s)}$$

where

M_{wet} = total mass of the discrete sample,

M_d = mass of the dry sample, and

s = salinity (assumed dimensionless constant at 0.035).

Bulk density

Bulk density is the density of a discrete core sample (ρ_b = Mwet/Vt). Total wet sample mass (Mwet) was measured immediately after collecting each discrete sample using the dual-balance system. Total sample volume assuming 100% saturation (Vt = Vg + Vpw) was determined from the pycnometer measurement of grain volume (Vg) and the calculated volume of pore water (Vpw). Solid grain and pore water volume were determined as

$$V_g = V_d - \frac{(M_{wet} - M_d)s}{\rho_{salt}(1-s)}$$

and

$$V_{pw} = \frac{M_{wet} - M_d}{\rho_{sw}(1-s)}$$

Where

V_d = dry volume,

ρ_{salt} = salt density, and

ρ_{sw} = standard seawater density.

Porosity and void ratio

Porosity (φ) relates the volume of the pores to total sample volume; void ratio (e) relates the pore volume to solid grain volume. They are calculated as

$$\varphi = \frac{\rho_b V_{pw}}{M_{wet}}$$

and

$$e = \frac{V_{pw}}{V_g}$$

Grain density

Grain density (ρ_g) was determined from measurements of dry mass and dry volume made with the balance and the pycnometer, respectively. Mass and volume were corrected for salt, yielding

$$\rho_g = \frac{M_d - M_{salt}}{\left\{V_d - \frac{(M_{wet} - M_d)s}{[\rho_{salt}(1-s)]}\right\}}$$

where the density of salt (ρ_{salt}) is assumed to be constant at 2.22 g/cm^3.

Penetration test

The penetrometer provides a measure of UCS of sediment samples. The UCS is calculated by dividing the penetration resistance generated by pushing a cylindrical probe into the core surface to a 5 mm penetration depth by the area of the penetration probe. All measurements in this expedition were conducted using a probe with a nominal diameter of 6.35 mm. The UCS values were calculated from the average of three penetration trials conducted at the point which collected sample for MAD. Typical spatial separation between trials was on the order of 1 cm. UCS were measured before collecting samples for MAD to remove the effects of collecting samples for MAD. The unit was converted from kg/cm^2 to kPa by the following equation as

$$UCS(kPa) = UCS(kg/cm^2) \times 9.81 \times 10$$

7.4. X-ray computed tomography and MSCL

X-ray computed tomography

X-ray computed tomography (CT) imaging provided information about structures and sedimentological features in the core and helped to assess sample locations and quality for whole-round samples. Our methods followed those in the measurement manual prepared by the Center for Deep Earth Exploration (CDEX) (X-ray CT Scanning, version 1.00, 26 Dec 2008) and used on previous expeditions (e.g., IODP Expeditions 315, 316, 319, 322, and 331). The manual is based on GE Healthcare (2006), Mees et al. (2003), and Nakano et al. (2000).

A LightSpeed Ultra 16 (GE Yokogawa Medical Systems, Ltd.), capable of generating sixteen 0.625 mm thick slice images every 0.5 s, the time for one revolution of the X-ray source around the sample, is the X-ray CT scanner on the *Chikyu*. Data generated for each core consist of core-axis-normal planes of X-ray attenuation values with dimensions of 512 × 512 pixels. Data were stored as Digital Imaging and Communication in Medicine (DICOM) formatted files. The theory behind X-ray CT has been well established through medical research and is very briefly outlined here. X-ray intensity varies as a function of X-ray path length and the linear attenuation coefficient (LAC) of the target material as

$$I = I_0 \times e^{-\mu L},$$

where

I = transmitted X-ray intensity,

I_0 = initial X-ray intensity,

μ = LAC of the target material, and

L = X-ray path length through the material.

LAC is a function of the chemical composition and density of the target material. The basic measure of attenuation, or radiodensity, is the CT number given in Hounsfield units (HU) and is defined as

$$\text{CT number} = [(\mu_t - \mu_w)/\mu_w] \times 1000,$$

where

μ_t = LAC for the target material, and

μ_w = LAC for water.

The distribution of attenuation values mapped to an individual slice comprises the raw data that are used for subsequent image processing. Successive 2-D slices yield a representation of attenuation values in 3-D voxels.

Analytical standards used during Expedition 333 were air (CT number = –1000), water (CT number = 0), and aluminum (2477 < CT number < 2487) in an acrylic core mock-up. All three standards were run once daily after air calibration. For each standard analysis, the CT number was determined for a 24.85 mm^2 area at fixed coordinates near the center of the cylinder.

X-ray CT scan data usage

X-ray CT scanning was done immediately after core cutting for time-sensitive (interstitial water, microbiology, and organic geochemistry) samples to finalize their selection. All whole-round core sections were screened to avoid destructive testing on intervals that may contain interesting structural or sedimentological features. This also facilitated identifying intervals with minimal drilling disturbance for whole-round sampling and for assessing heterogeneity (essential for post-expedition studies of frictional, geotechnical, and hydrogeological properties).

MSCL-W

GRA density

Bulk density can be used to evaluate pore volume in sediment, which provides information on the consolidation state of sediment. GRA density is based on the detection of a gamma ray beam produced by a cesium source. The beam, produced by a ^{137}Cs gamma ray source at a radiation level of 370 MBq within a lead shield with a 5 mm collimator, is directed through whole-round cores. The gamma ray detector includes a scintillator and an integral photomultiplier tube to record the gamma rays that pass through the whole-round core. GRA bulk density (ρ_b) is calculated as

$$\rho_b = \ln(I/I_0)\mu d,$$

where

I_0 = gamma ray source intensity,

I = measured intensity of gamma rays passing through the sample,
μ = Compton attenuation coefficient, and
d = sample diameter.

The Compton attenuation coefficient (μ) and source intensity (I_0) are treated as constants, so ρ_b can be calculated from I. The gamma ray detector is calibrated with a sealed calibration core (a standard core liner filled with pure water [Elix] and aluminum cylinders of various diameters). To establish the calibration curves, gamma ray counts were taken through each aluminum cylinder for 60 s. Each aluminum cylinder has a density of 2.7 g/cm^3, and d is 1, 2, 3, 4, 5, or 6 cm. The relationship between I and μd is

$$\ln(I) = A(\mu d) + B,$$

where A and B are coefficients determined from the calibration experiment. GRA density measurements on core samples were conducted every 4 cm for 4 s. The spatial resolution was 5 mm.

Magnetic susceptibility

Magnetic susceptibility is the degree to which a material can be magnetized by an external magnetic field. Therefore, magnetic susceptibility provides information on sediment composition. A Bartington loop sensor with an 8 cm diameter was used to measure magnetic susceptibility. An oscillator circuit in the sensor produces a low intensity (~80 A/m RMS), non-saturating, alternating magnetic field (0.565 kHz). This pulse frequency is converted into magnetic susceptibility. The spatial resolution of the loop sensor is 23–27 mm, and it is accurate to within 5%. Magnetic susceptibility data were collected every 4 cm along the core.

Natural gamma radiation

Natural gamma radiation measurements provide insights into sediment composition and thus can be used to identify lithology. Whole-round cores were monitored for natural gamma ray (NGR) emissions to obtain spatial variability in radioactivity and establish gamma ray logs of cores for correlation to downhole gamma ray logs. A lead-shielded counter, optically coupled to a photomultiplier tube and connected to a bias base that supplies high-voltage power and a signal preamplifier, is used. Two horizontal and two vertical sensors are mounted in a lead, cube-shaped housing. The NGR system records radioactive decay of long-period isotopes ^{40}K, ^{232}Th, and ^{238}U. NGR has a resolution of 120–170 mm and was measured every 16 cm with a count time of 30 s. Background radiation noise was determined by taking measurements on a water-filled calibration core.

***P*-wave velocity**

P-wave data can be used to evaluate small-strain moduli, to correlate between log and core data, and to evaluate pore structure and cementation. *P*-wave (compressional) velocity (V_P) is defined by the time required for a compressional wave to travel a set distance:

$$V_P = d/t_{core},$$

where
d = path length of the wave across the core, and
t_{core} = traveltime through the core.

P-wave velocity transducers on the MSCL-W system measure total traveltime of the compressional wave between transducers. The wave travels horizontally across the whole core and core liner. The total traveltime observed is composed of
t_{delay} = time delay related to transducer faces and electronic circuitry,
t_{pulse} = delay related to the peak detection procedure,
t_{liner} = transit time through the core liner, and
t_{core} = traveltime through the sediment or rock.

The system is calibrated using a core liner filled with distilled water, which provides control for t_{delay}, t_{pulse}, and t_{liner}. With these calibrations, core velocity (V_P) can be calculated on whole-round specimens in core liners as follows:

$$V_P = (d_{cl} - 2d_{liner})/(t_o - t_{pulse} - t_{delay} - 2t_{liner}),$$

where
d_{cl} = measured diameter of core and liner,
d_{liner} = liner wall thickness, and
t_o = measured total travel time.

The above equation assumes that the core completely fills the core liner.

Electrical resistivity

Within limits, electrical resistivity may be useful for estimating other sediment physical properties, including porosity, tortuosity, permeability, and thermal conductivity. Bulk electrical resistivity is controlled by solid grain resistivity, interstitial water resistivity, pore space distribution, and pore connectivity. Electrical resistivity (ρ) is defined by the electrical resistance and geometry of the core measured:

$$\rho = R(A/L),$$

where

R = electrical resistance,

L = length of measurement, and

A = cross-sectional area of the core.

The noncontact resistivity sensor on the MSCL-W system induces a high-frequency magnetic field in the core with a transmitter coil. This generates an electrical current in the bulk sediment that is inversely proportional to its resistivity. The secondary magnetic field generated by this induced electrical current is measured by a receiver coil. To measure this smaller magnetic field accurately, a differencing technique has been developed that compares readings from the sample core to readings from an identical set of coils operating in air. Electrical resistivity data were obtained at 4 cm intervals on the MSCL-W.

MSCL-I: Photo image logger (archive half)

The GeoTek photo image logger (MSCL-I) scans the surface of the archive half and creates a digital image. The line-scan camera (Nikon Lens: AF Nikkor 50 mm 1:1.8D) is equipped with three charge-coupled devices, each with 2048 arrays. The reflected light from the core surface is split into three channels (red, blue, and green) by a beam splitter inside the line-scan camera. The signals are combined, and the digital image is processed. A correction is made for any mechanical differences among the charge-coupled vice responses. Calibrations are conducted before scanning each core to compensate for pixel-to-pixel response variation, uneven lightning, and lens effects. Optical distortion is avoided by precise movement

7.5 Paleomagnetism

Paleomagnetic and rock magnetic investigations were conducted to determine the characteristic of remanence directions for use in magnetostratigraphic and structural studies. Archive halves and discrete samples were measured with the superconducting rock magnetometer (SRM). The paleomagnetism laboratory on board the *Chikyu* houses a large (7.3 m × 2.8 m × 1.9 m) magnetically shielded room, with its long axis parallel to the ship transverse. The total magnetic field inside the room is ~1% of Earth's magnetic field. The room is large enough to comfortably handle standard IODP core sections (~1.5 m). The shielded room houses the equipment and instruments described in this section. The long-core SRM is a liquid helium free cooling system (4K SRM: WSGI); the 4K SRM uses a Cryomech pulse tube cryocooler to achieve the required 4ºK operating temperatures without the use of any liquid helium. The differences between the pulse tube cooled system and the liquid helium cooled magnetometers have very significant impact on the system ease of use, convenience, safety and long-term reliability. The SRM system is ~6 m long with an 8.1 cm diameter access bore. A 1.5 m split core liner can pass through a magnetometer, an alternating-field (AF) demagnetizer, and an anhysteretic remanent magnetizer (Figure 7.1). The system includes three sets of superconducting pickup coils, two for transverse moment measurement (x- and y-axes), and one for axial moment measurement (z- axis). The noise level of the magnetometer is $<10^{-7}$ A/m for a 10 cm^3 volume rock. An automated sample handler system (2G804) included in the magnetometer consists of aluminum and fiberglass channels and designated to support and guide long core movement. The core itself is positioned in a nonmagnetic fiberglass carriage that is pulled through the channels by a rope attached to a geared high-torque stepper motor. A 2G600 sample degaussing system is coupled to the SRM to allow automatic demagnetization of samples up to 100 mT. The system is controlled by an external computer and enables programming of a complete sequence of measurements and degauss cycles without removing the long core from the holder.

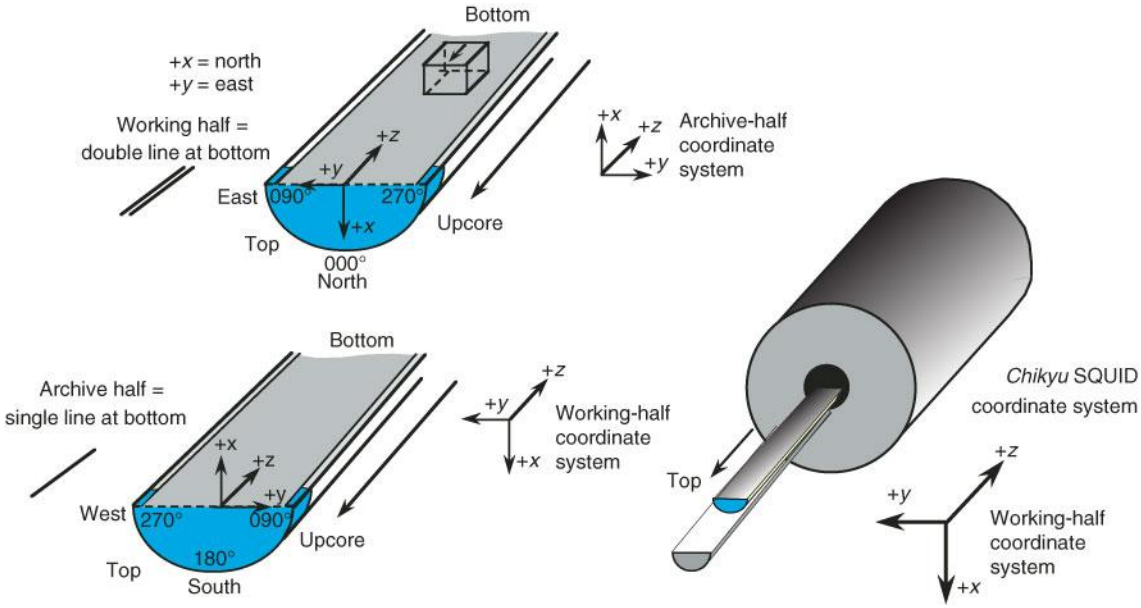

Figure 7.1 Relation of orientation between an archive halve and a cube sample

8. Preliminary Results

8.1 Lithostratigraphy

The sedimentary succession recovered at Site C9035 is dominated by silty sediments with numerous coarse-grained (coarse silt–very fine sand) layers and some volcanic ash layers and spots (Figure 8.1). The section is divided into two major lithological units (Unit I and II), distinguished on the basis of sedimentary facies. Some coring disturbances such as flow-in and fall-in are observed. Flow-in sediments occur in the middle to lower part of Cores 8H, 10F and 11F, and fall-in sediments occur at the core-top of Cores 5H, 8H, 9H, 10F and 11F. Gas expansion is significant at the middle to lower part of Unit I, and artificial disturbances to release gases before core cutting are found in cores.

Unit description

Unit I

Intervals: C9035A 1H-1, 0 cm through 1H-cc 29.4 cm; C9035B 1H-1, 0 cm through 6H-1 10.2 cm.

Depths: C9035A = 0 – 10.00 m CSF-B; C9035B = 0 – 42.10 m CSF-B.

Lithology and structures: Unit I consists of bioturbated silt and layered coarse silt–very fine sand with massive silt. Silt contains large amounts of biogenic materials such as diatom, sponge spicules, foraminifera and calcareous nannoplankton. Numerous intercalations of coarse silt–very fine sand layers characterize this lithological unit. The layers have a sharp (and sometimes erosional) basal contact and grades upward into massive silt. Parallel lamination is common. Mud laminae is also found in some layers. These structures suggest the layer is muddy (fine-grained) turbidite. Turbidite mud is thick in the upper part, but thin or absent in the lower part. Total 194 turbidite beds with their averaged thickness of 9.2 cm occur in Unit I of Hole C9035B. Rhythmic occurrence (4–5 layers/section) of the fine-grained turbidites is a characteristic feature of Unit I. Some burrows destroy sedimentary structures of the coarse silt–very fine sand layers, suggesting high benthos activities. Discrete tephra (volcanic ash) layers and spots are intercalated in bioturbated silt.

Unit II

Interval: C9035B 6H-1, 10.2 cm through 12H-cc 80.3 cm.

Depth: C9035B = 42.10 – 80.19 m CSF-B.

Lithology and structures: Unit II is characterized by matrix-supported gravelly mud–muddy gravel (Subunit IIB). Angular mudstone gravel is predominant. Large (>a few tens cm) siltstone blocks with distorted layer or bedding are found. Very fine sand layers with massive silt covers gravelly mud–muddy gravel, and form Subunit IIA.

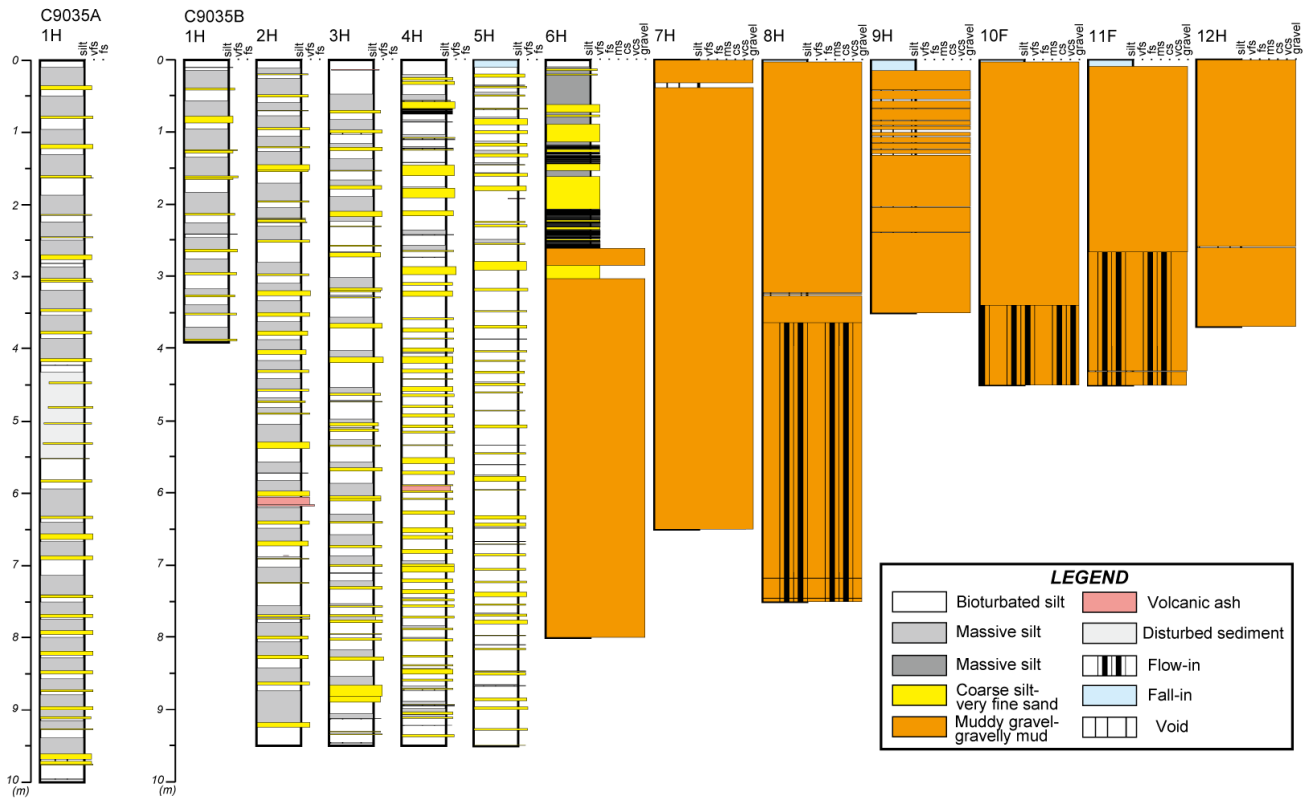

Figure 8.1 Summary of VCD. Core lengths are adjusted to CSF-B. In the upper part of core 6H, the massive silt (dark gray) of Unit II shows a minor color different to that (massive silt in light gray) of Unit I. Besides, numerous thin coarse silt layers are marked in black color.

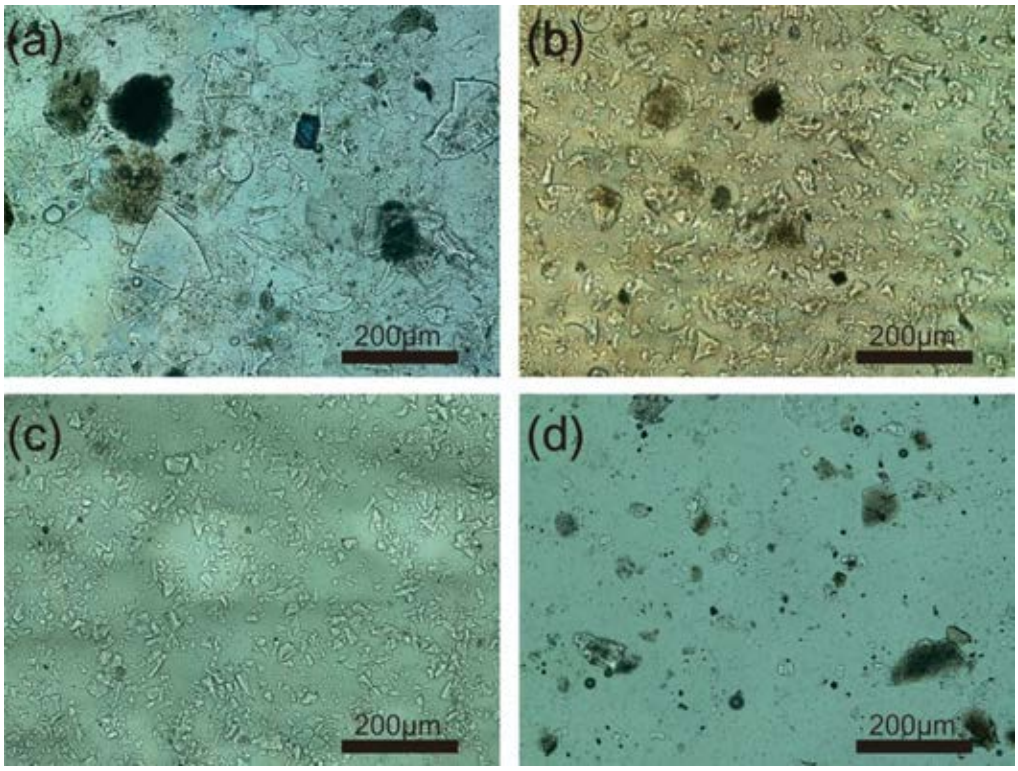

Figure 8.2 Plane-polarized light microscopic images of clear glass fragments of (a) 2H-5A-86 cm, (b) 3H-1A-14.5 cm, (c) 4H-6A-60 cm, (d) 6H-5-57 cm.

8.2 Smear slides

During this expedition, two samples from C9035A and 22 samples from C9035B were selected for smear slide. One or more smear slide samples per core were made to observe the main lithology. The depth of each sample used for preparation of smear slide was listed in Table 1. The sediment is mainly dominated by silt and silty clay. In C9035B, three intervals including clear glass fragments were observed in: 2H-5A-86 cm, 3H-1A-14.5 cm, 4H-6A-60 cm. The slide in 6H-5-57 cm also included part of clear glass fragments (Figure 8.2). The composition of the samples includes terrigenous and biogenic materials in each slide, except the ash samples. Terrigenous sediments mainly include quartz, feldspar, rock fragments, and mica. Biogenic sediments mainly include nannofossils, foraminifera, diatoms, and sponge spicules.

In general, the calcareous nannofossils abundance has a decreasing trend from very abundant (top to 7H-2A) to common (8H-3A to bottom). Besides, the *Discoaster sp*. can be observed in the 7H-2A to the bottom.

8.3 Physical property measurements

MAD measurements

The MAD data from 19 samples of Hole C9035B are shown in Figure 8.3. In Figures 8.3 A and 8.3B shows water contents (Wc[wet]: Figure 8.3A; Wc[dry]: Figure 8.3B). The trend of Figures 8.3A and 8.3B are similar. The trend decreased sharply from 2.160 mCSF to 7.577 mCSF and from 42.225 mCSF to 48.055 mCSF. From 7.558 mCSF to 20.268 mCSF and from 24.926 mCSF to 40.319 mCSF, these gradually decreased with core depth. Dry density (Figure 8.3C) increased sharply from 2.16 mCSF to 7.577 mCSF and from 42.225 mCSF to 48.055 mCSF and were nearly constant from 7.558 mCSF to 42.244 mCSF.

Below 42.244 mCSF, values increased while oscillating. Grain density (Figure 8.3D) gradually decreased from 11.269 mCSF to 55.209 mCSF. Porosity (Figure 8.3E) and void ratio (Figure 8.3F) have a similar tendency which shows inverse correlation with dry density.

Penetration test

The downhole profiles of penetration strength are shown in Figure 8.3G. UCS gradually increased with depth to ~84.20 kPa at 20.268 mCSF and were nearly constant from 31.5 mCSF to 40.319 mCSF. Below 42.244 mCSF, the amplitude of UCS increased with depth and the values also increased.

Table 8.1 Sample depth and sample id for smear slide from 24 samples of Holes A and B.

Sample	Depth of samples below the sea floor (mcsf-A)	J-CORES sample id	note
Hole A-1H-5, 74 cm	0.740	CKY000000000001146350	
Hole A-1H-CC, 8 cm	9.805	CKY000000000001146450	
Hole B-1H-2, 130 cm	1.530	CKY000000000001146550	
Hole B-2H-4, 97 cm	9.170	CKY000000000001147250	
Hole B-2H-5, 86 cm	10.475	CKY000000000001147350	ash
Hole B-2H-7, 129 cm	12.559	CKY000000000001147450	
Hole B-3H-1, 14.5 cm	13.645	CKY000000000001147550	ash
Hole B-3H-4, 25 cm	17.960	CKY000000000001147650	
Hole B-3H-7, 100 cm	22.055	CKY000000000001147750	
Hole B-4H-2, 30 cm	23.420	CKY000000000001148050	
Hole B-4H-6, 60 cm	29.335	CKY000000000001148250	ash
Hole B-5H-2, 63 cm	34.530	CKY000000000001148850	
Hole B-5H-3, 30 cm	35.605	CKY000000000001148950	
Hole B-5H-7, 110 cm	42.025	CKY000000000001149050	
Hole B-6H-1, 12 cm	42.120	CKY000000000001149150	
Hole B-6H-5, 57 cm	48.240	CKY000000000001149250	have part glass
Hole B-7H-2, 95 cm	52.350	CKY000000000001149350	
Hole B-8H-2, 3 cm	57.260	CKY000000000001149650	
Hole B-8H-3, 51 cm	59.140	CKY000000000001150250	
Hole B-9H-3, 10 cm	66.700	CKY000000000001150350	
Hole B-10F-3, 50 cm	69.825	CKY000000000001150450	
Hole B-11F-1, 80 cm	72.800	CKY000000000001150550	
Hole B-12H-CC, 20 cm	79.585	CKY000000000001150650	
Hole B-12H-CC, 30 cm	79.685	CKY000000000001150750	

Table 8.2 J-CORES sample ID, averaged cohesive strength and MAD results from 21 samples of Holes A and B.

Sample source	J-CORES sample ID	Averaged cohesive strength (kg/cm^2)	MAD		
			Wet bulk mass (g)	Dry bulk mass (g)	Dry bulk volume (cm^3)
Hole A-1H-5W, 101.5-103.5 cm	CKY000000000001146650	0.62	12.2808	6.9786	2.6908
Hole A-1H-2W, 76.0-78.0 cm	CKY000000000001146750	0.30	8.0809	3.8914	1.4266
Hole B-2H-3W, 94.0-96.0 cm	CKY000000000001146850	0.67	7.6288	4.5382	1.6470
Hole B-2H-6W, 62.0-64.0 cm	CKY000000000001146950	0.80	8.8024	5.3216	2.0113
Hole B-3H-3W, 103.5-105.5 cm	CKY000000000001147050	1.30	10.4166	6.5178	2.4390
Hole B-3H-6W, 12.0-14.0 cm	CKY000000000001147150	1.72	17.4969	11.0823	4.1929
Hole B-4H-3W, 53.5-55.5 cm	CKY000000000001147850	0.90	16.2332	9.9184	3.7705
Hole B-4H-8W, 54.5-56.5 cm	CKY000000000001147950	1.47	15.7507	9.9967	3.7168
Hole B-5H-3W, 58.0-60.0 cm	CKY000000000001148150	1.43	16.8082	10.8661	4.0492
Hole B-5H-6W, 124.0-126.0 cm	CKY000000000001148350	1.27	15.6095	10.2826	3.7884
Hole B-6H-1W, 24.0-26.0 cm	CKY000000000001148450	0.70	14.3028	8.9833	3.3193
Hole B-6H-5W, 77.0-79.0 cm	CKY000000000001148550	1.90	18.9779	14.6698	5.4240
Hole B-7H-2W, 104.0-105.0 cm	CKY000000000001148650	1.63	18.7539	14.3266	5.2483
Hole B-7H-5W, 27.0-29.0 cm	CKY000000000001148750	2.53	16.9182	13.2946	4.8552
Hole B-8H-2W, 79.0-81.0 cm	CKY000000000001149450	1.63	18.7648	14.0914	5.0360
Hole B-8H-4W, 31.0-33.0 cm	CKY000000000001149550	3.40	18.8354	14.9863	5.4876
Hole B-9H-3W, 17.0-19.0 cm	CKY000000000001149750	2.10	15.5433	11.7889	4.3959
Hole B-10F-2W, 76.0-78.0 cm	CKY000000000001149850	1.47	18.5660	14.9708	5.4775
Hole B-10F-4W, 35.0-37.0 cm	CKY000000000001149950	4.63	22.5402	19.0294	6.9697
Hole B-11F-2W, 23.0-25.0 cm	CKY000000000001150050	2.40	19.1212	15.3534	5.6760
Hole B-12H-CCW, 28.0-30.0cm	CKY000000000001150150	3.17	17.9994	14.6084	5.4415

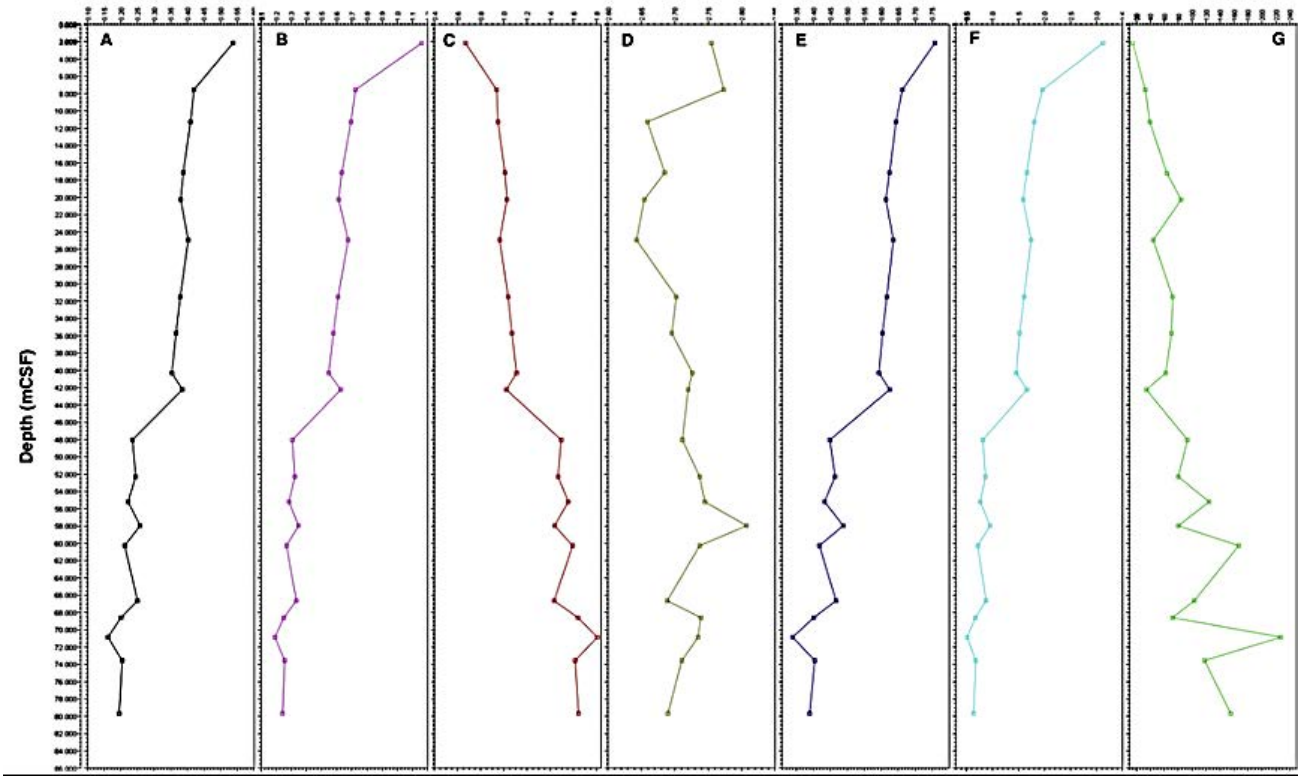

Figure 8.3 Moisture and density data from 19 samples of Hole C9035B include: (A, B) water contents, (C) dry density, (D) grain density, (E) porosity, (F) void ratio, and (G) penetration strength.

8.4 X-ray CT scanning and MSCL

Hole C9035A

Because mud line cannot be identified in C9035A-1H core, it is decided to make Hole B in 10-m southeast to Hole A. P-wave, Magnetic susceptibility, GRA density, natural gamma radiation, and Electric resistivity were measured on C9035A-1H core (Figure 8.4). The obtained data could be correlated to the somewhere of sections of Hole B. Cyclic fluctuating variations in magnetic susceptibility, GRA density, and Electric resistivity are observed.

Hole C9035B

Since P-wave amplitude below 14.0 CSF-B m become lower value such as 40, P-wave velocity is invalid below the horizon (Figure 8.5). The general P wave velocity is about 1500 m/sec. GRA density is generally show a constant value ca. 1.6-1.7 g/cc in the interval between 10.0 and 43.0 CSF-B m. The GRA density suddenly increase at 43.0-46.0 CSF-B m **(**Figure 8.4**)**. The GRA density fluctuates between values between 1.9-2.2 g/cc in the interval between 46.0-76.0 CSF-B m. The extremely lower value in the bottom could be due to core treatment on the rig floor (see coring operation). In detailed, High GRA density corresponds to sandy layer occurrence. General trend of magnetic susceptibility gradually decreases to 0 to 20.0 CSF-B m, hump in the interval of 26-30 CSF-B m. Below 38.0 CSF-B m, magnetic susceptibility keeps relatively low value.

In the core 2H for example, magnetic susceptibility peaks roughly correspond to the sandy layer occurrence in Unit I **(**Figure 8.6**)**. Bases of layers shows a spiky high value and decrease gradually upward. Electric resistivity gradually increases downward. The fluctuation pattern of resistivity shows mirror images to magnetic susceptibility and GRA density. The downhole variation of Natural Gamma radiation is similar to the trend of GRA density. There is a large gap around 44 CSF-B m (Figure 8.4).

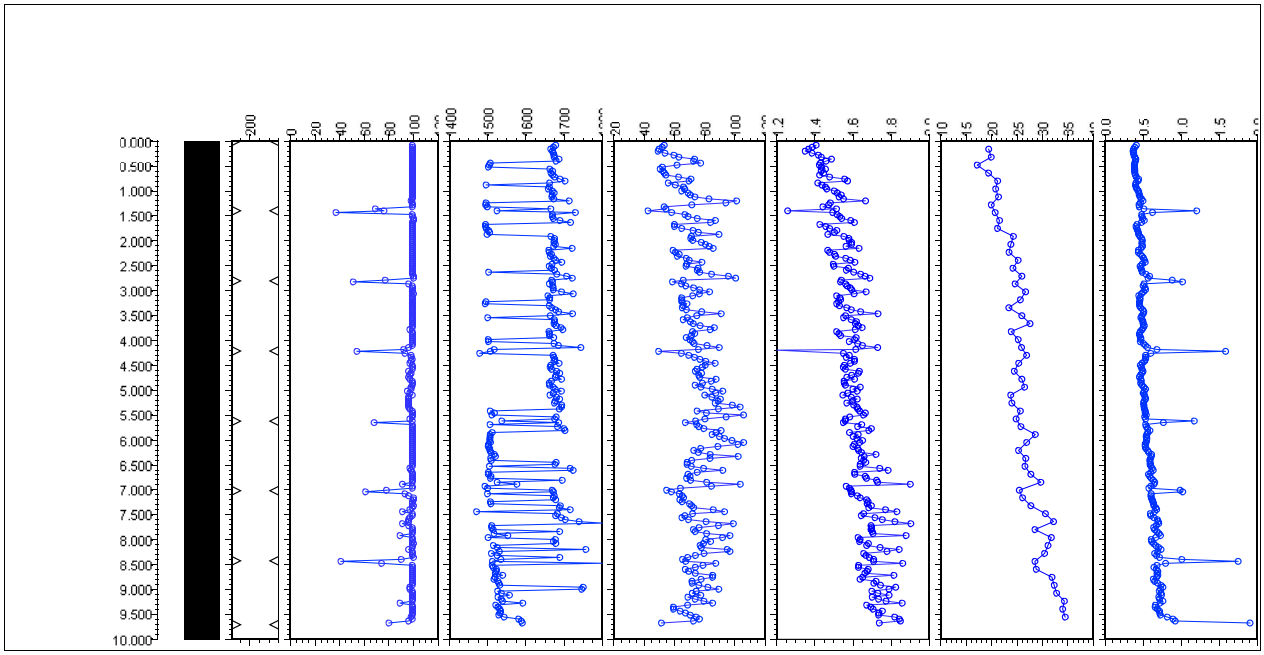

Figure 8.4 MSCL-W results of Hole C9035A. CSF = core depth below seafloor.

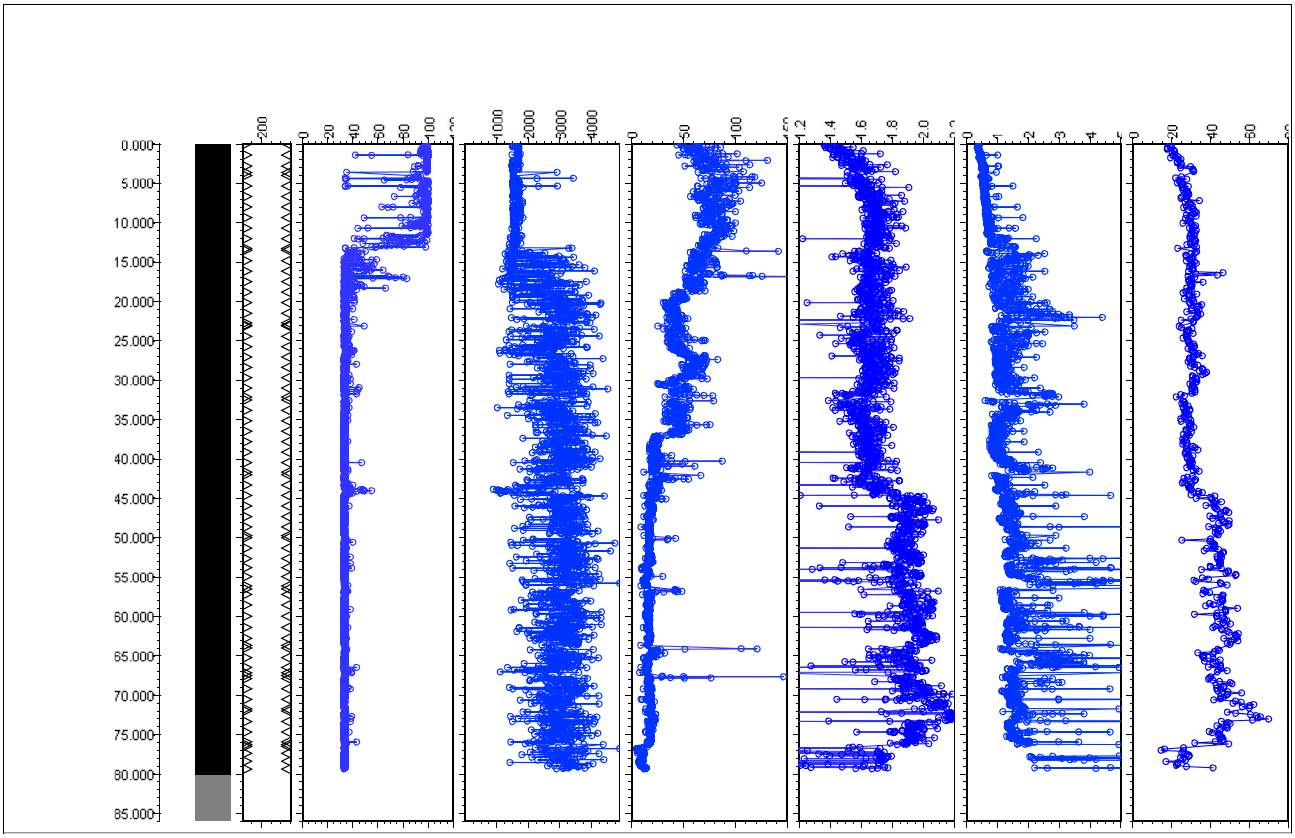

Figure 8.5 MSCL-W results of Hole C9035B. CSF = core depth below seafloor.

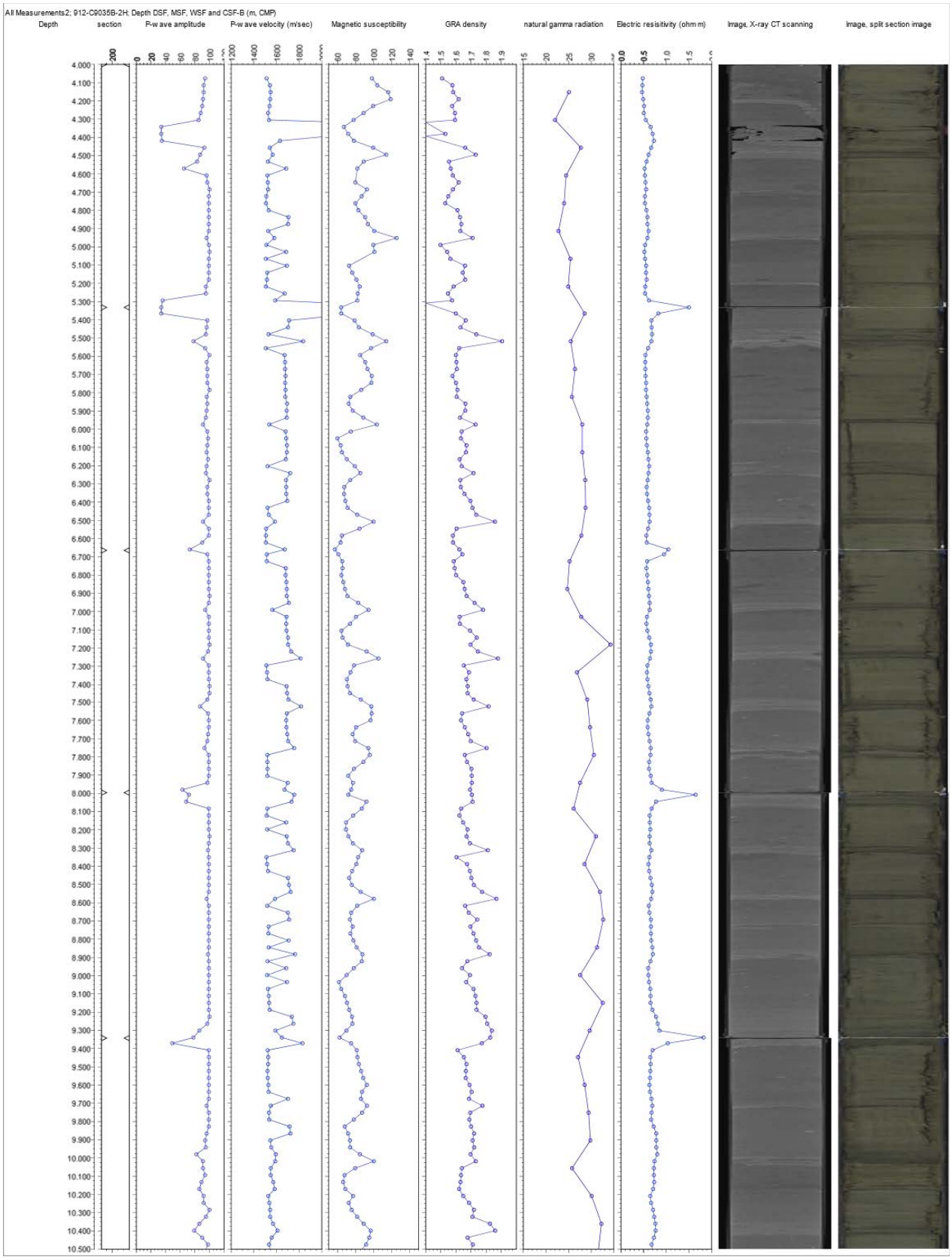

Figure 8.6 MSCL-W results of core 2H, Hole C9035B. CSF = core depth below seafloor.

8.5 Paleomagnetism

Holes C9035A and C9035B

Remanent magnetizations of archive-half sections from Holes C9035A and C9035B were measured at demagnetization levels of 0, 10, and 20 mT peak fields in order to recognize stable magnetic components. It is confirmed that low-coercivity components can be removed by demagnetizations step of 10 mT (Figure 8.7). Inclinations, declinations and intensity after 20 mT are shown in Figures 8.8 and 8.9. Because the mud line was unrecognized in the first core at Hole A, a continuous coring was made at Hole B. Inclination in Hole B gently changes downward. Deviation in the inclination suddenly changes around 42.0 m CSF-B. Inclination becomes widely scattered in the interval between 42-80 m CSF-B (Figure 8.8). Declination is generally constant within each core interval. But gaps occur at core boundaries. This is obviously due to different core orientation in respective HPCS. Declination is scattered in the interval between 42.0 and 80.0 m CSF-B. Intensity decreases from 0 to 42 m CSF-B, and quickly from 42 to 48 m CSF-B. A constant weak interval between 48.0 to 80.0 m CSF-B is recognized. The changes in inclination, declination, and intensity around 42 m CSF-B is corresponded to the lithologic boundary at 42 m CSF-B (refer to 8.1 Lithostratigraphy).

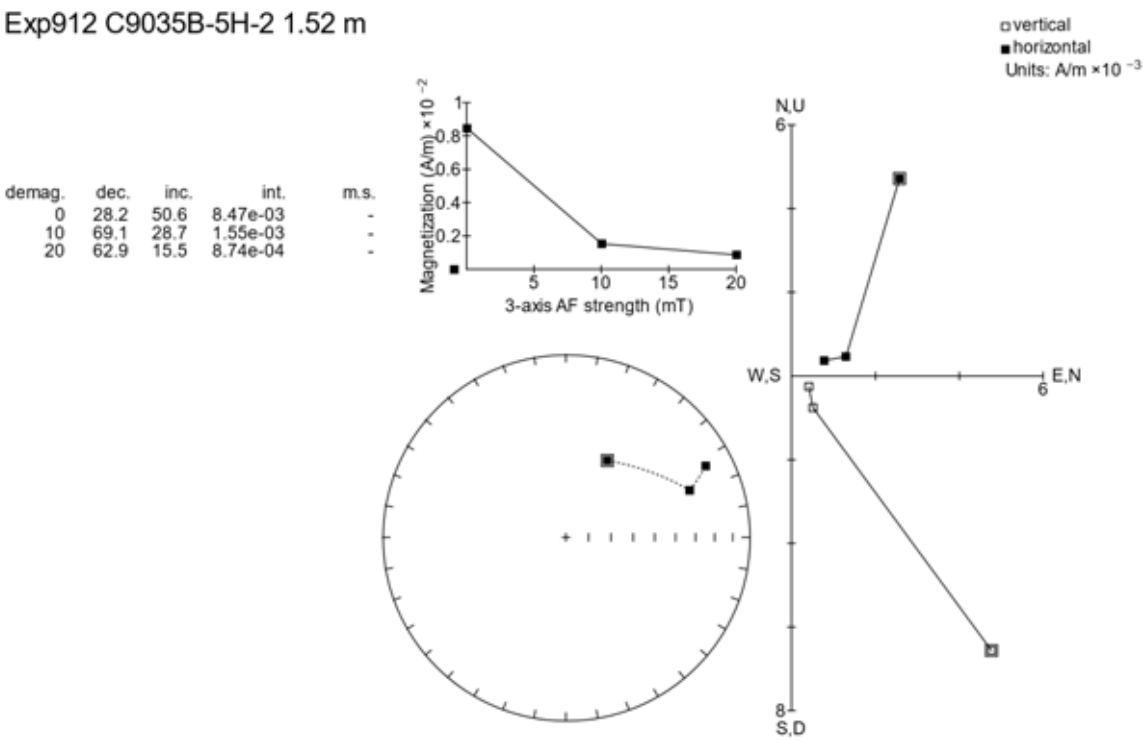

Figure 8.7 Vector endpoint and stereonet magnetization directions showing the results of AF demagnetization for Exp912 C9035B-5H-2 1.52m. Black and white squares = projection of magnetization vector endpoint on the horizontal and vertical planes, respectively. NRM = natural remanent magnetization. Figure is produced using software "PuffinPlot" by Lurcock and Wilson (2012).

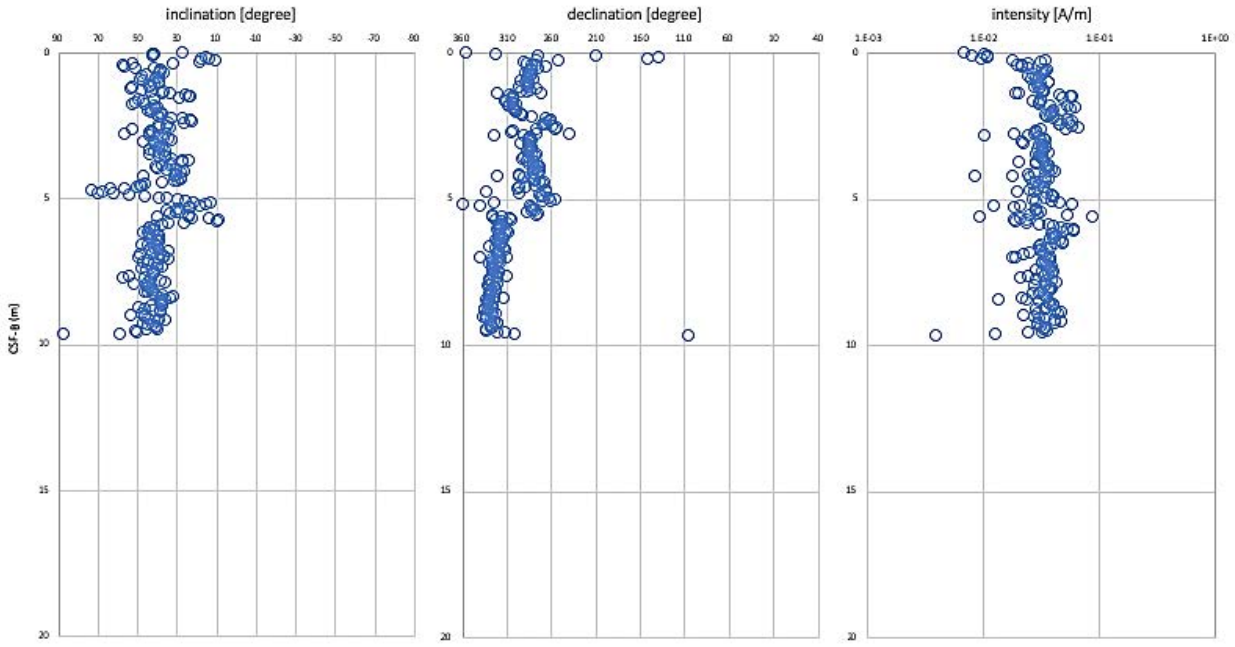

Figure 8.8 Inclination and declination after 20 mT alternating-field (AF) demagnetization of Hole **C9035A**. CSF = core depth below seafloor.

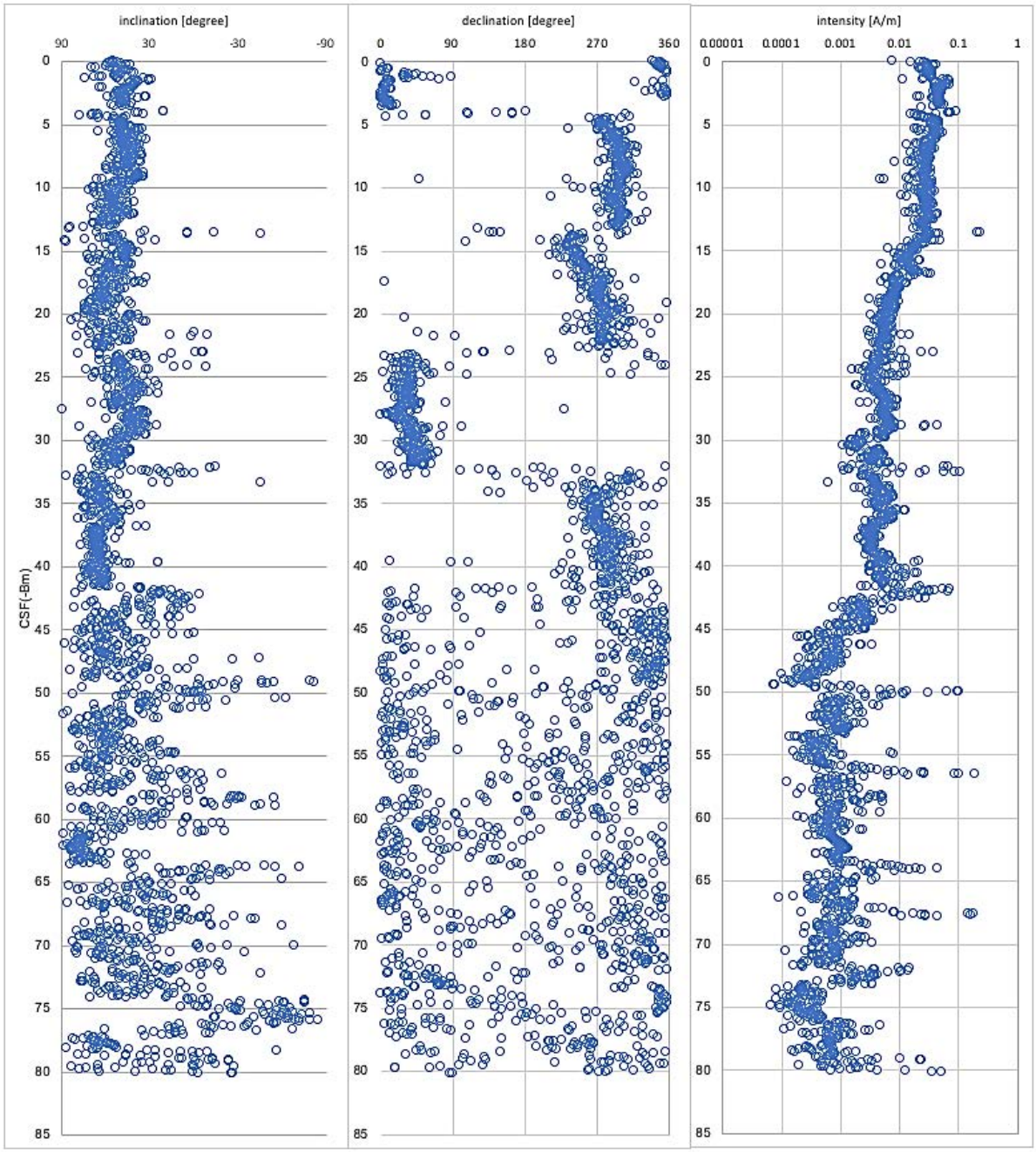

Figure 8.9 Inclination and declination after 20 mT alternating field (AF) demagnetization of Hole **C9035B**. CSF = core depth below seafloor.

9. Post-cruise research plan

Ken Ikehara: According to the submitted sample requests, I plan to conduct two major studies using the obtained cores. First, to recognize range of each turbidite bed and confirm turbidite stratigraphy, high-resolution XRF core scanning will be conducted at the Geological Survey of Japan, AIST, by using U- (or LL-) channel samples collected for on shore paleomagnetic measurements. Distinction between turbidite mud and hemipelagic mud is essential not only for turbidite stratigraphy but also for paleoceanographic study using core C9035B. Combined with VCD and the other physical and magnetic properties, turbidite stratigraphy will be confirmed. Coupled with age model for the obtained core, temporal recurrence pattern of turbidite will be obtained. Another study is to confirm the depositional processes of muddy turbidites in Unit I. There are several mechanisms to initiate the earthquake-induced turbidity currents. To evaluate the contribution of surface sediment remobilization for formation of earthquake-induced turbidites, paired radiocarbon age determinations both of turbidite mud and underlying hemipelagic mud will be conducted for some selected turbidite beds. At least 10 pairs of turbidite beds for upper part (possible Holocene sequence) of Unit I and the other 10 pairs for middle to lower part (last glacial maximum and before) will be selected based on VCD and the other measurement results.

Toshiya Kanamatsu: We propose ^{14}C age dating, which is one of primary items in this project for the chronology of turbidite. We will carefully select the sampling place based on shipboard data. About paleo and rock magnetic studies, we propose to recover paleomagnetic secular variation records from the obtained sedimentary sequences. We believe that this can be one of key measurements for precise age modeling of obtained cores. Because we consider that it functions under the high sedimentation rate condition larger than several ten cm/kyr. Shipboard preliminary results show that background sedimentation in C9035 is ideal condition for this study. Other our interest is to distinct paleo and rock magnetic property of each event deposit. For example, Upward grain fining of magnetic mineral granulometry in the interval of turbidites will be studied to understand turbidite depositional properties. Remanent directions of turbidite is an interesting topic to understand the depositional remanent magnetization, which could be information of hydrodynamic status during deposition.

Kan-Hsi Hsiung: The main scope of my post cruise research is to evaluate the flow direction of the significant turbidite beds of C9035A and C9035B. The first step is to distinguish the turbidites and hemipelagites, based on lithology, CT images, particle size, and chemical ratios of ITRAX (by co-requester Ikehara). The continuous ITRAX results may help to determine the sediment types precisely. Second, we will choose appropriate turbidite mud and underlying hemipelagic mud (about 10 events) including the related bottom/upper boundaries to take plastic cubes along the middle of each section after the visual core description. The anisotropy of magnetic susceptibility (AMS) and related magnetic measurements will be conducted.

Io Miura: We will measure radiocarbon dating of total organic carbon for turbidite dating. Our research plan consists of three steps: detailed observation of the core, measurement of carbon content, and radiocarbon dating. First, the turbidite layer is certified by conducting detailed observations of the core. In this case, the data measured onboard is also used. By making this observation, we can sample the semi-pelagic mud just below the turbidite layer. Next, measure carbon content using EA. It is expected that this will not only determine the amount of sample required for radiocarbon measurement but also clarify the origin of organic matter. Finally, the radiocarbon dating of the TOC is measured using an accelerator mass spectrometer at the Atmosphere and Ocean Research Institute, the University of Tokyo. These steps are expected to clarify the history of the Nankai Trough giant earthquake.

10. References

Ando, M. (1975). Source mechanisms and tectonic significance of historical earthquakes along the Nankai Trough, Japan. Tectonophysics, 27(2), 119-140.

Arai, K., Okamura, Y., Ikehara, K., Ashi, J., Soh, W., & Kinoshita, M. (2006). Active faults and tectonics on the upper forearc slope off Hamamatsu City, central Japan. JOURNAL-GEOLOGICAL SOCIETY OF JAPAN, 112(12), 749.

Arai, K., (2008). Geological map of Enshu Nada. Marine Geological Map Series, no. 65 (CD), Geological Survey of Japan, AIST.

Ashi, J. (1997). Distribution of cold seepage at the fault scarp of the eastern Nankai accretionary prism. JAMSTEC Jour. Deep Sea Res., 13, 495-501.

Channell, J. E. T., & Kleiven, H. F. (2000). Geomagnetic palaeointensities and astrochronological ages for the Matuyama–Brunhes boundary and the boundaries of the Jaramillo Subchron: palaeomagnetic and oxygen isotope records from ODP Site 983. Philosophical Transactions of the Royal Society of London. Series A: Mathematical, Physical and Engineering Sciences, 358(1768), 1027-1047.

Earthquake Research Committee, (2013). Long-term evaluation of seismicity along Nankai Trough (2nd version) (in Japanese). Headquarters for Earthquake Research Promotion.

Goldfinger, C., Ikeda, Y., Yeats, R. S., & Ren, J. (2013). Superquakes and supercycles. Seismological Research Letters, 84(1), 24-32.

Ikehara, K. (2001). Recurrence interval of large earthquakes along the eastern Nankai Trough inferred from deep-sea turbidites. Journal of Geography (Chigaku Zasshi), 110(4), 471-478.

Ikehara, K., Kanamatsu, T., Nagahashi, Y., Strasser, M., Fink, H., Usami, K., ... & Wefer, G. (2016). Documenting large earthquakes similar to the 2011 Tohoku-oki earthquake from sediments deposited in the Japan Trench over the past 1500 years. Earth and Planetary Science Letters, 445, 48-56.

Ishizuka, O., Uto, K., & Yuasa, M. (2003). Volcanic history of the back-arc region of the Izu-Bonin (Ogasawara) arc. In: Larter, R.D., Leat, P.T. (Eds.), Intra-oceanic Subduction Systems: Tectonic and Magmatic Processes, vol. 2. Geological Society, London, Special Publications, 219(1), 187-205.

Kodaira, S., Kurashimo, E., Park, J. O., Takahashi, N., Nakanishi, A., Miura, S., ... & Kaneda, Y. (2002). Structural factors controlling the rupture process of a megathrust earthquake at the Nankai trough seismogenic zone. Geophysical Journal International, 149(3), 815-835.

Kodaira, S., Nakanishi, A., Park, J. O., Ito, A., Tsuru, T., & Kaneda, Y. (2003). Cyclic ridge subduction at an inter-plate locked zone off central Japan. Geophysical research letters, 30(6).

Lurcock, P. C., & Wilson, G. S. (2012). PuffinPlot: A versatile, user-friendly program for paleomagnetic analysis. Geochemistry, Geophysics, Geosystems, 13(6).

Mazzotti, S., Lallemant, S. J., Henry, P., Le Pichon, X., Tokuyama, H., & Takahashi, N. (2002). Intraplate shortening and underthrusting of a large basement ridge in the eastern Nankai subduction zone. Marine geology, 187(1-2), 63-88.

Nakanishi, A., Kodaira, S., Park, J. O., & Kaneda, Y. (2002). Deformable backstop as seaward end of coseismic slip in the Nankai Trough seismogenic zone. Earth and Planetary Science Letters, 203(1), 255-263.

Park, J. O., Moore, G. F., Tsuru, T., Kodaira, S., & Kaneda, Y. (2004). A subducted oceanic ridge influencing the Nankai megathrust earthquake rupture. Earth and Planetary Science Letters, 217(1-2), 77-84.

Rothwell, R. G. (1989). Minerals and mineraloids in marine sediments; an optical identification guide: Elsevier Appl. Sci, London, United Kingdom.

Satake, K. (2015). Geological and historical evidence of irregular recurrent earthquakes in Japan. Philosophical Transactions of the Royal Society A: Mathematical, Physical and Engineering Sciences, 373(2053), 20140375.

The Research group for active submarine faults off Tokai, (1999). Active Submarine Faults Off Tokai, 151p.

Yokota, Y., Ishikawa, T., Sato, M., Watanabe, S. I., Saito, H., Ujihara, N., ... & Mochizuki, M. (2015). Heterogeneous interplate coupling along the Nankai Trough, Japan, detected by GPS-acoustic seafloor geodetic observation. Progress in Earth and Planetary Science, 2(1), 10.

Wang, K., & Bilek, S. L. (2014). Invited review paper: Fault creep caused by subduction of rough seafloor relief. Tectonophysics, 610, 1-24.

Wessel, P., & Smith, W. H. (1991). Free software helps map and display data. Eos, Transactions American Geophysical Union, 72(41), 441-446.

APPENDIX 1

Split core images and X-CT image

C9035A_1H_1 C9035A_1H_2 C9035A_1H_3 C9035A_1H_4 C9035A_1H_5 C9035A_1H_6

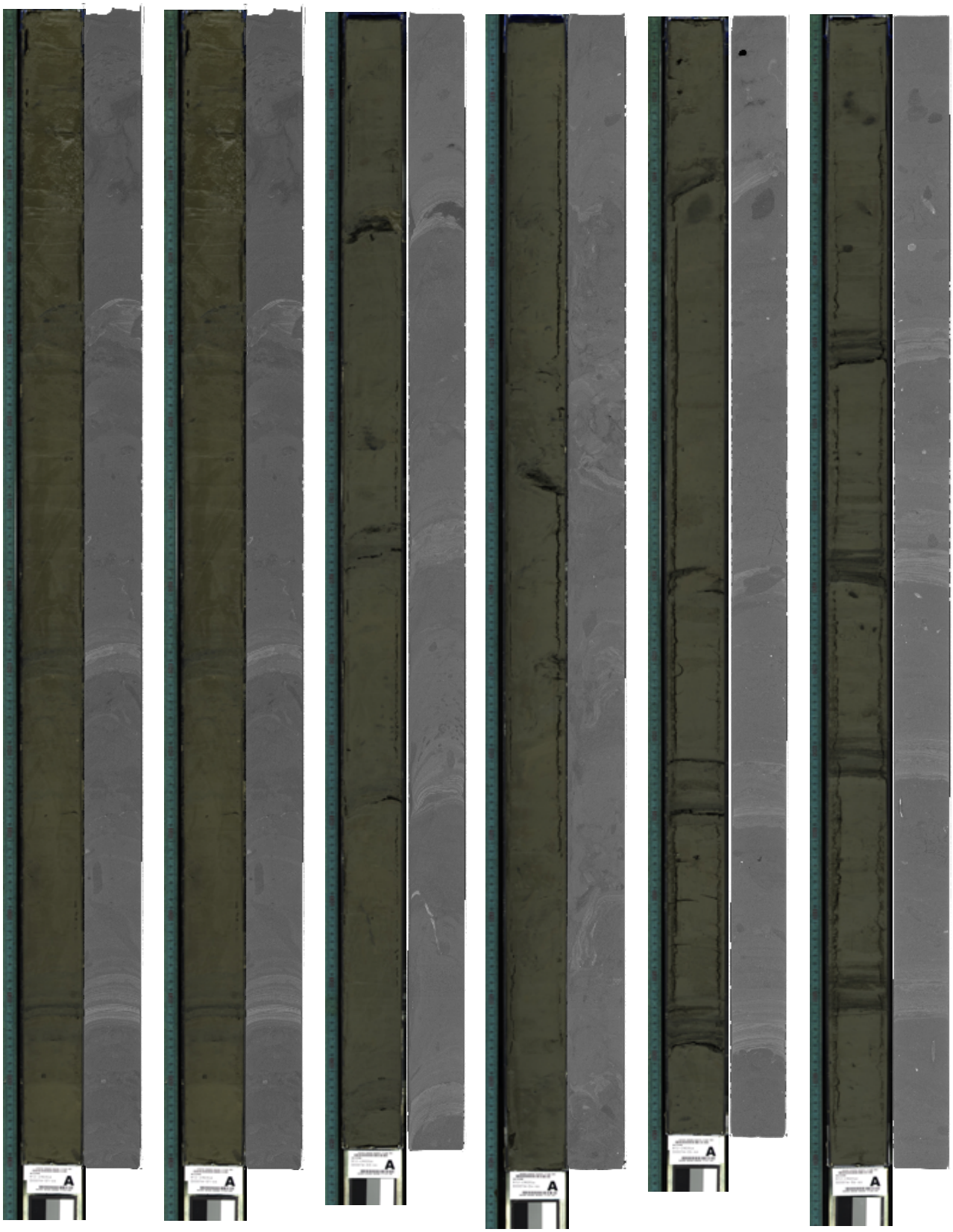

C9035A_1H_7

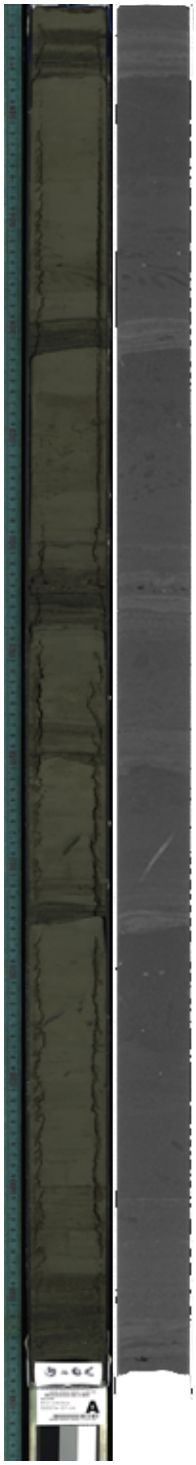

C9035A_1H_CC

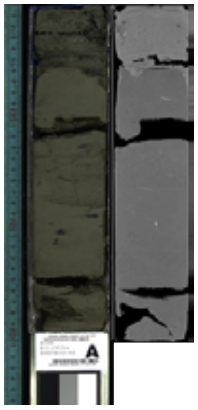

C9035B_1H_1

C9035B_1H_2

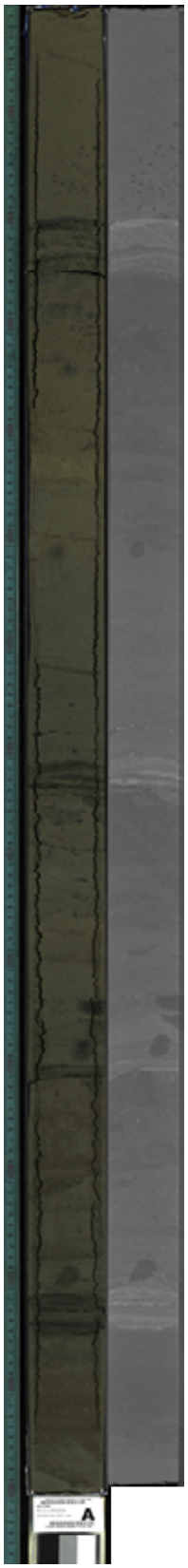

C9035B_1H_3

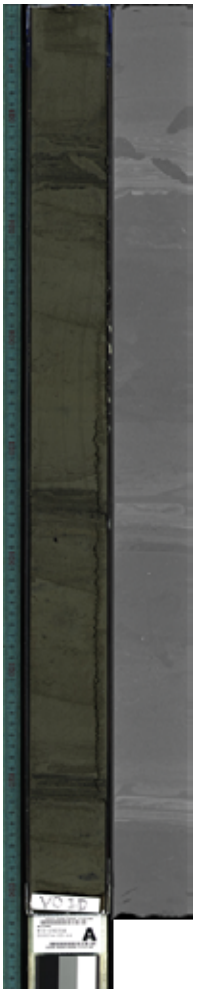

C9035B_1H_CC

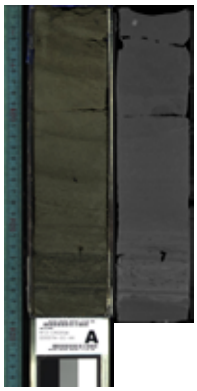

C9035B_2H_1

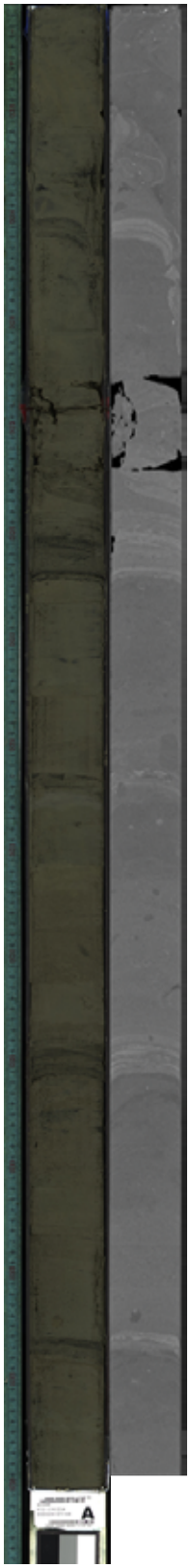

C9035B_2H_2

C9035B_2H_3

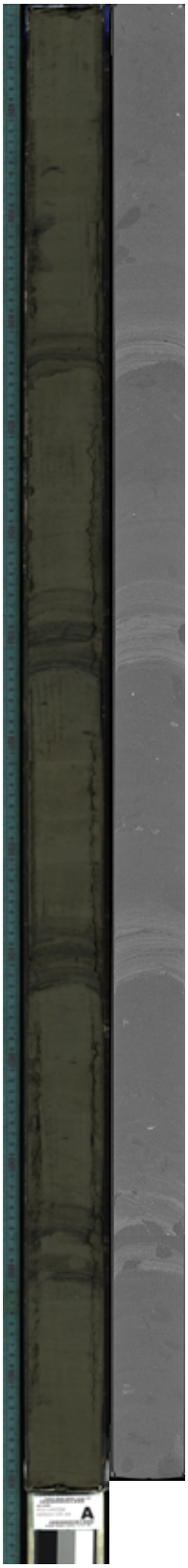

C9035B_2H_4

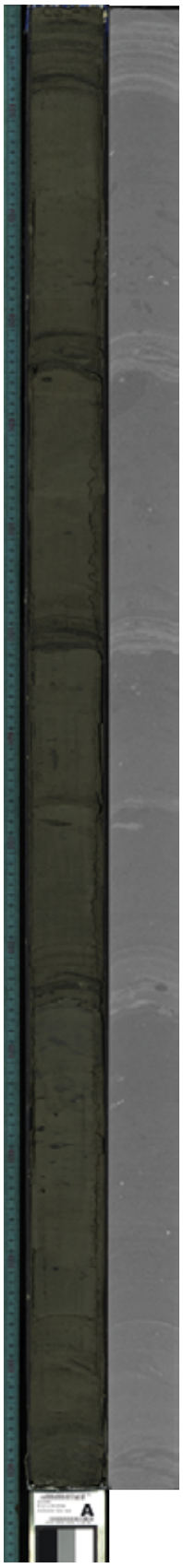

C9035B_2H_5

C9035B_2H_6

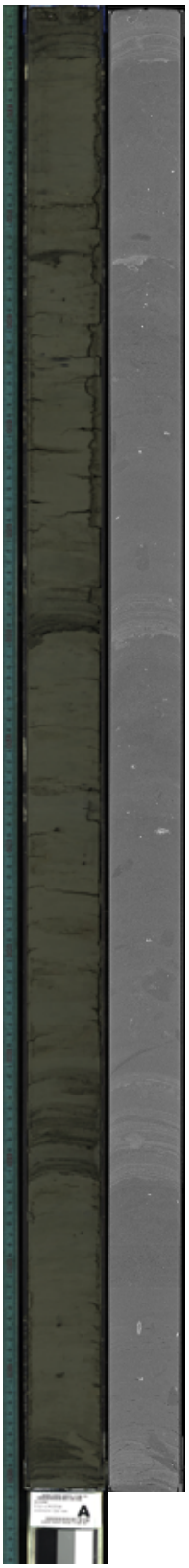

C9035B_2H_7

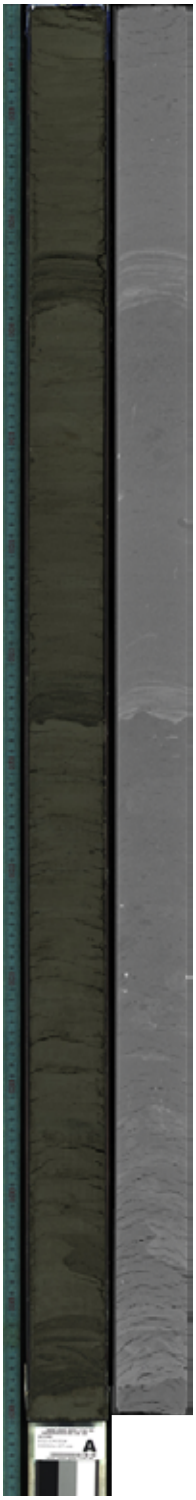

C9035B_2H_CC

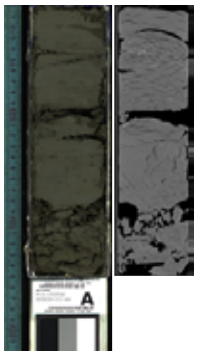

C9035B_3H_1 C9035B_3H_2 C9035B_3H_3 C9035B_3H_4 C9035B_3H_5 C9035B_3H_6

C9035B_3H_7

C9035B_3H_CC

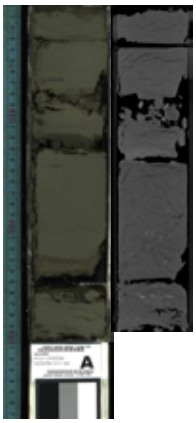

C9035B_4H_1

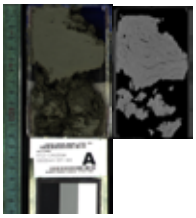

C9035B_4H_2

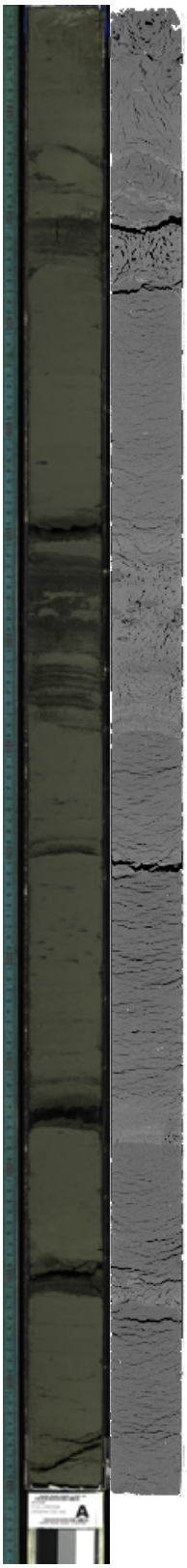

C9035B_4H_3

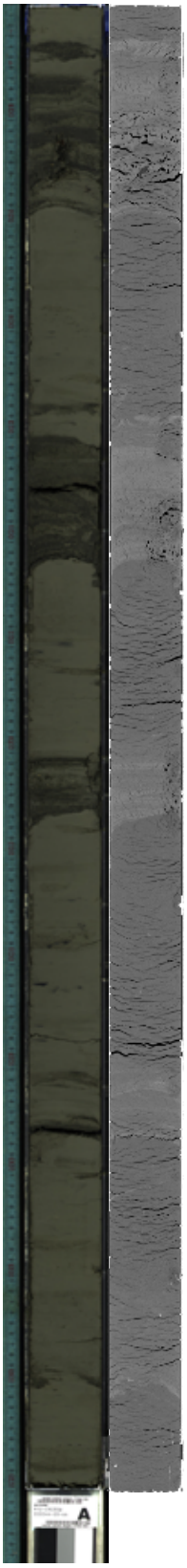

C9035B_4H_4

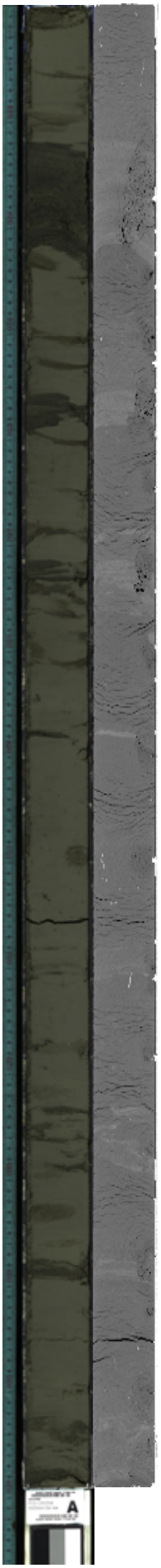

C9035B_4H_5

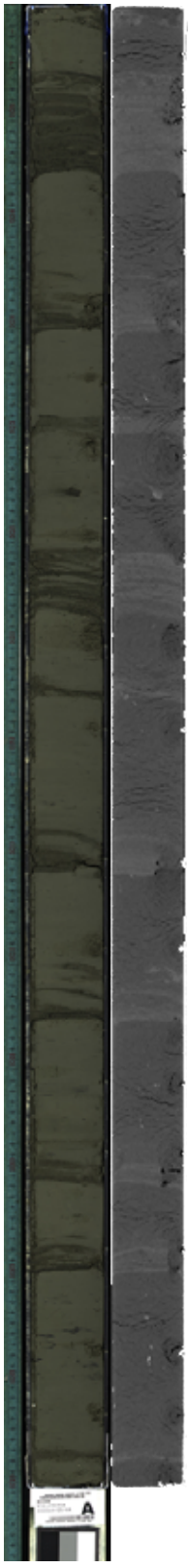

C9035B_4H_6

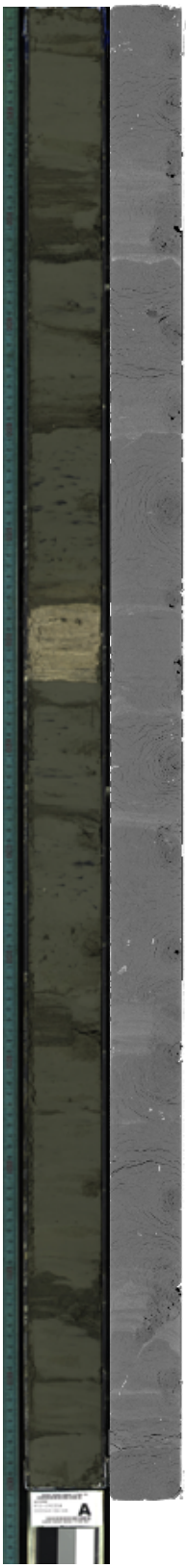

C9035B_4H_7

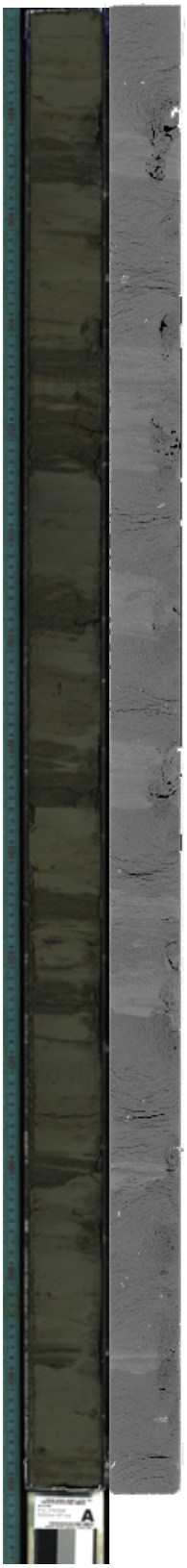

C9035B_4H_8

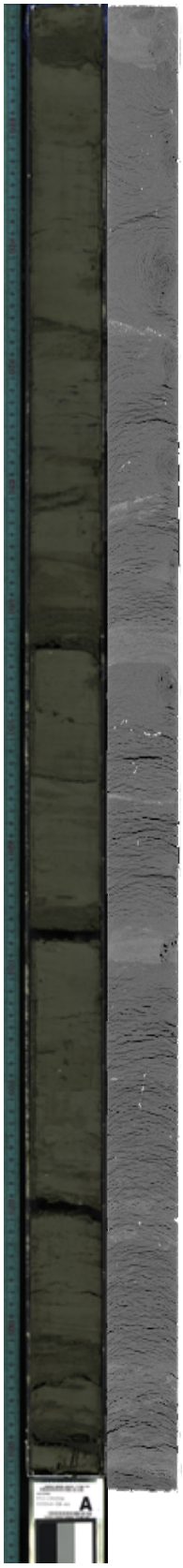

C9035B_4H_CC

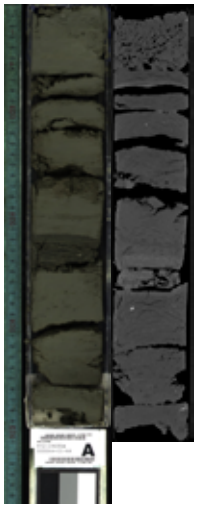

C9035B_5H_1

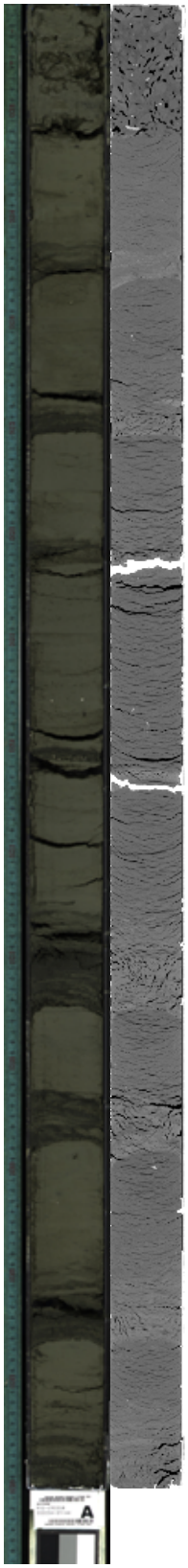

C9035B_5H_2 C9035B_5H_3 C9035B_5H_4 C9035B_5H_5 C9035B_5H_6 C9035B_5H_7

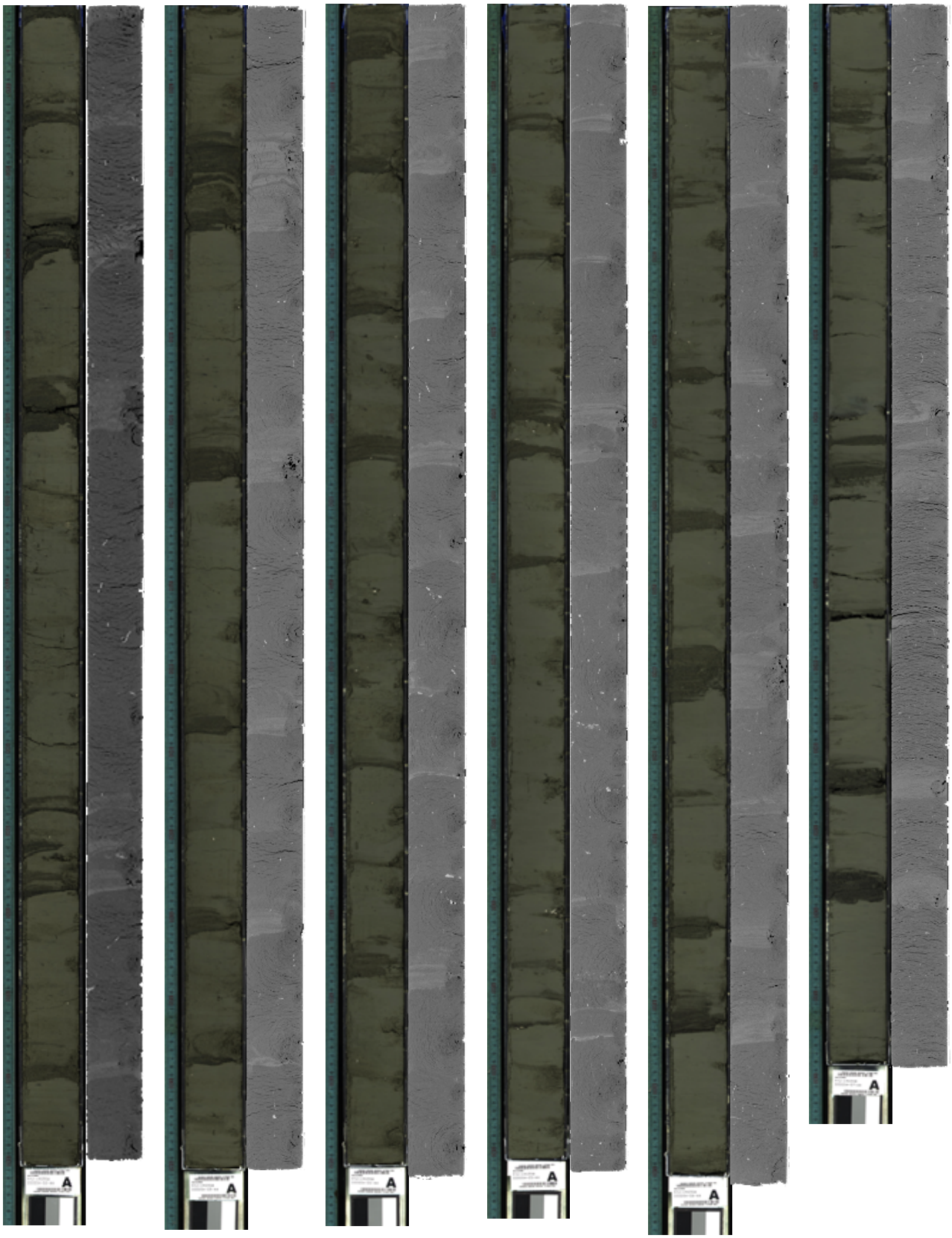

C9035B_5H_CC

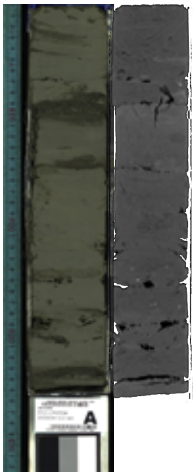

C9035B_6H_1

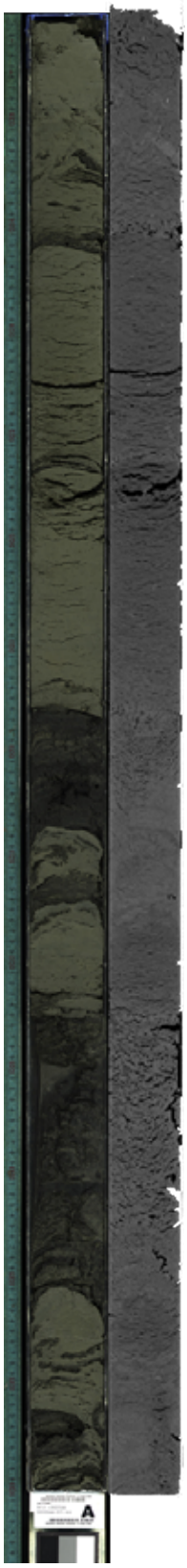

C9035B_6H_2

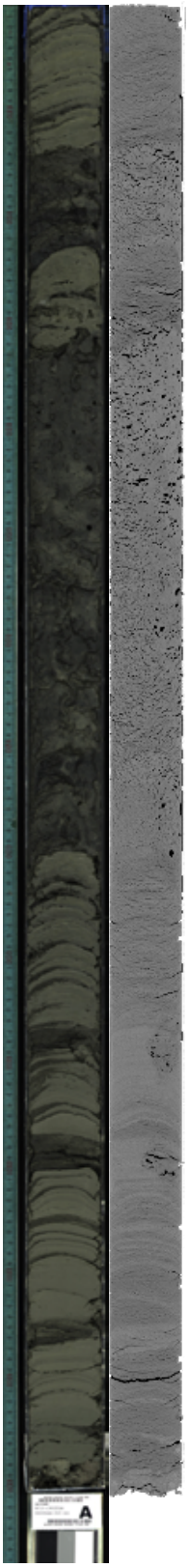

C9035B_6H_3

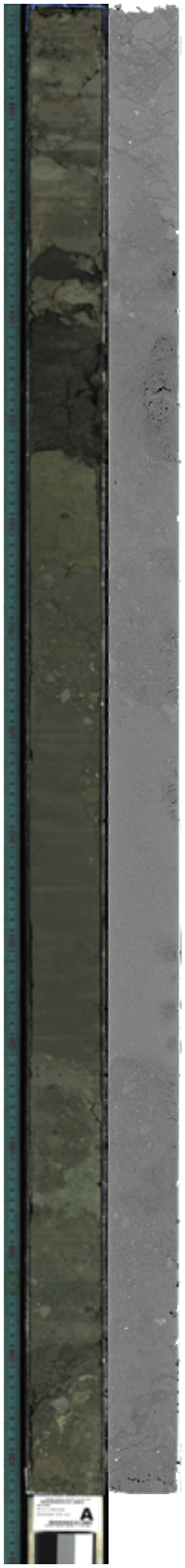

C9035B_6H_4

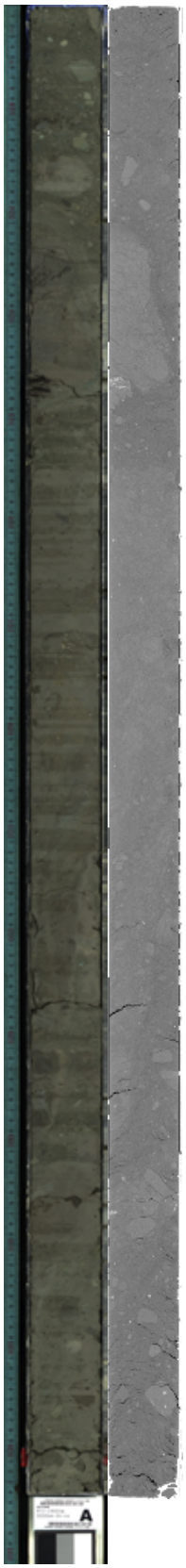

C9035B_6H_5

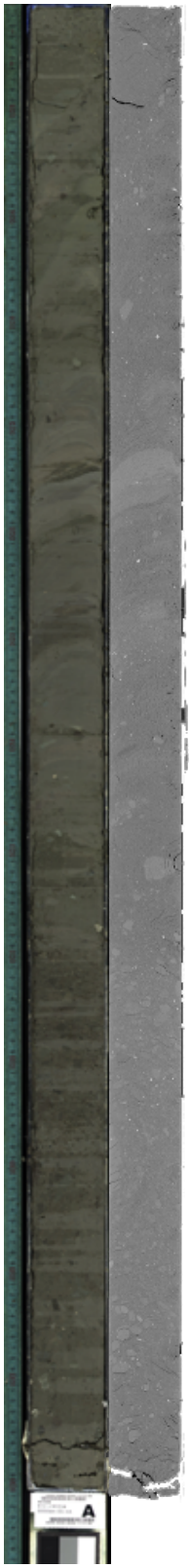

C9035B_6H_6 C9035B_6H_CC C9035B_7H_1 C9035B_7H_2 C9035B_7H_3 C9035B_7H_4

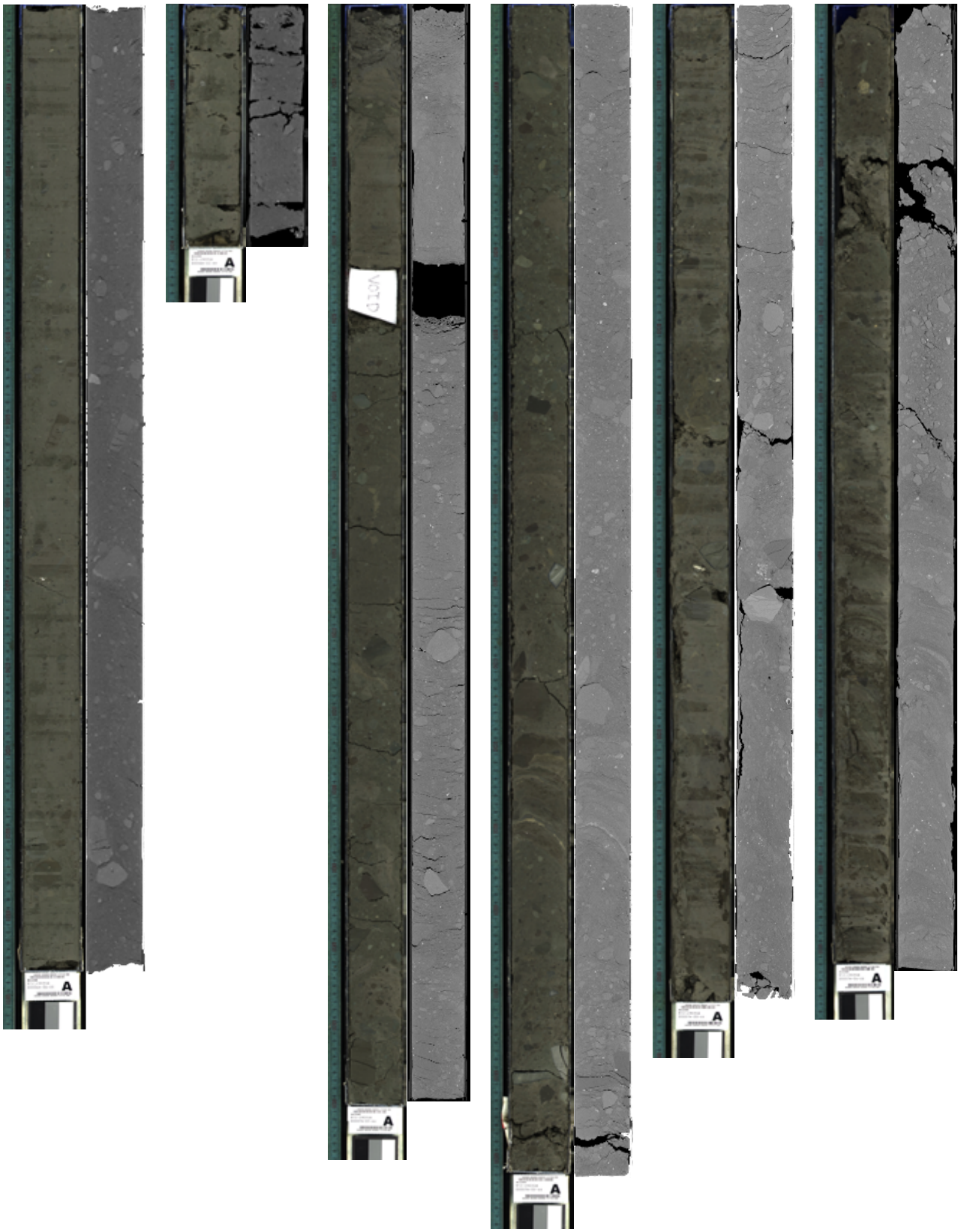

C9035B_7H_5 C9035B_7H_CC C9035B_8H_1 C9035B_8H_2 C9035B_8H_3 C9035B_8H_4

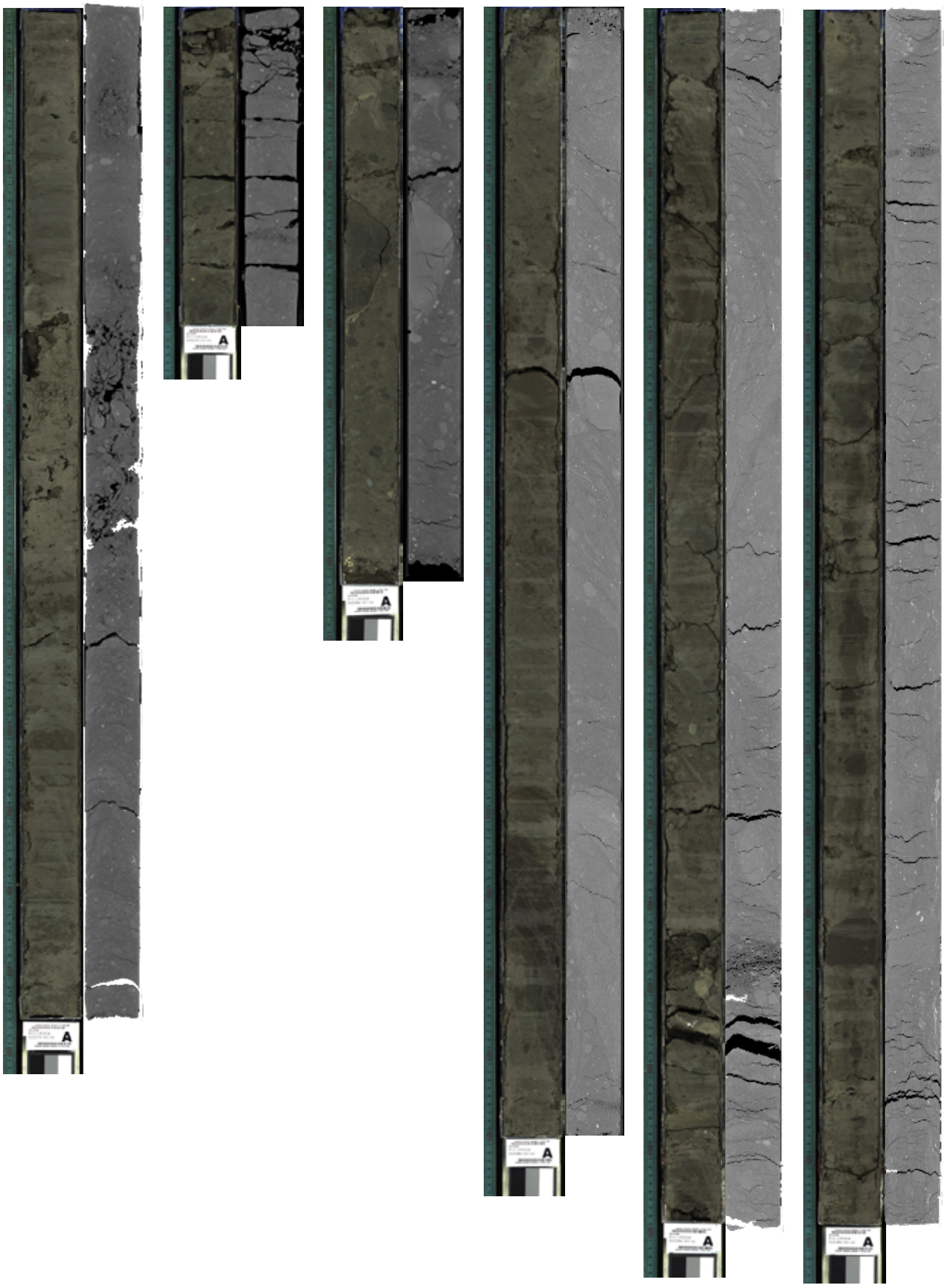

C9035B_8H_5 C9035B_8H_6 C9035B_8H_CC C9035B_9H_1 C9035B_9H_2 C9035B_9H_3

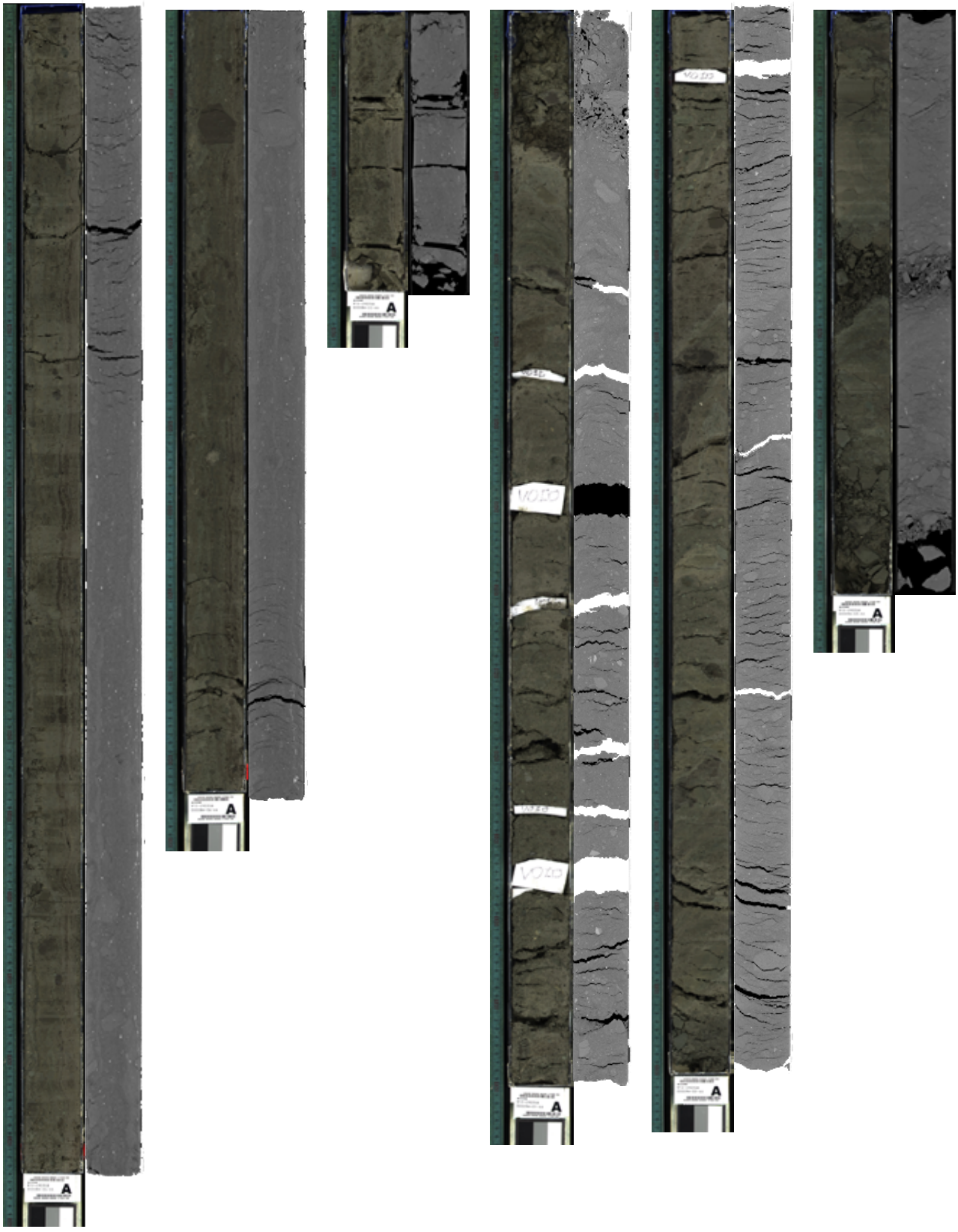

C9035B_9H_CC

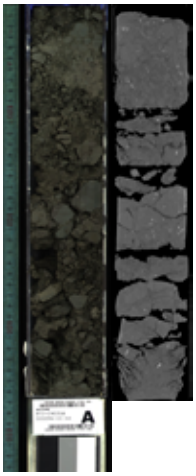

C9035B_10F_1

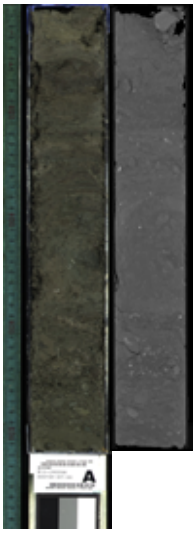

C9035B_10F_2

C9035B_10F_3

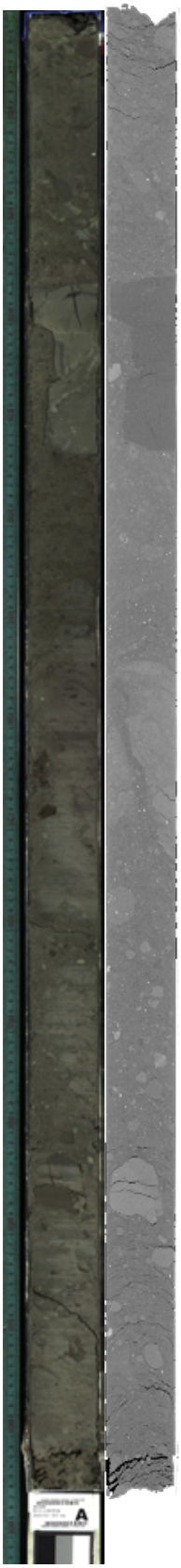

C9035B_10F_4

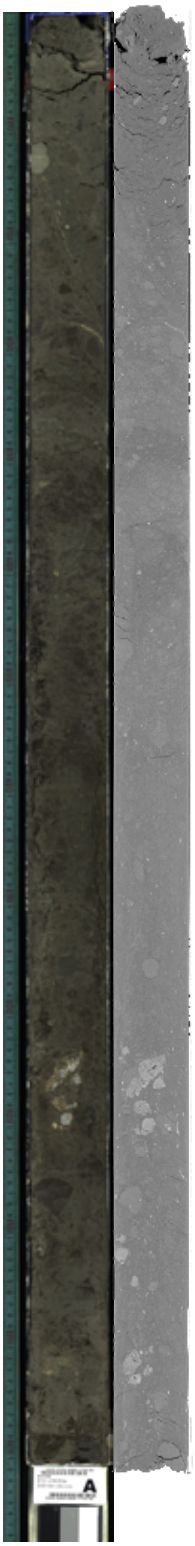

C9035B_10F_CC

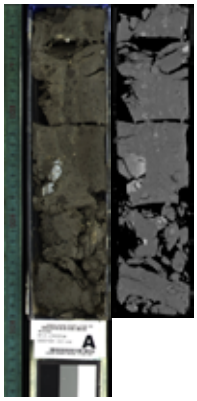

C9035B_11F_1

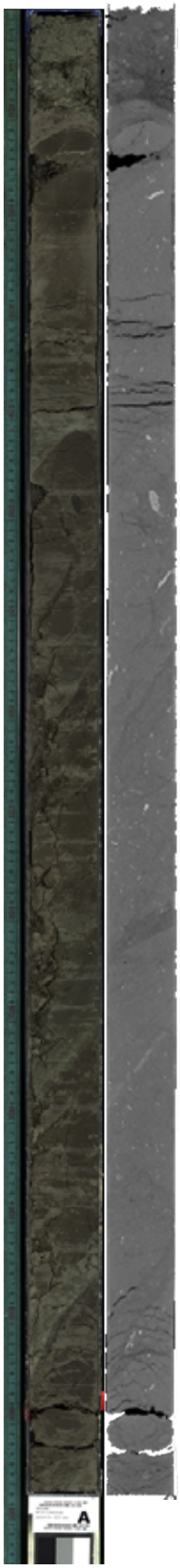

C9035B_11F_2

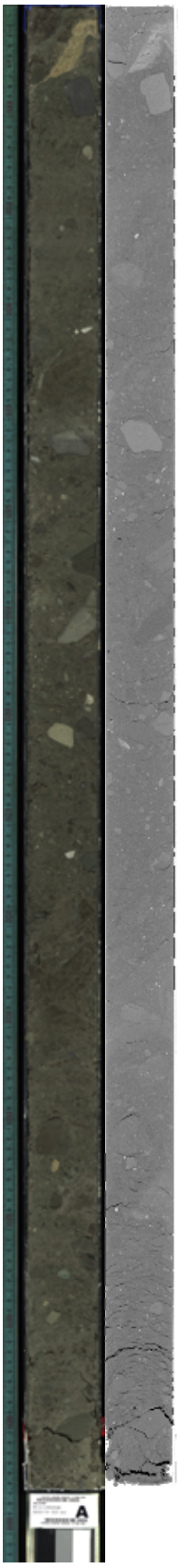

C9035B_11F_3

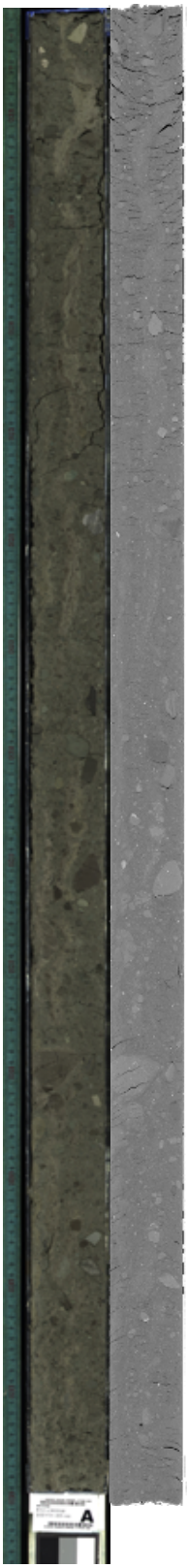

C9035B_11F_4

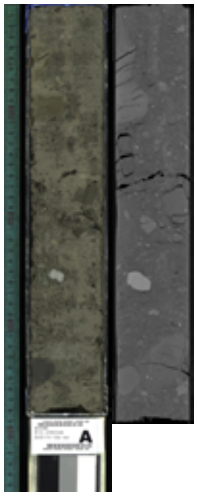

C9035B_11F_CC

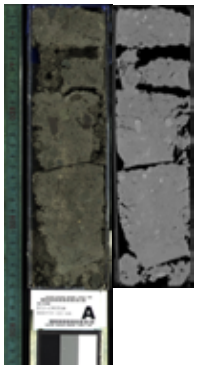

C9035B_12H_1

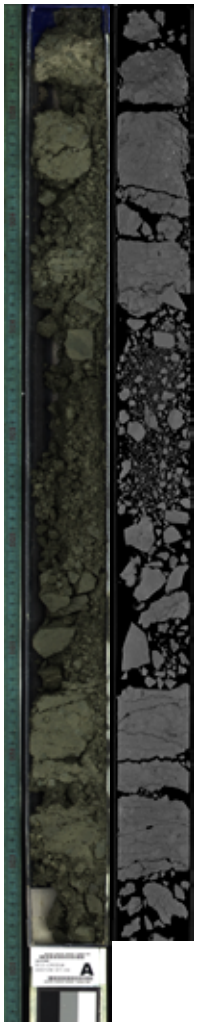

C9035B_12H_2 C9035B_12H_3 C9035B_12H_CC

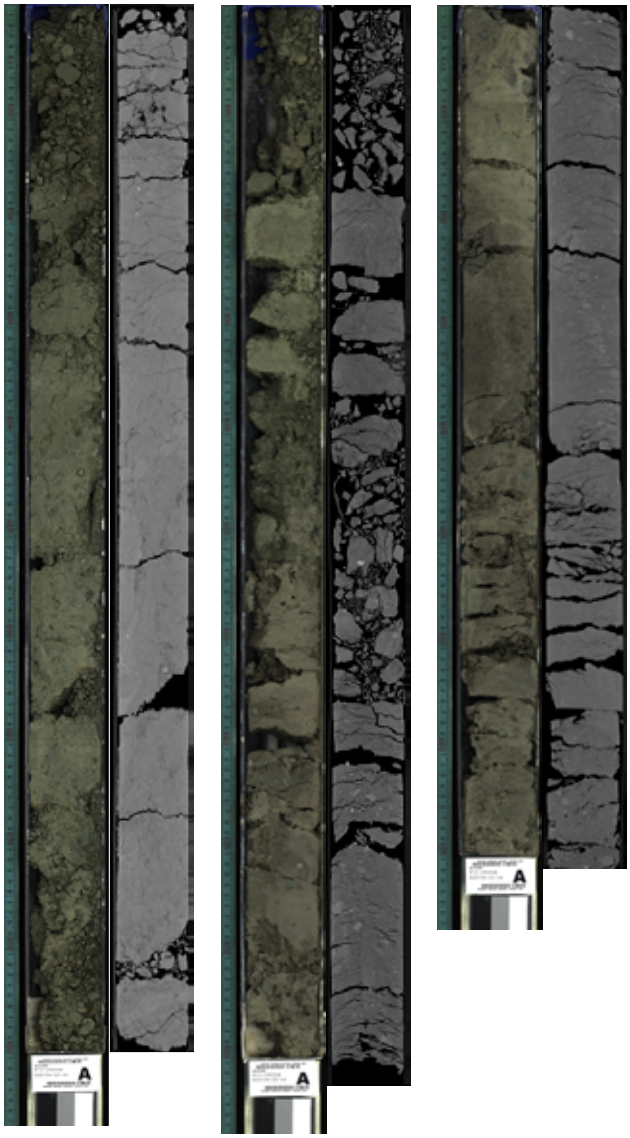

APPENDIX 2

Visual Core Description

International Ocean Discovery Program

Visual Core Description

NO.
DATE: 1/6/20
EXP.: 912
SITE/HOLE: C9035/A
CORE: 1H
SECTION: 1A
TOP DEPTH (m CSF): 0 – 140.1
cm
OBSERBER: Ken

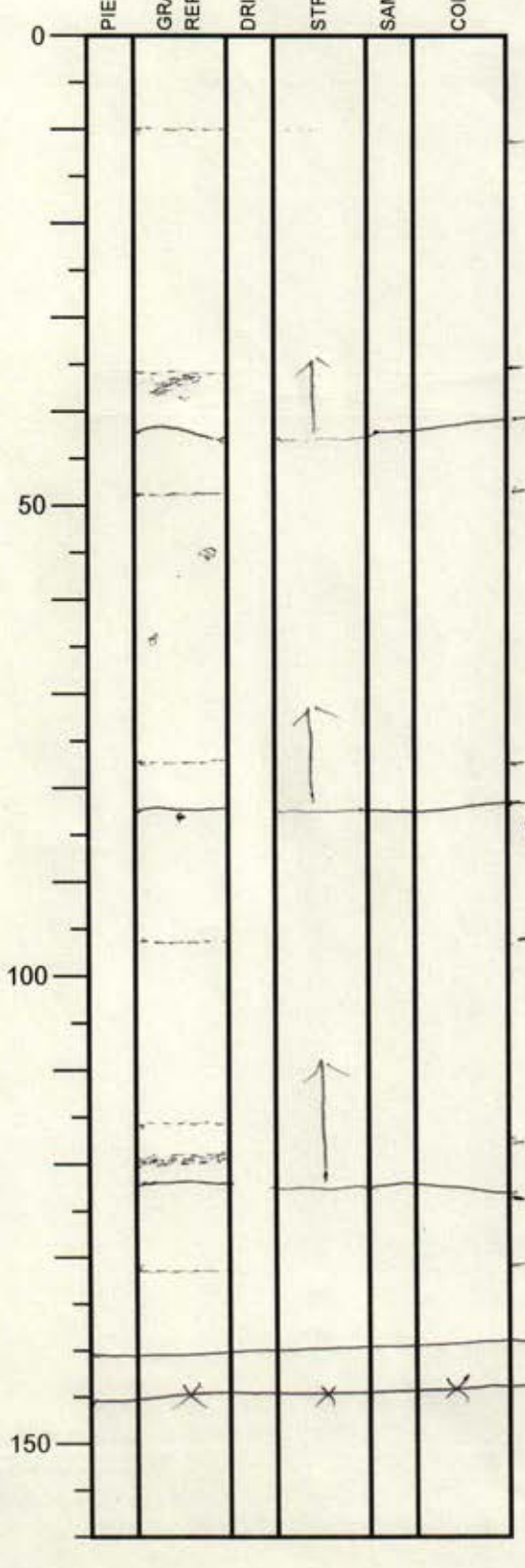

International Ocean Discovery Program

Visual Core Description

NO.
DATE: 1/6/20
EXP.: 912
SITE/HOLE: C9035 / A
CORE: 1H
SECTION: 2A
TOP DEPTH (m CSF): 140.1 — 280.9
OBSERBER:

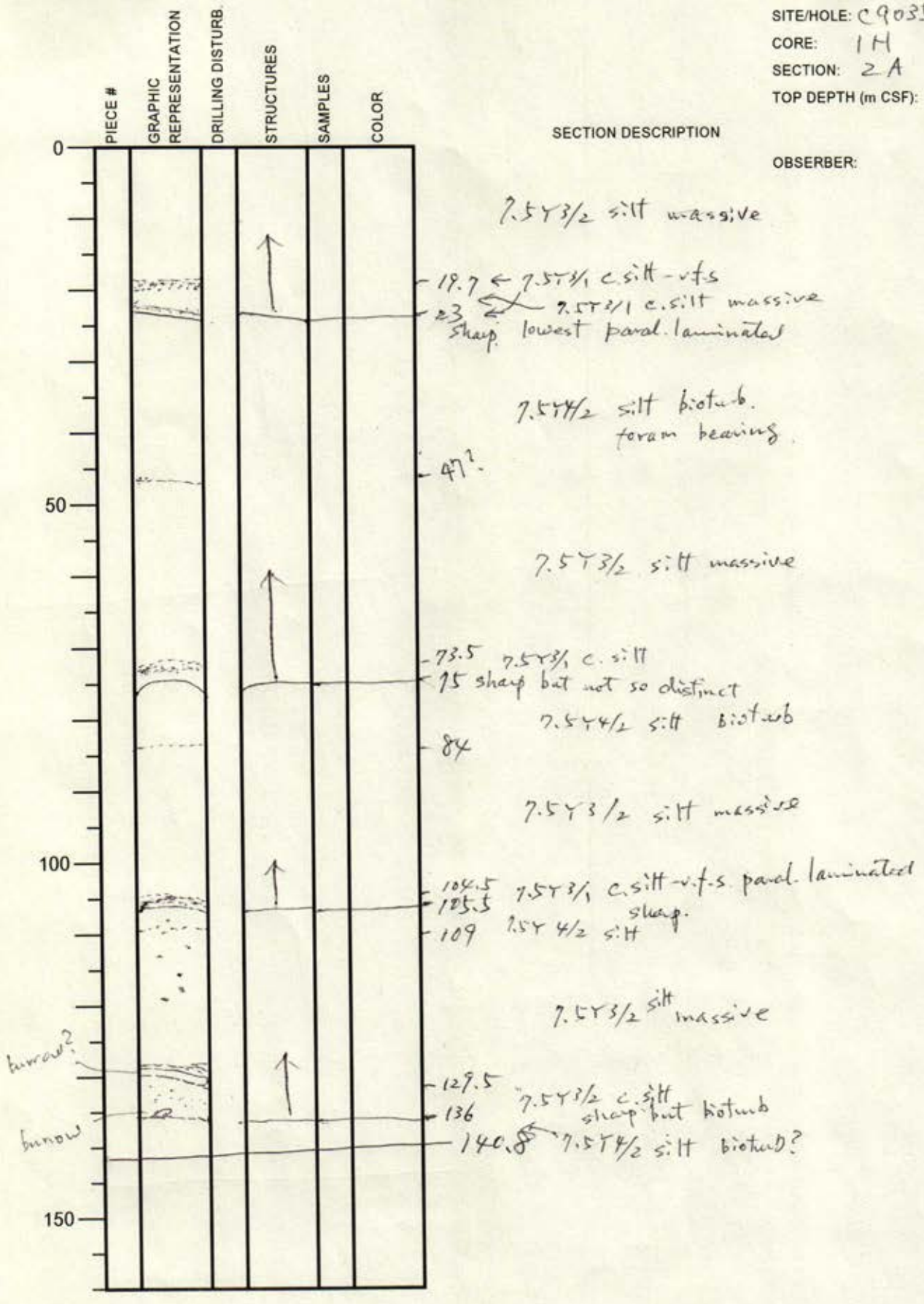

International Ocean Discovery Program

Visual Core Description

NO.
DATE: 1/6/20
EXP.: 912
SITE/HOLE: C9035/A
CORE: 1H
SECTION: 3A
TOP DEPTH (m CSF): 280.9 – 420.9
OBSERBER:

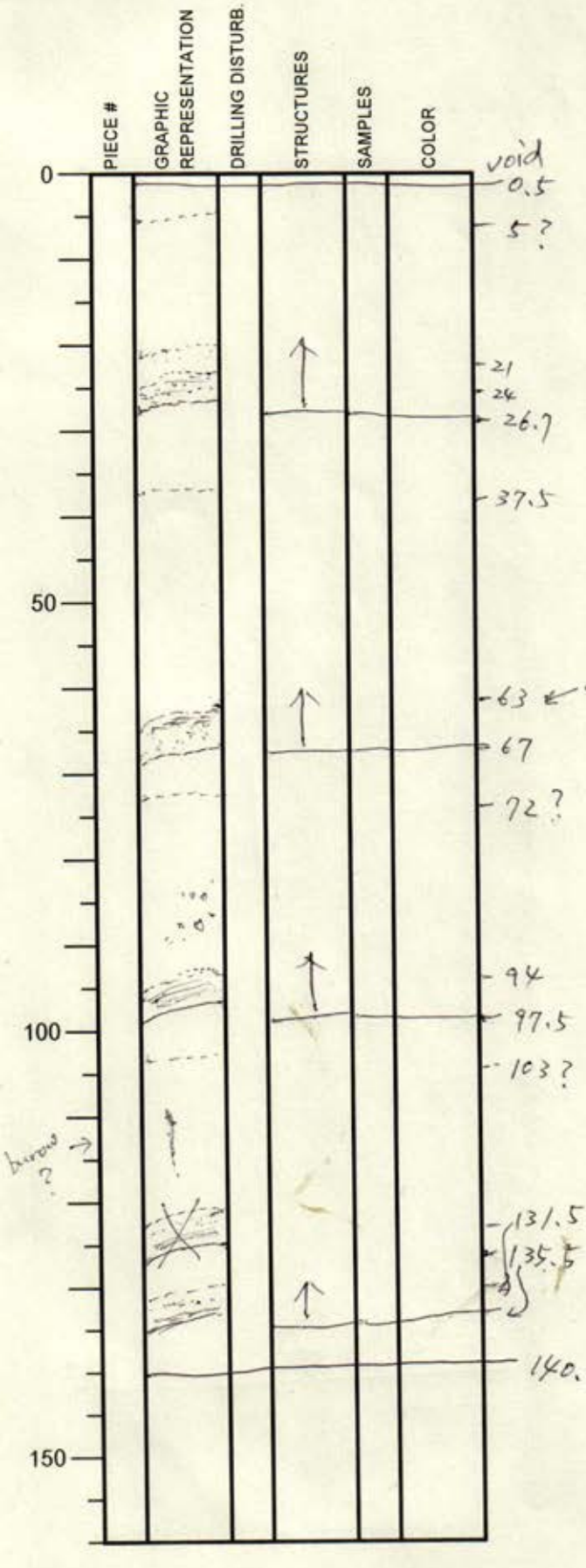

7.5YR4/2 silt massive

7.5YR3/2 c.silt massive

7.5YR3/1 v.f.s-c.silt paral laminated sharp.

7.5YR3/2 silt biotub? foram?

7.5YR3/2 silt massive

coarset at top of coarse layer.

7.5YR3/2 c.silt sharp a little forams.

7.5YR4/2 silt biotub. amount of

7.5YR3/2 silt massive

7.5YR3/1 c.silt paral. laminated sharp

7.5YR3/2 silt biotub?

7.5YR3/2 silt massive

7.5YR3/1 c.silt paral. laminated at lower part. sharp

7.5YR3/2 silt biotub.

International Ocean Discovery Program

Visual Core Description

NO.
DATE: 1/8/20
EXP.: 912
SITE/HOLE: C9035 / A
CORE: 1 H
SECTION: 4 A
TOP DEPTH (m CSF): 420.9 – 561.4
OBSERBER:

International Ocean Discovery Program

Visual Core Description

NO.
DATE: 1/8/20
EXP.: 912
SITE/HOLE: C9035 / A
CORE: 1H
SECTION: 5A
TOP DEPTH (m CSF): 561.4 - 700.9
OBSERBER:

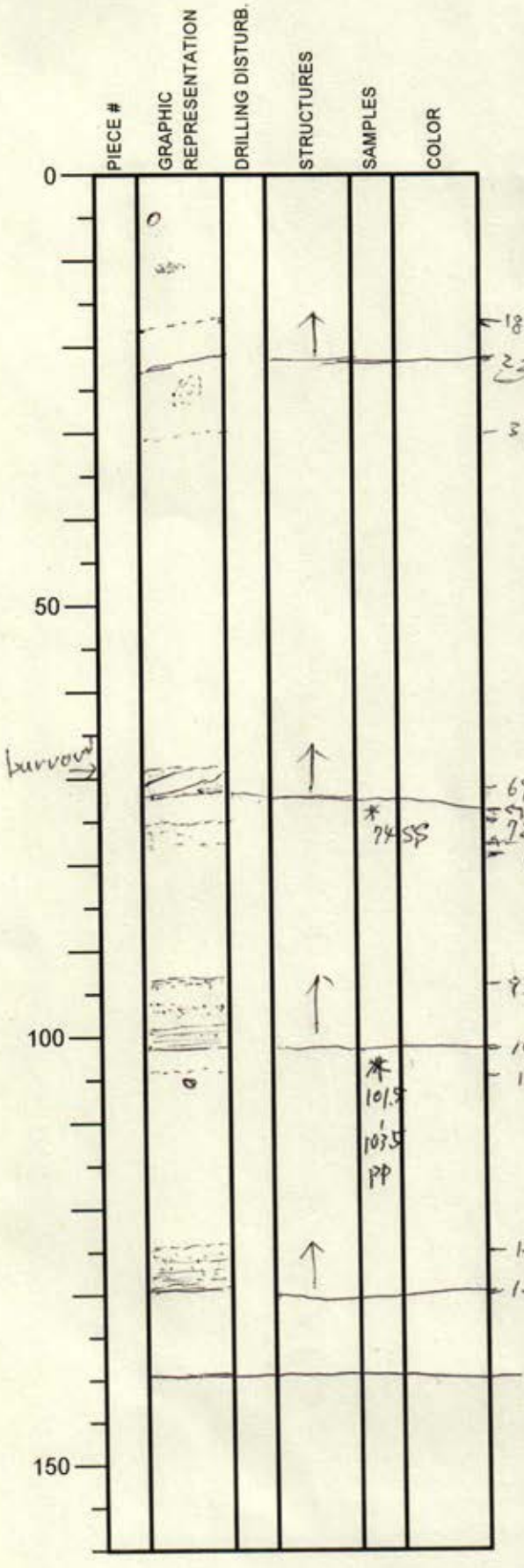

International Ocean Discovery Program

Visual Core Description

NO.
DATE: 1/7/20
EXP.: 912
SITE/HOLE: C9035 / A
CORE: 1 H
SECTION: 6 A
TOP DEPTH (m CSF): 700.9 – 841.3
OBSERBER:

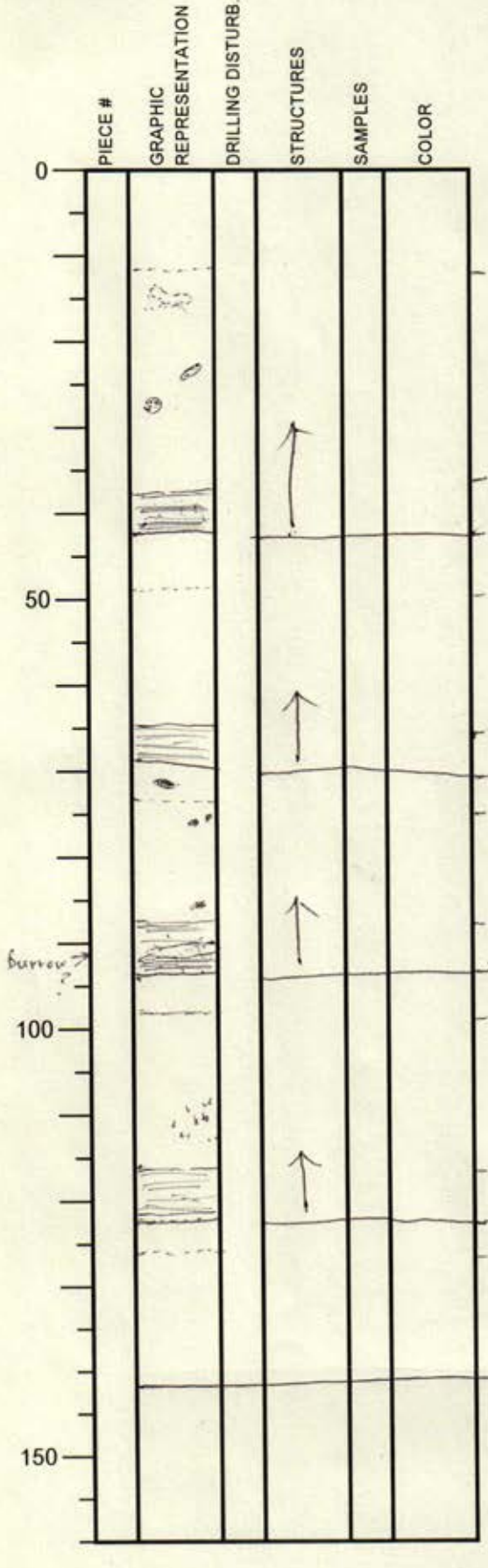

SECTION DESCRIPTION

7.5Y3/2 silt bioturb foram bearing

11?

7.5Y3/2 silt massive mica? bearing

38

7.5Y3/1 c.silt-vf.s paral.-cross-laminated

42.2 sharp

7.5Y3/2 silt bioturb

48?

7.5Y3/2 silt massive mica? bearing

65

7.5Y3/1 c.silt-vf.s paral. laminated

69.5

7.5Y3/2 silt bioturb

72?

7.5Y3/2 silt massive

89.5

7.5Y3/1 c.silt-vf.s paral. laminated

93 sharp

7.5Y3/2 silt bioturb

97.

7.5Y3/2 silt massive

116

7.5Y3/1 c.silt-vf.s paral-cross laminated

122 sharp

125?

7.5Y3/2 silt bioturb

7.5Y3/2 silt massive

140.4

International Ocean Discovery Program

Visual Core Description

NO.
DATE: 1/7/20
EXP.: 912
SITE/HOLE: C9035 / A
CORE: 1 H
SECTION: 7 A
TOP DEPTH (m CSF): 841.3 – 969.8.
OBSERBER:

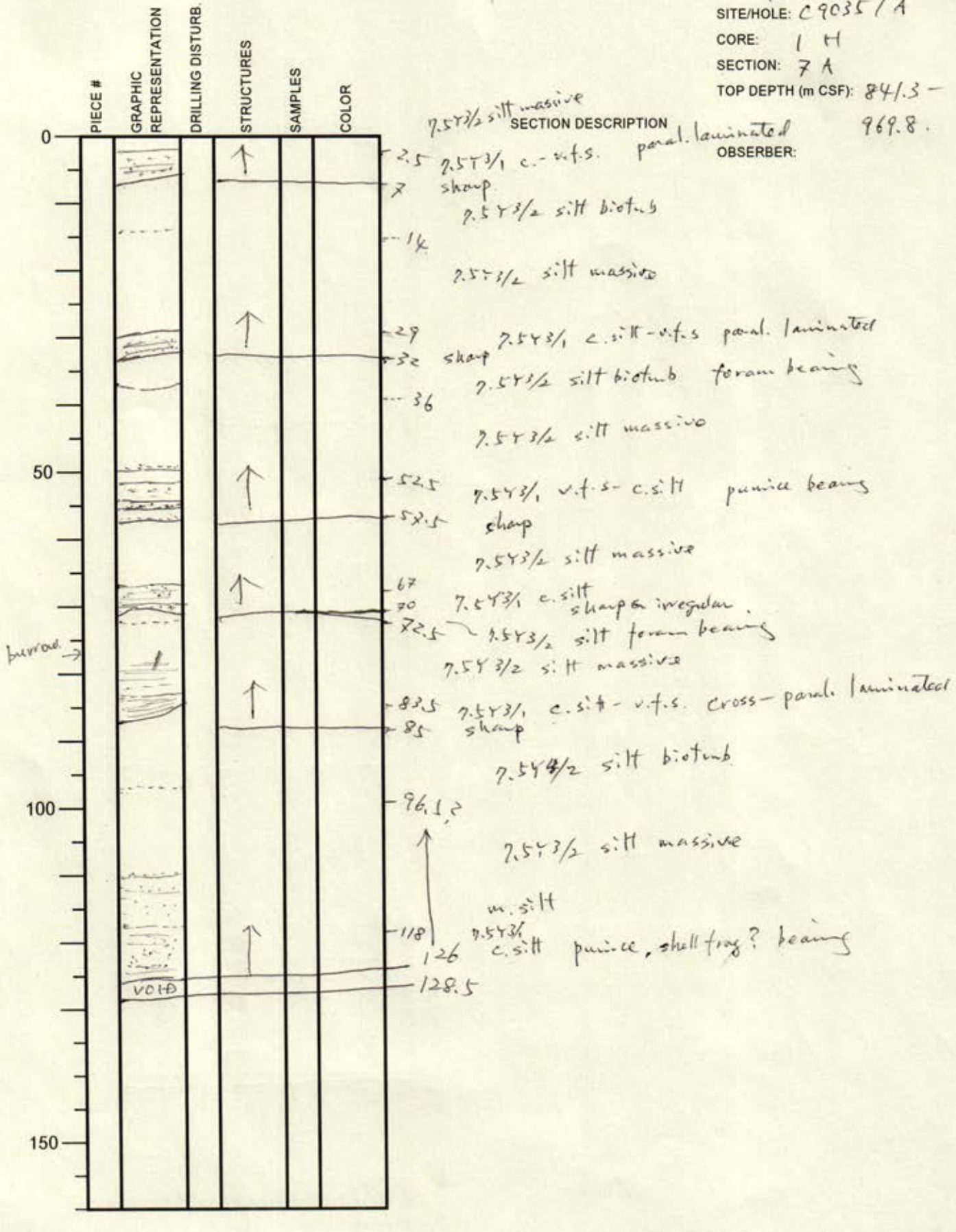

International Ocean Discovery Program

Visual Core Description

NO.
DATE: 1/7/20
EXP.: 912
SITE/HOLE: C9035 / A
CORE: ~~CC A~~ 1H
SECTION: CC A
TOP DEPTH (m CSF): 969.8 – 999.3
OBSERBER:

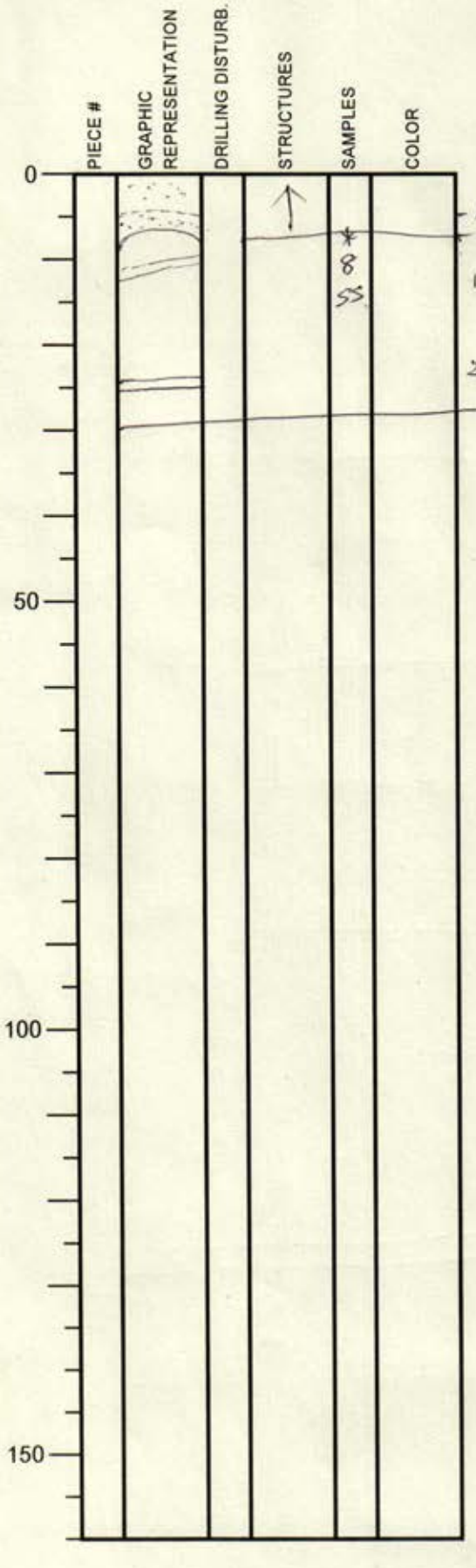

VCD_sheet_160629.xlsx

International Ocean Discovery Program

Visual Core Description

NO.
DATE: 1/7/20
EXP.: 912
SITE/HOLE: C9035 / B
CORE: 1 H
SECTION: 1 A
TOP DEPTH (m CSF): 0 – 138.8

OBSERBER:

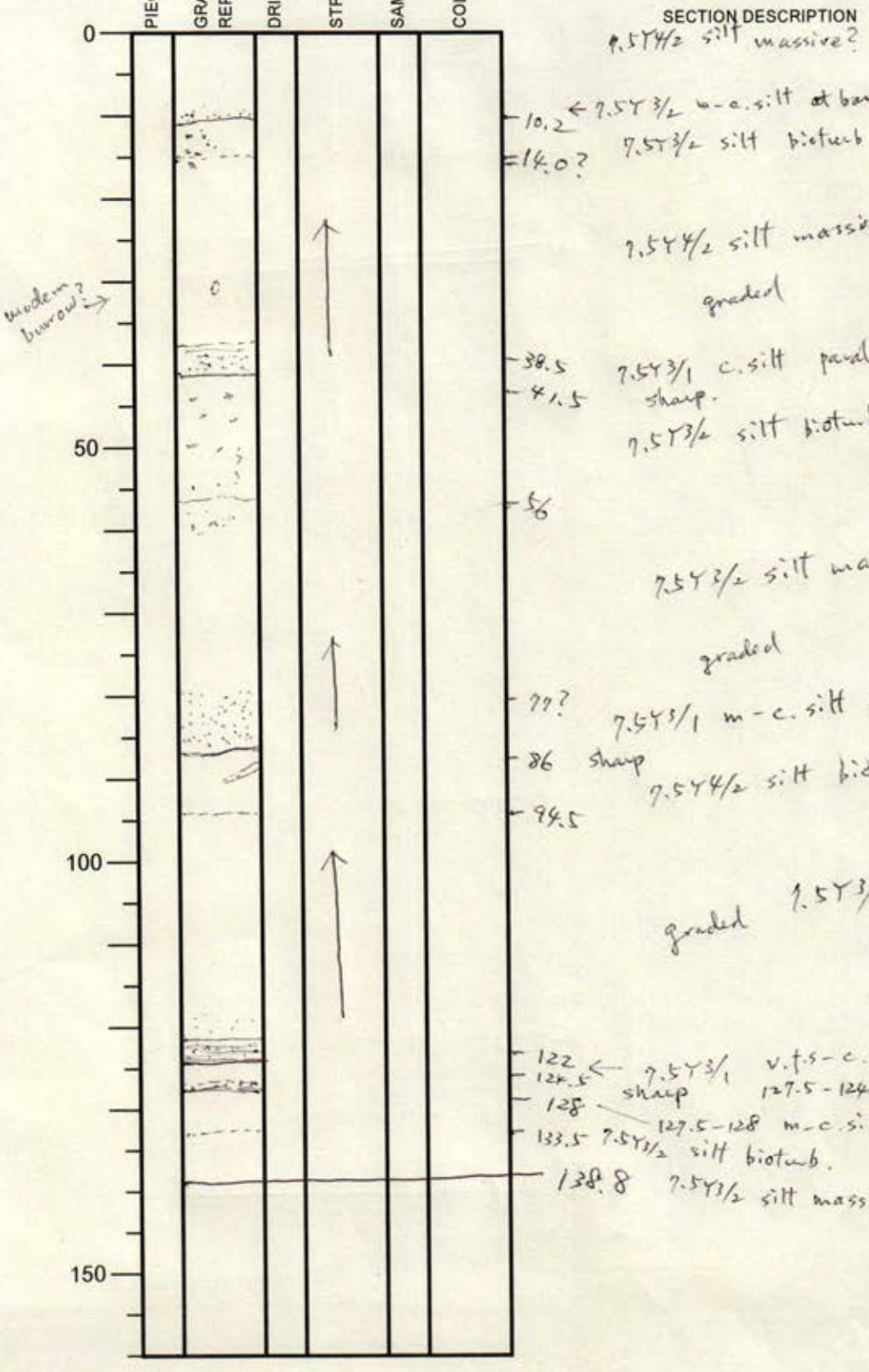

International Ocean Discovery Program

Visual Core Description

NO.
DATE: 1 / 7/ 20
EXP.: 912
SITE/HOLE: C9035 / B
CORE: 1 H
SECTION: 2 A
TOP DEPTH (m CSF): 138.8 – 278.8
OBSERBER:

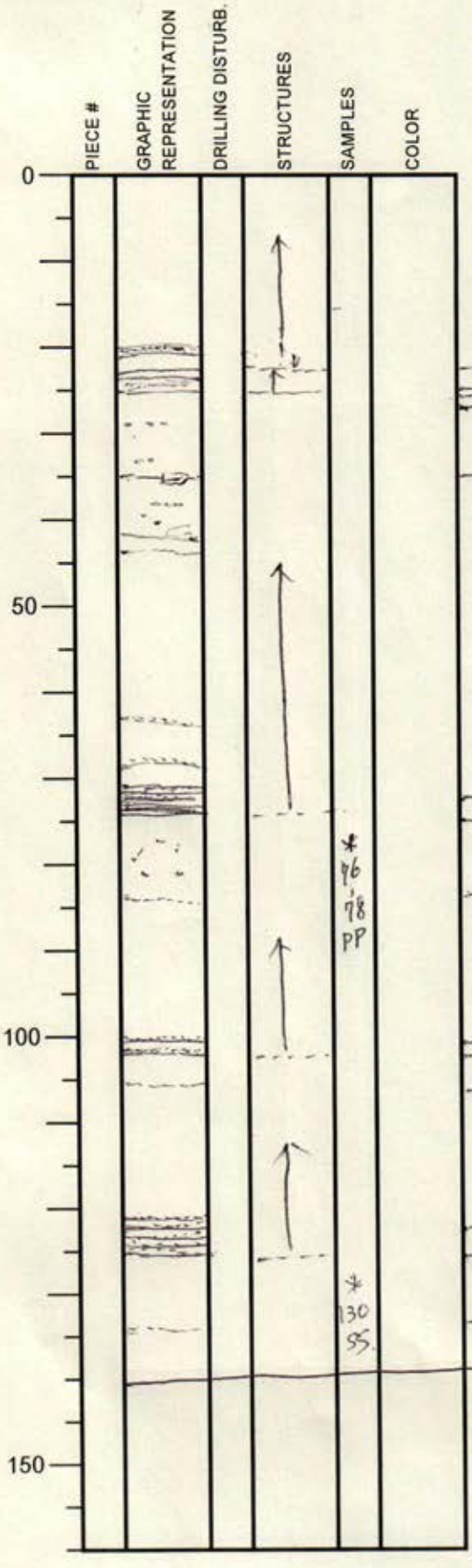

International Ocean Discovery Program

Visual Core Description

NO.
DATE: 1/7/20
EXP.: 912
SITE/HOLE: C9035 / B
CORE: 1 H
SECTION: 3A
TOP DEPTH (m CSF): 278.8 – 360.8
OBSERBER:

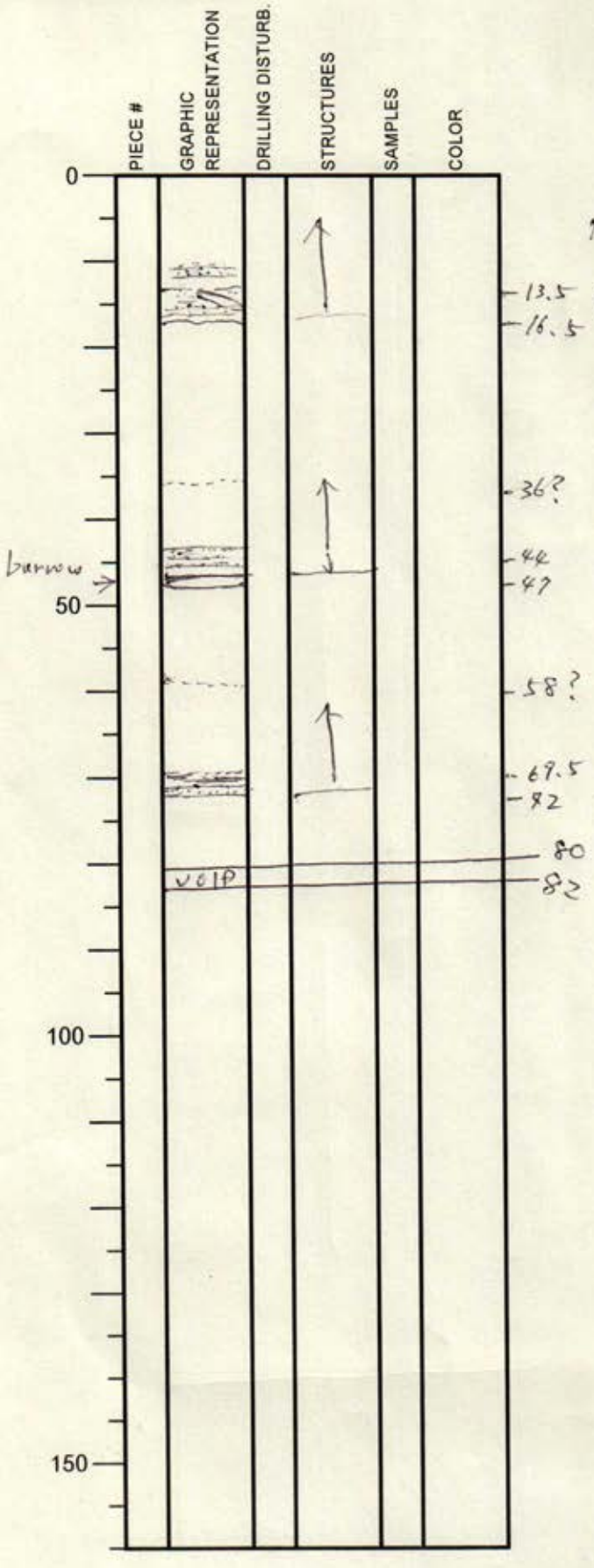

7.5Y3/2 silt massive

7.5Y3/1 c.silt-v.f.s. bedded (banded?) sharp

7.5Y3/2 silt biotub foram bearing

7.5Y3/2 silt massive

7.5Y3/1 c.silt sharp 45.8-47 m - c.silt.

7.5Y4/2 silt biotub.

7.5Y3/2 silt massive

7.5Y3/1 c.silt-v.f.s. bedded sharp.

7.5Y3/2 silt biotub. foram bearing

International Ocean Discovery Program

Visual Core Description

NO.
DATE: 1/3/20
EXP.: 912
SITE/HOLE: C9035 / B
CORE: 1H
SECTION: CC A
TOP DEPTH (m CSF): 360.8 - 389.0
OBSERBER:

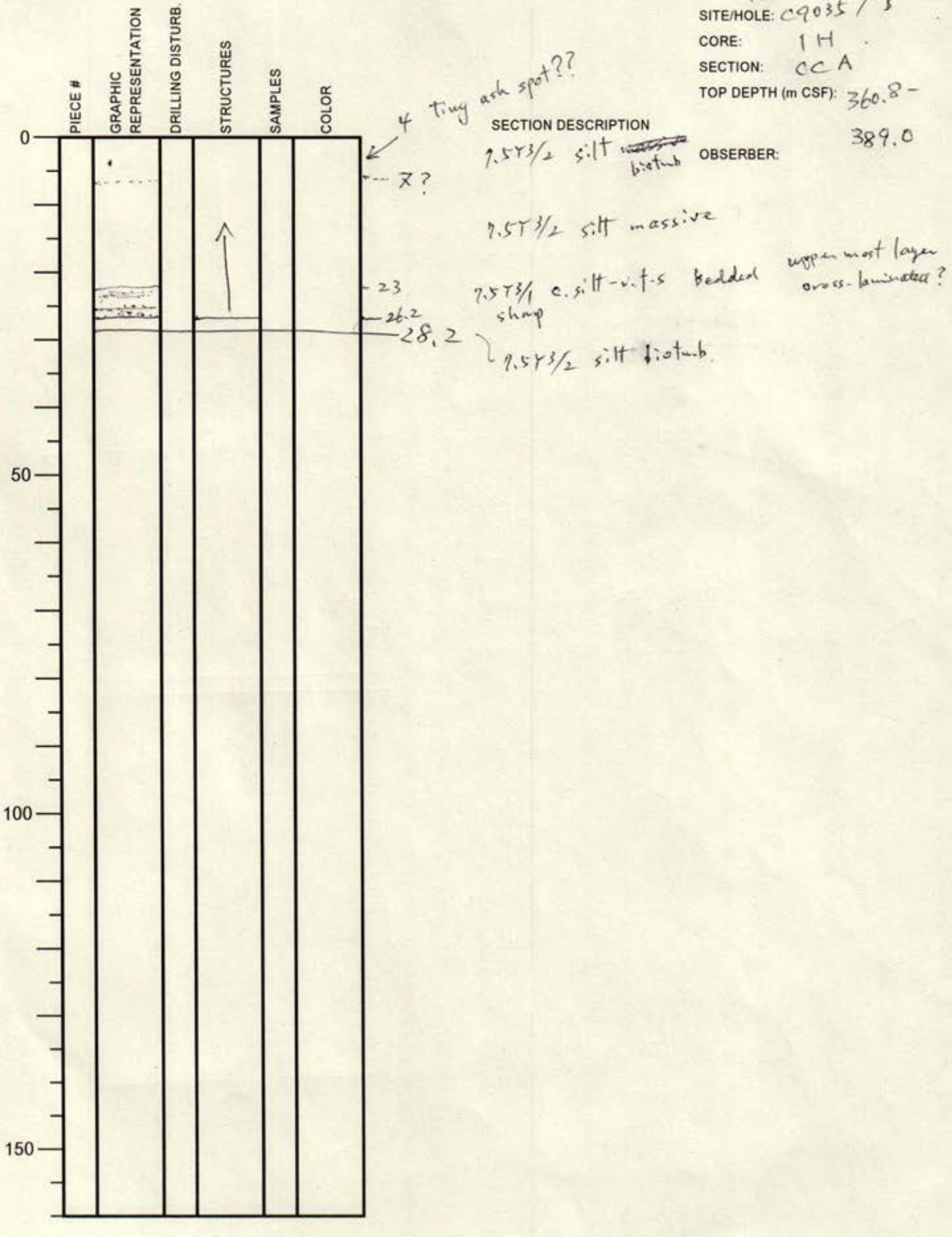

International Ocean Discovery Program

Visual Core Description

NO.
DATE: 1/7/20
EXP.: 912
SITE/HOLE: C9035/B
CORE: 2H
SECTION: 1A
TOP DEPTH (m CSF): 389.0 – 529.0
OBSERBER:

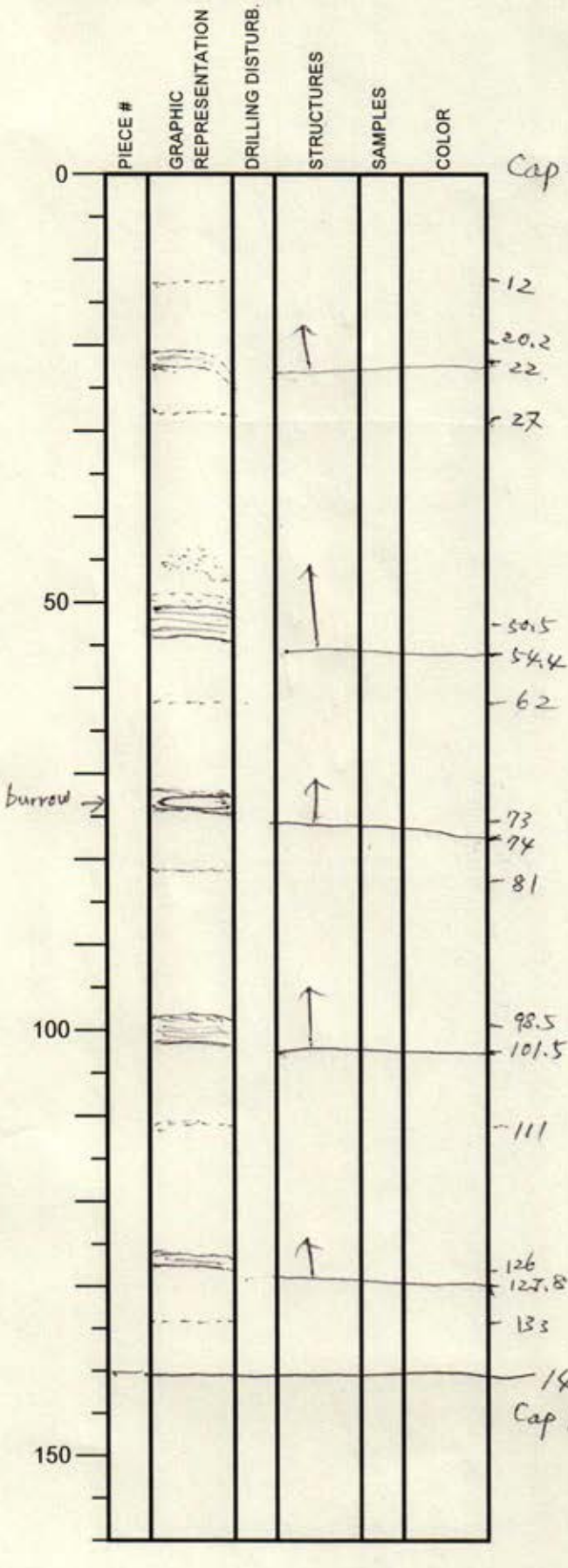

Cap – 0.1

SECTION DESCRIPTION

7.5Y3/2 silt. biotub.

7.5Y3/2 silt massive.

7.5Y3/1 c.silt paral. laminated
sharp

7.5Y3/2 silt biotub

7.5Y3/2 silt massive

← 38.1 Linear patch

7.5Y3/1 c.silt paral. laminated
sharp
foram bearing.

7.5Y3/2 silt biotub

7.5Y3/2 silt massive

7.5Y3/1 c.silt paral. laminated (burrowed)
maybe sharp 7.5Y3/2 silt biotub

7.5Y4/2 silt massive.

uppermost

7.5Y3/1 c.silt-v.f.s paral-cross laminated
sharp

7.5Y3/2 silt biotub

7.5Y4/2 silt massiv

7.5Y3/1 c silt-v.f.s. coarsest at the uppermost
sharp

7.5Y3/2 silt biotub

7.5Y3/2 silt massive

Cap 140.3

VCD_sheet_160629.xlsx

International Ocean Discovery Program

Visual Core Description

NO.
DATE: 1/2/20
EXP.: 912
SITE/HOLE: C9035 / B
CORE: 2H
SECTION: 2A
TOP DEPTH (m CSF): 529.0 – 669.5
OBSERBER: I

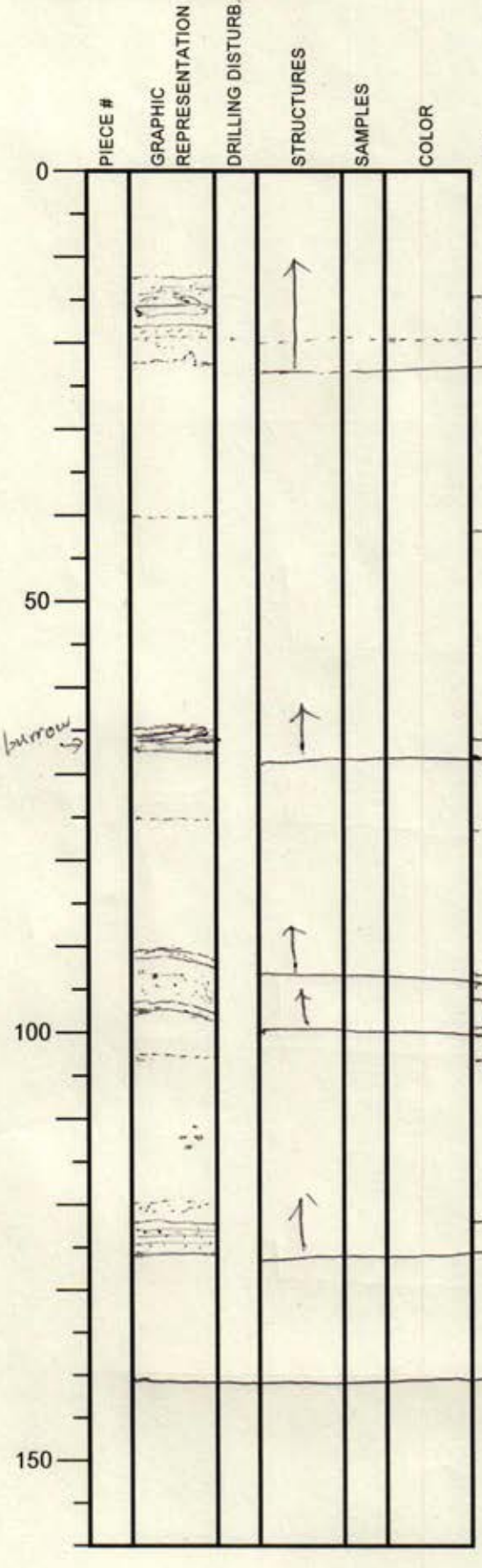

cap -0.2

SECTION DESCRIPTION

7.5YR 5/2 silt massive.

12.5 7.5Y 3/1 c.silt-v.f.s paral. laminated
20 sharp
23 7.5Y 3/1 c.silt sharp

7.5Y 4/2 silt bioturb.
foram bearing.

39

7.5Y 4/2 silt massive
mica(?) bearing

65
67 7.5Y 3/1 c.silt-v.f.s. paral. laminated
sharp.
7.5Y 3/2 silt bioturb sponge spicules.

75

7.5Y 3/2 silt massive

90 7.5Y 3/2 m.silt sharp
91 7.5Y 3/2 silt massive
96
97 7.5Y 3/2 m-c.silt paral. laminated
sharp
102 7.5Y 3/2 silt bioturb

7.5Y 3/2 silt massive

122
125.5 7.5Y 3/1 c.silt-v.f.s. paral. laminated
sharp
7.5Y 3/2 silt bioturb.

140.1
cap 140.5

International Ocean Discovery Program

Visual Core Description

NO.
DATE: 1 / 7 / 20
EXP.: 912
SITE/HOLE: C9035 / B
CORE: 2H
SECTION: 3A
TOP DEPTH (m CSF): 669.~~8~~ 1 – 809.~~6~~ 2
OBSERBER:

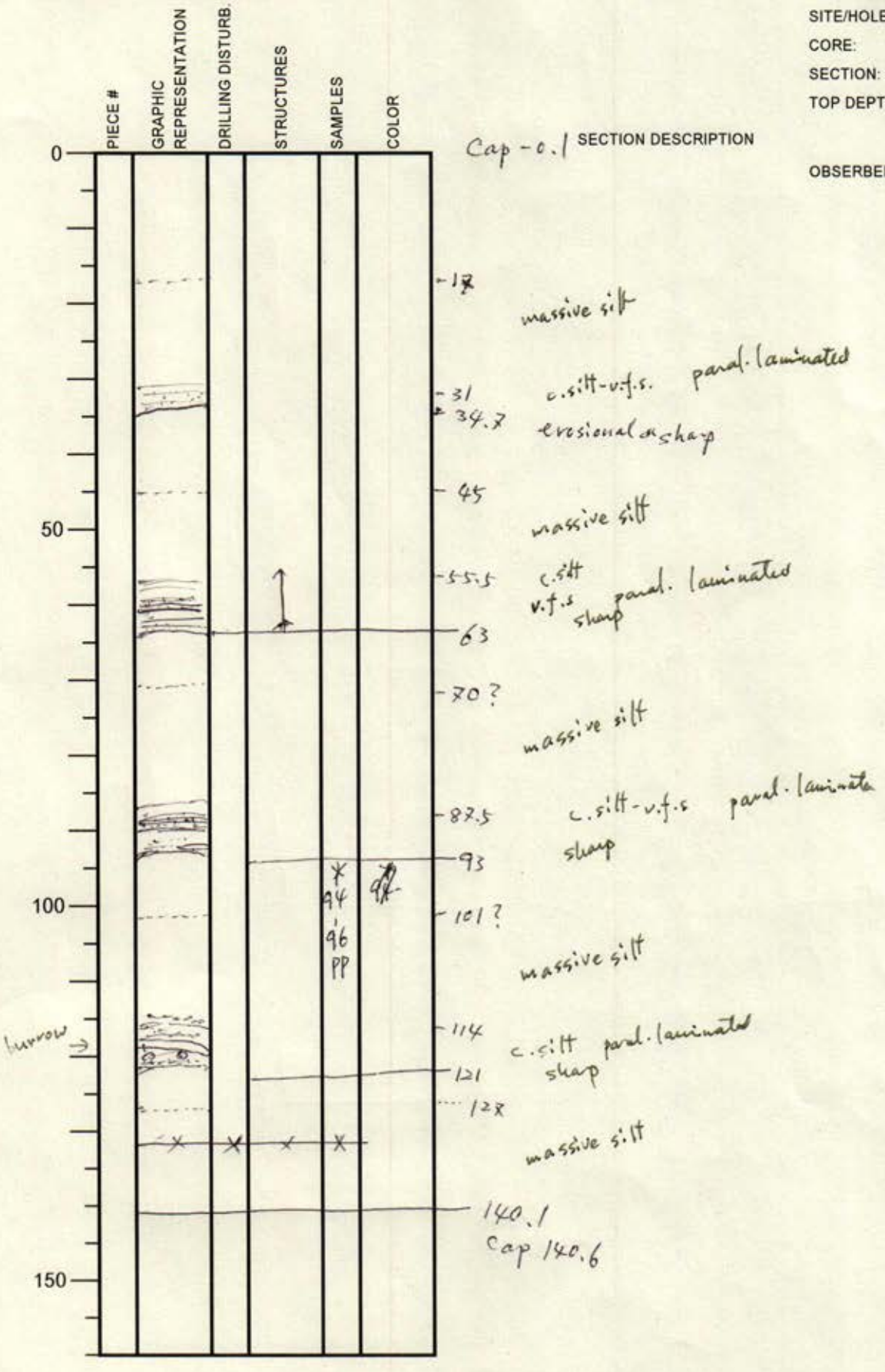

International Ocean Discovery Program

Visual Core Description

NO.
DATE: 1/8/20
EXP.: 912
SITE/HOLE: C9035 / B
CORE: 2H
SECTION: 4A 2
TOP DEPTH (m CSF): 809.7 – 950.6
OBSERBER: 2

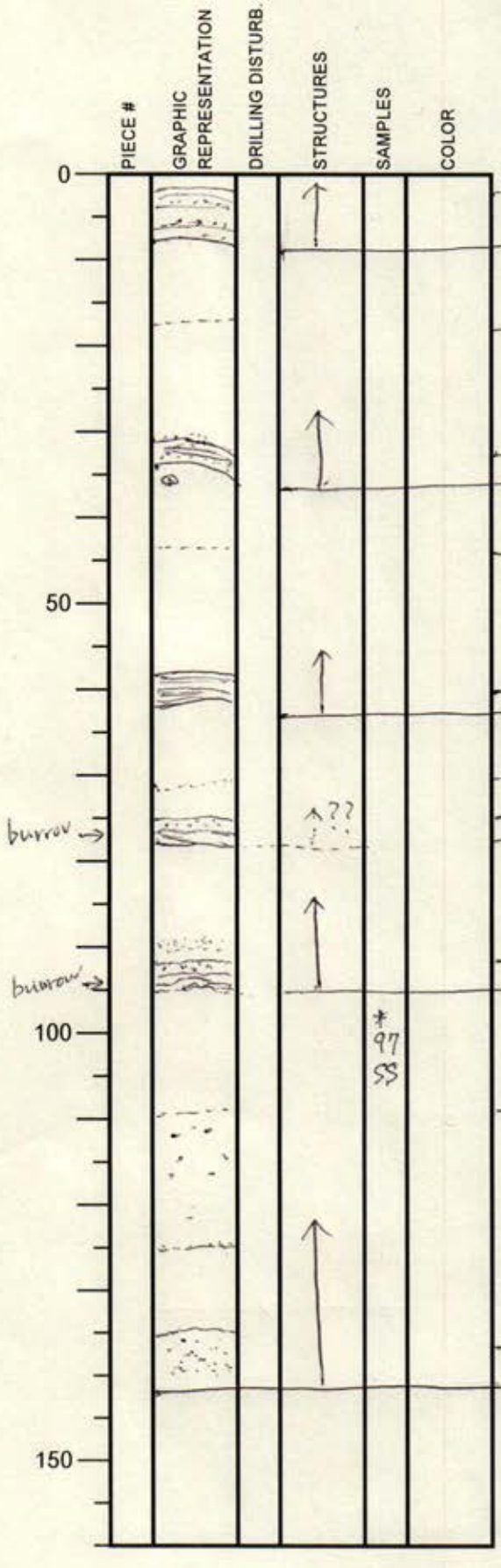

Carp -0.2 SECTION DESCRIPTION

1.5
7.5Y3/1 c.silt-v.f.s. paral. laminated
8.2 sharp
7.5Y3/2 silt biotumb
17
7.5Y3/2 silt massive
31
7.5Y3/1 c.silt-v.f.s sharp paral. laminated
34.5
7.5Y3/2 silt biotumb.
43
7.5Y3/2 silt massive
58.5
7.5Y3/1 c.silt-v.f.s. paral.-cross laminated sharp
61.5
7.5Y3/2 silt biotumb
71?
7.5Y3/2 silt massive
75.5
7.5Y3/2 m-f.silt burrow fill??
78
7.5Y3/2 silt massive
93
7.5Y3/1 c.silt-v.f.s. sharp & irregular
95
7.5Y3/2 silt biotumb
109
7.5Y3/2 silt massive
135
7.5Y3/1 c.silt massive.
141
linear 140.5
Carp 141.4

International Ocean Discovery Program

Visual Core Description

NO.
DATE: 1/2/20
EXP.: 912
SITE/HOLE: C9035/B
CORE: 2H
SECTION: 5A 2
TOP DEPTH (m CSF): 950.6 - 1090.8
OBSERBER: Z

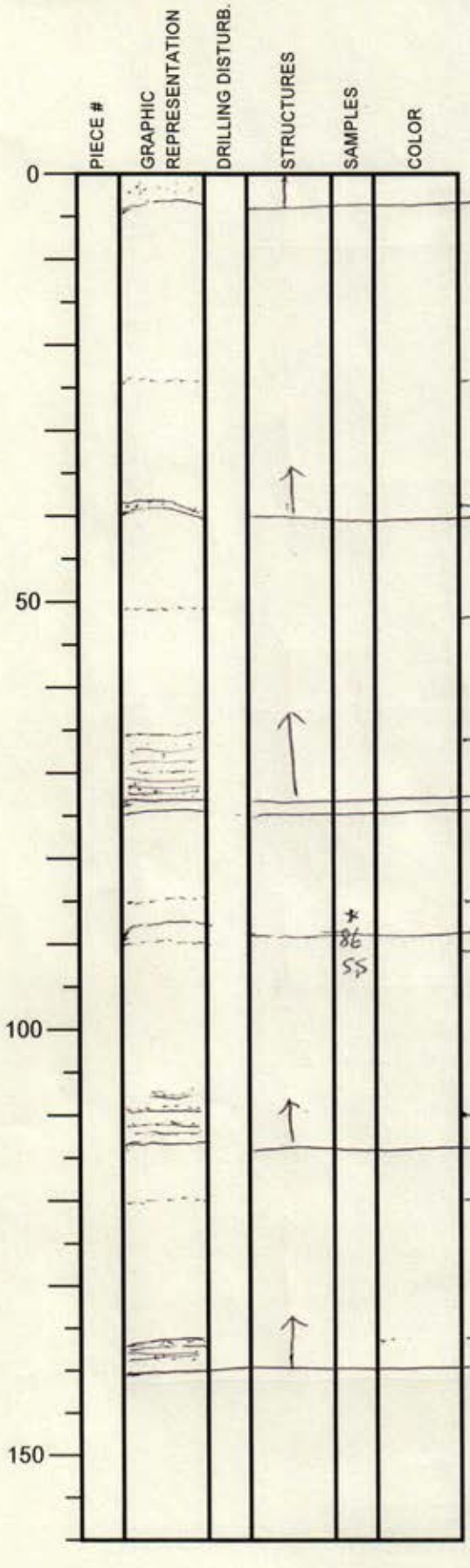

Cap -0.2

SECTION DESCRIPTION

7.5Y3/1 c.silt - v.f.s sharp
massive?
foram bearing.

7.5Y3/2 silt bioturb.

7.5Y3/2 silt massive

7.5Y3/1 c.silt sharp.

7.5Y3/2 silt bioturb

7.5Y3/2 silt massive

7.5Y3/1, c.silt - v.f.s paral. laminated
sharp sharp top
volcanic ash 5Y4/1 m. silt sized ash.

2.5Y4/1 c.silt sized ash.
sharp.

7.5Y3/2 silt bioturb.

7.5Y3/2 silt massive.

7.5Y3/1 c.silt paral. laminated or bedded
sharp

7.5Y4/1 silt bioturb

7.5Y4/2 silt massive

7.5Y3/1 c.silt paral. laminated or bedded

Cap 140.4

VCD_sheet_160629.xlsx

International Ocean Discovery Program

Visual Core Description

NO.
DATE: 1/8/20
EXP.: 912
SITE/HOLE: C9035/B
CORE: 2H
SECTION: 6A
TOP DEPTH (m CSF): 1090.6 – 1231.8

OBSERBER:

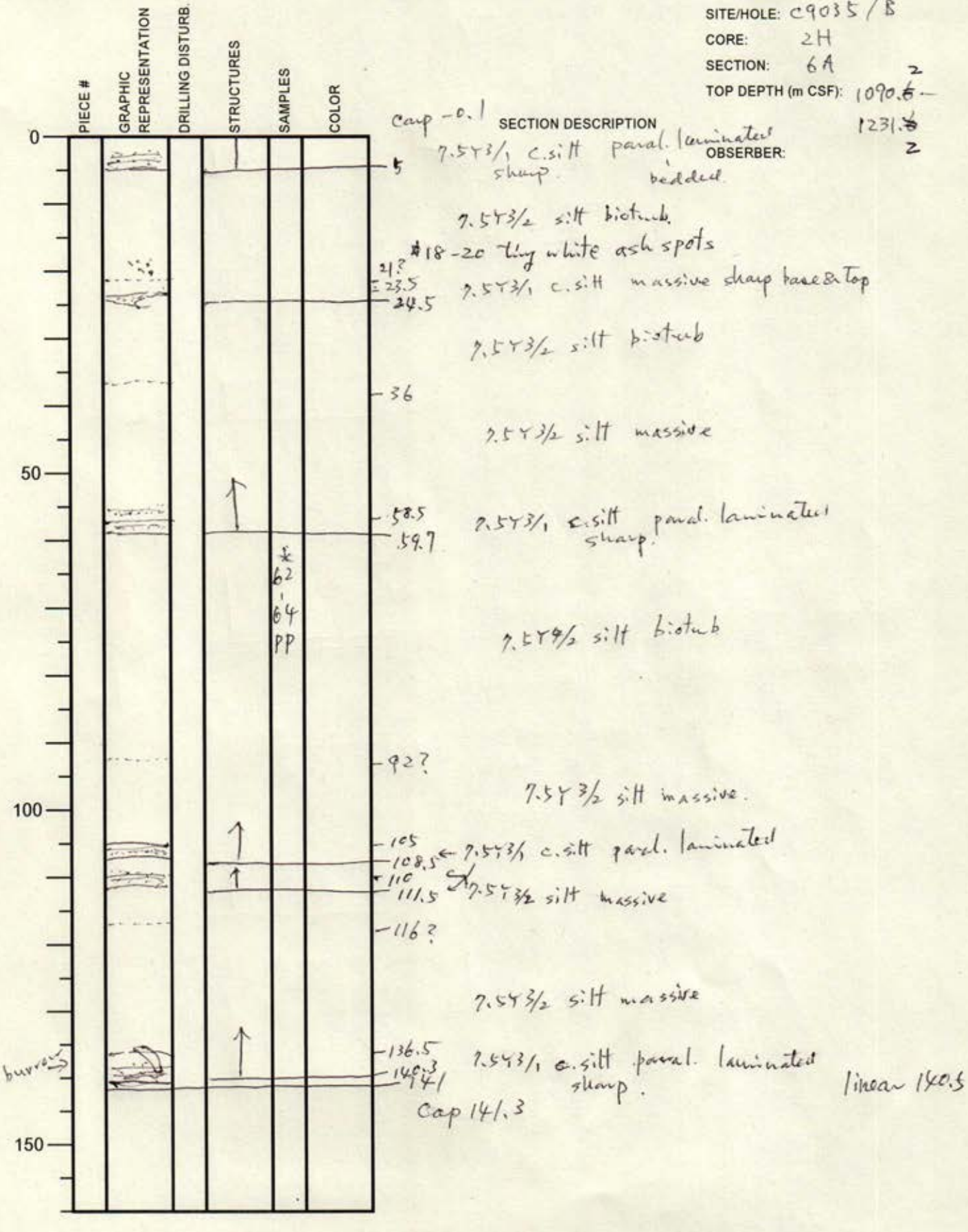

VCD_sheet_160629.xlsx

International Ocean Discovery Program

Visual Core Description

NO.
DATE: 1 / 8 / 20
EXP.: 912
SITE/HOLE: C9035 / B
CORE: 2H
SECTION: 7A
TOP DEPTH (m CSF): 1231.8 - 1361.2
OBSERBER: b

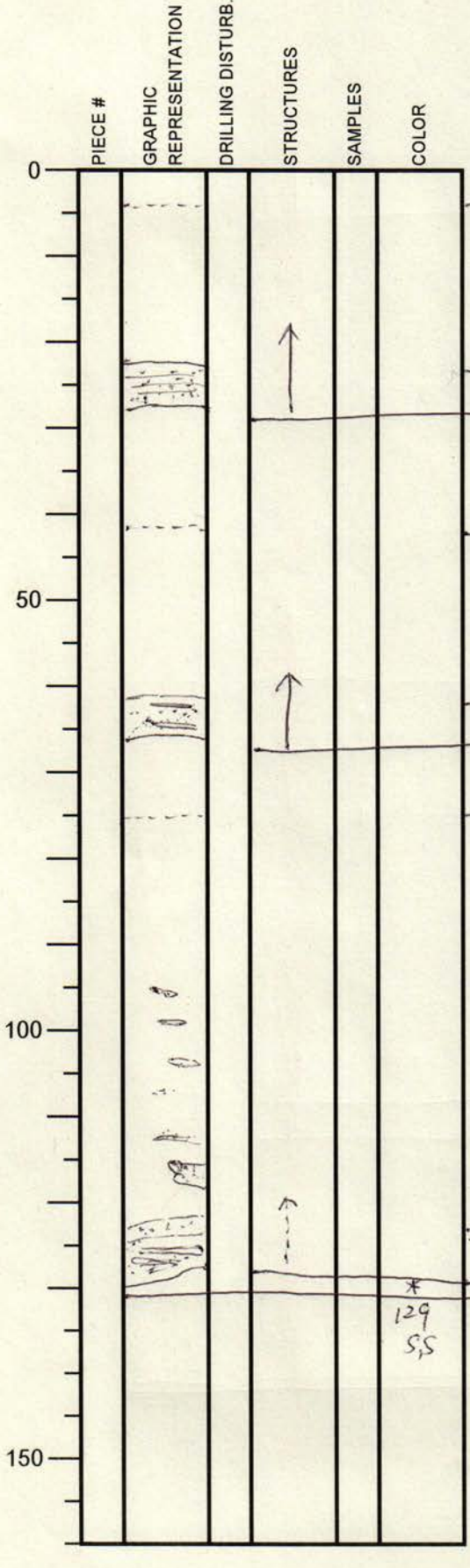

International Ocean Discovery Program

Visual Core Description

NO.
DATE: 1 13 / 20
EXP.: 912
SITE/HOLE: C9035 / B
CORE: 2H
SECTION: cc A 1.6
TOP DEPTH (m CSF): 136~~8.0~~ 1386.7
OBSERBER: 5

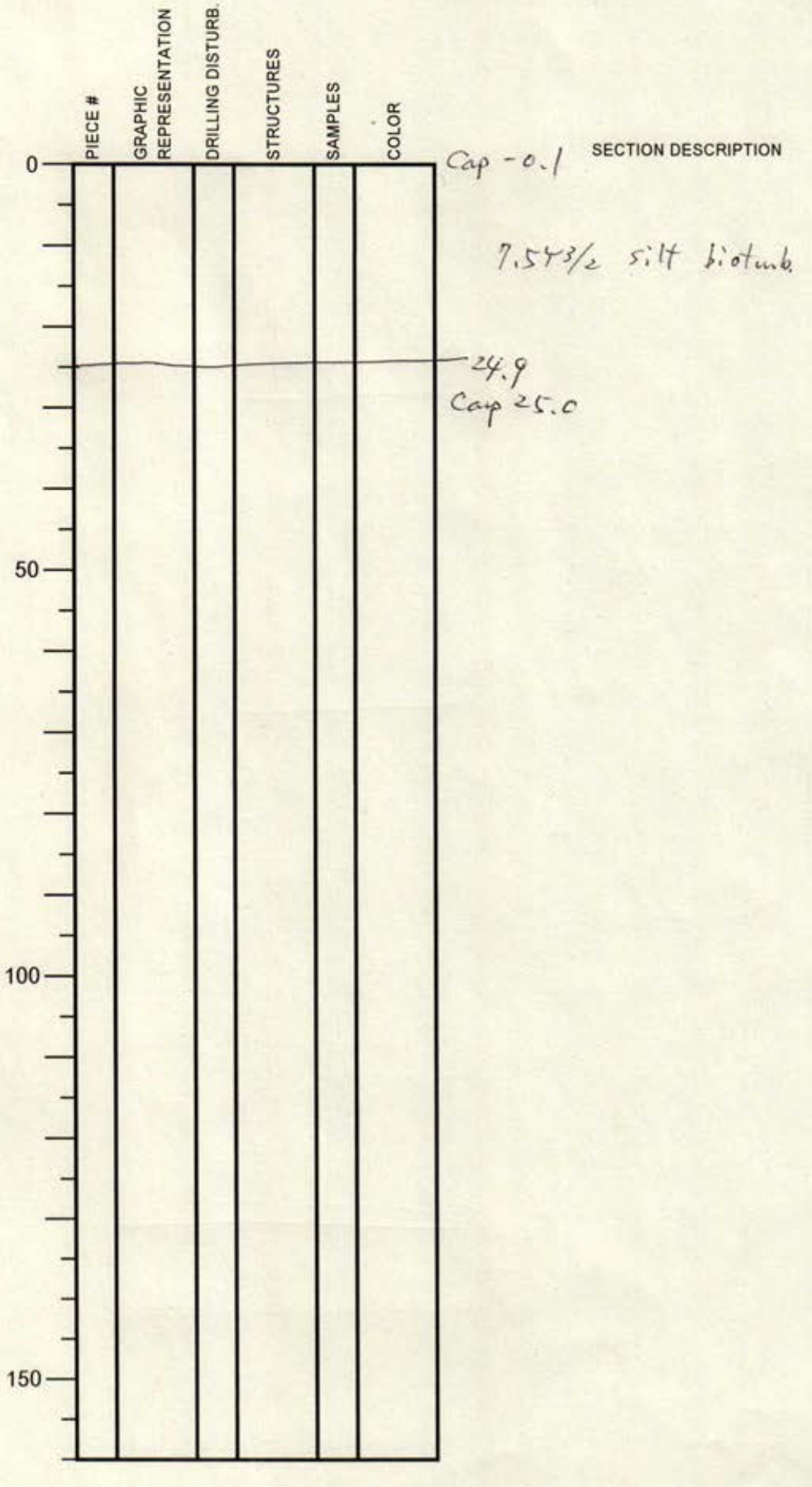

International Ocean Discovery Program

Visual Core Description

NO.
DATE: 1 / 19 / 20
EXP.: 912
SITE/HOLE: C9035 / B
CORE: 3H
SECTION: 1 A
TOP DEPTH (m CSF): 1386.9 – 1526.9
OBSERBER:

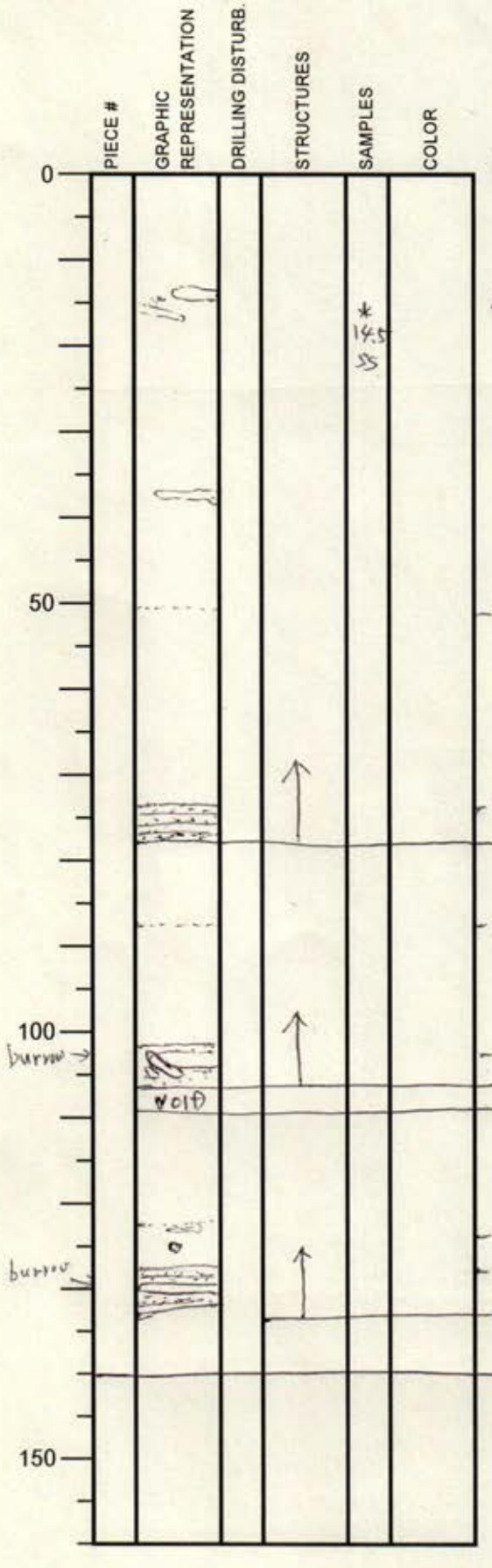

Cap -0.2 SECTION DESCRIPTION

7.5Y4/2 silt biotub

14-15 7.5Y5/1 m-c. silt-sized ash ☆

7.5Y3/2 silt biotub
sponge spicule

50

7.5Y3/2 silt massive

73.8
78 7.5Y3/1 c.silt-v.f.s shell frag? bearing
7.5Y4/2 silt biotub sharp
foram?
82.5

7.5Y3/2 silt massive

102.5
107 7.5Y3/1 c.silt-v.f.s. shell bearing
109 ~1/10 cm

7.5Y4/2 silt biotub?

122.5
128 7.5Y3/2 silt massive
133.3 7.5Y3/1 c.silt. v.f.s para. laminated
sharp
140 7.5Y3/2 silt biotub.

Cap 140.1

International Ocean Discovery Program

Visual Core Description

NO.
DATE: 1/8/20
EXP.: 912
SITE/HOLE: C9035/B
CORE: 3H
SECTION: 2A
TOP DEPTH (m CSF): 1526.7 - 1667 6.8

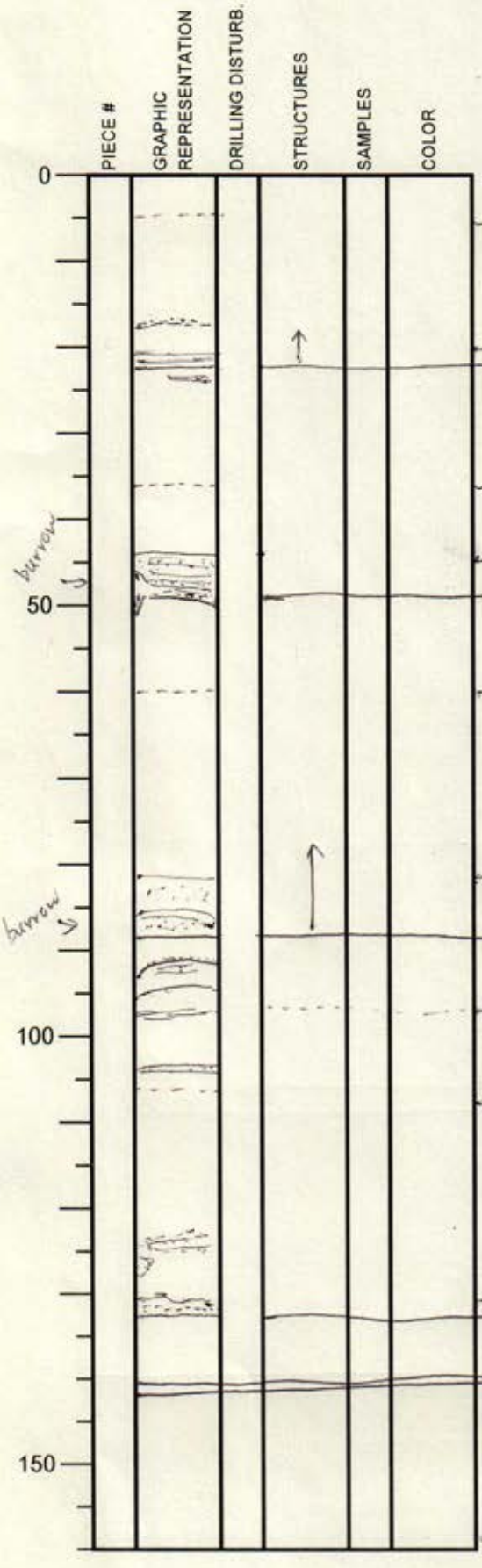

International Ocean Discovery Program

Visual Core Description

NO.
DATE: 1/8/20
EXP.: 912
SITE/HOLE: C9035 / B
CORE: 3H
SECTION: 3A
TOP DEPTH (m CSF): 166~~7.0~~ 6.8 – 180~~7.0~~ 6.8
OBSERBER:

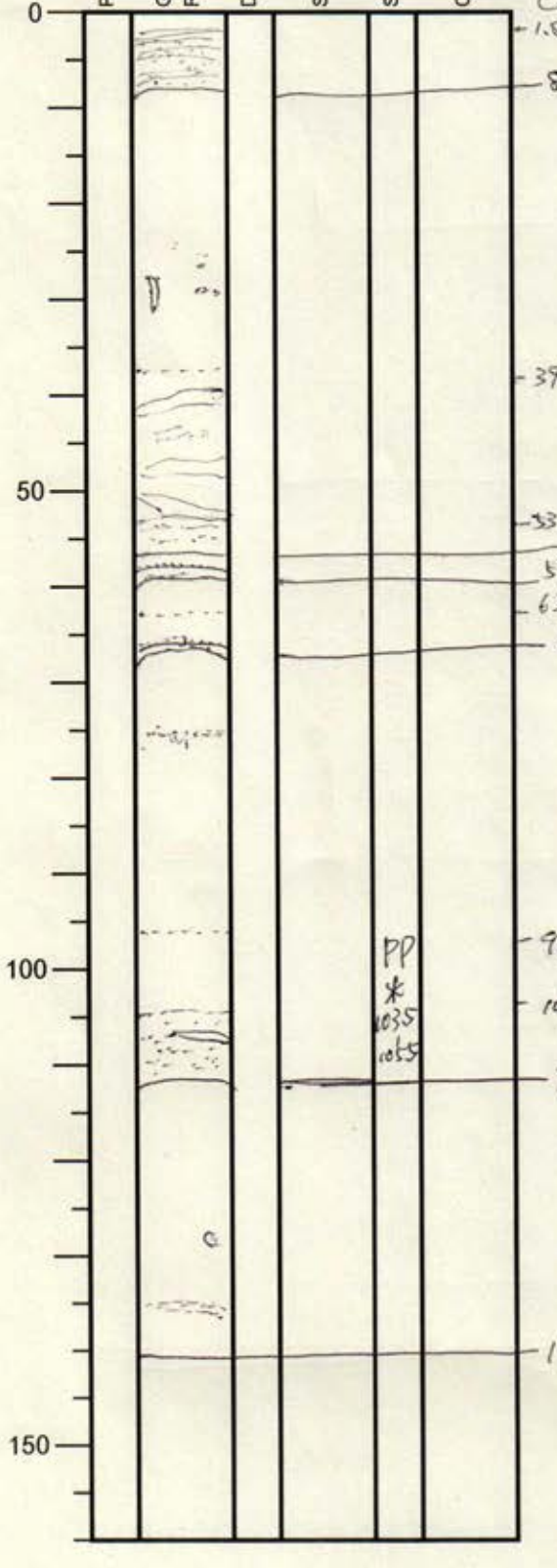

Cap -0.1 SECTION DESCRIPTION

1.8 – 7.5Y3/1 c.silt paral. laminati – bedded
8 – sharp

7.5Y3/2 silt biotumb

39

7.5Y3/2 silt massive? but highly burrowed

33

59 – 7.5Y 3/1 c.silt-v.f.s paral. laminate

63? – banded 7.5Y3/1 c.silt sharp

7.5Y3/2 silt biotumb

7.5Y3/2 silt massive

67.8 banded 7.5Y3/1 c.silt

7.5Y 4/2 silt biotumb.

96

7.5Y3/2 silt massive

105

7.5Y 3/1 c.silt-v.f.s paral laminate

112.3 – sharp

7.5Y 4/2 silt biotumb.

140

Cap 140.5

linear 139.9

International Ocean Discovery Program

Visual Core Description

NO.
DATE: 1 / 8 / 20
EXP.: 912
SITE/HOLE: C9035 / B
CORE: 3H
SECTION: 4A 6.8
TOP DEPTH (m CSF): 1807~~70~~ – 1947.2
OBSERBER: O

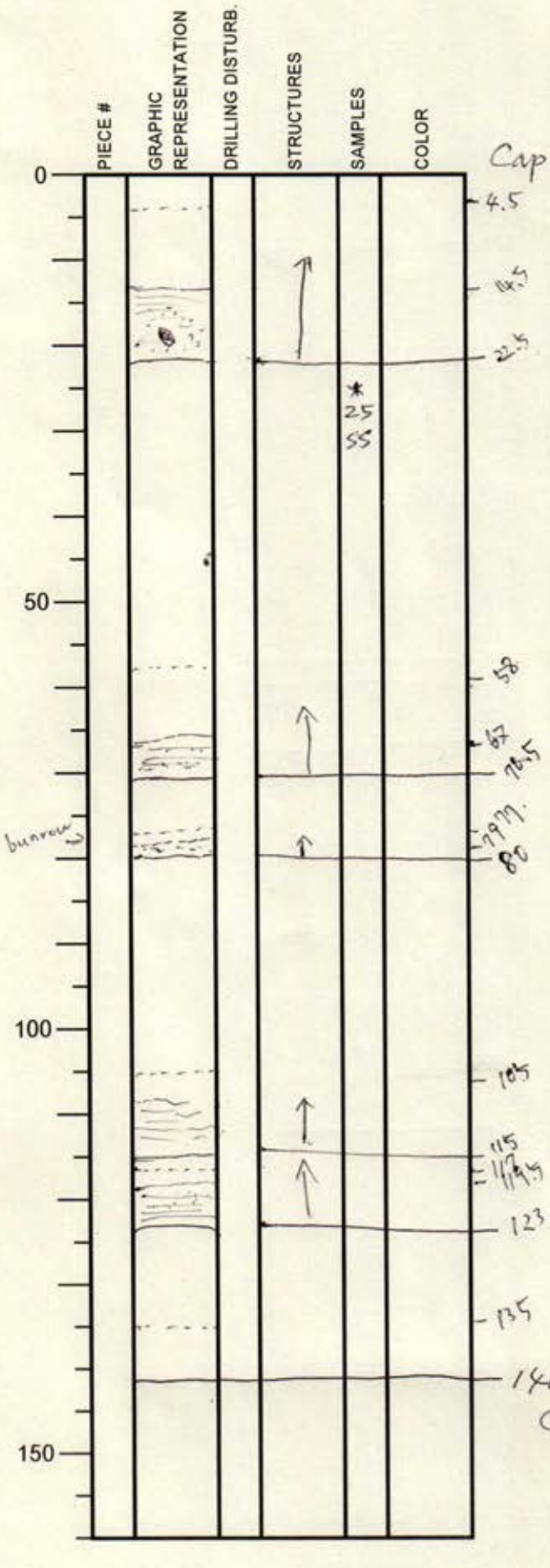

Cap -0.1 SECTION DESCRIPTION

7.5Y3/2 silt massive

7.5Y3/1 v.f.s paral. laminated
sharp 19-20 shell frag.

7.5Y4/2 silt biotub.
sponge spicule

7.5Y3/2 silt massive

7.5Y3/2 c.silt paral-cross laminated
sharp
7.5Y3/2 silt biotub foram?

7.5Y3/2 c.silt sharp massive?

7.5Y 3/2 silt biotub.

massive
7.5Y 3/2 m-c. silt paral. laminated
7.5Y3/2 silt biotub.

7.5Y3/1 c.silt-v.f.s paral laminated
sharp

7.5Y3/2 silt biotub sponge spicule

7.5Y3/2 silt massive

linear 139.8

Cap 140.5

International Ocean Discovery Program

Visual Core Description

NO.
DATE: 1/8/20
EXP.: 912
SITE/HOLE: C9035/B
CORE: 3H
SECTION: 5A
TOP DEPTH (m CSF): 1947.0 - 2087.8
OBSERBER:

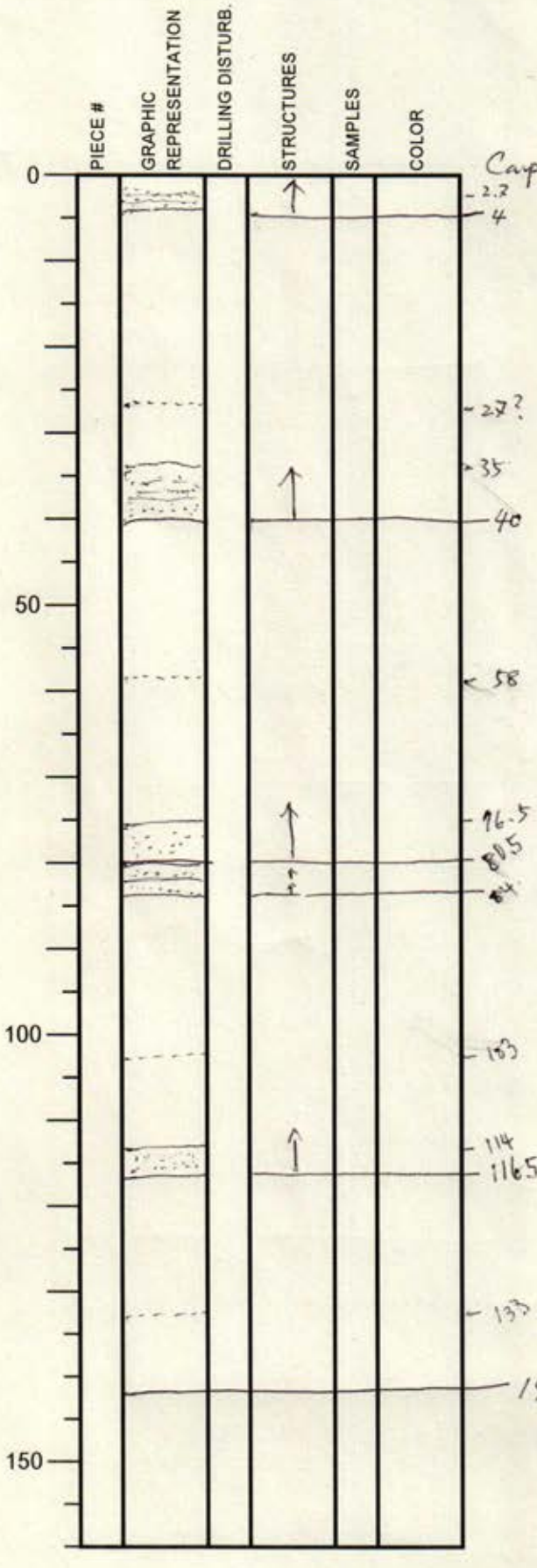

Cap -0.1 SECTION DESCRIPTION

7.5Y3/1 c.silt paral. laminated sharp

7.5Y3/2 silt bioturb sponge spicule

7.5Y3/2 silt massive

7.5Y3/1 c.silt-vfs. paral. laminated sharp

7.5Y4/2 silt bioturb sponge spicules

7.5Y3/2 silt massive

7.5Y3/1 c.silt paral. laminated sharp

c.silt band 84-83.3 83-80.5 laminated c.silt

7.5Y4/2 silt bioturb.

7.5Y3/2 silt massive

7.5Y3/1 c.silt graded sharp.

7.5Y3/2 silt bioturb sponge spicule

7.5Y3/2 silt massive

140.6 linear 140.1

Cap 140.9

International Ocean Discovery Program

Visual Core Description

NO.
DATE: 1/8/20
EXP.: 912
SITE/HOLE: C9035 / B
CORE: 3H
SECTION: 6A
TOP DEPTH (m CSF): 2082.6 - 2230.6
OBSERBER: 6

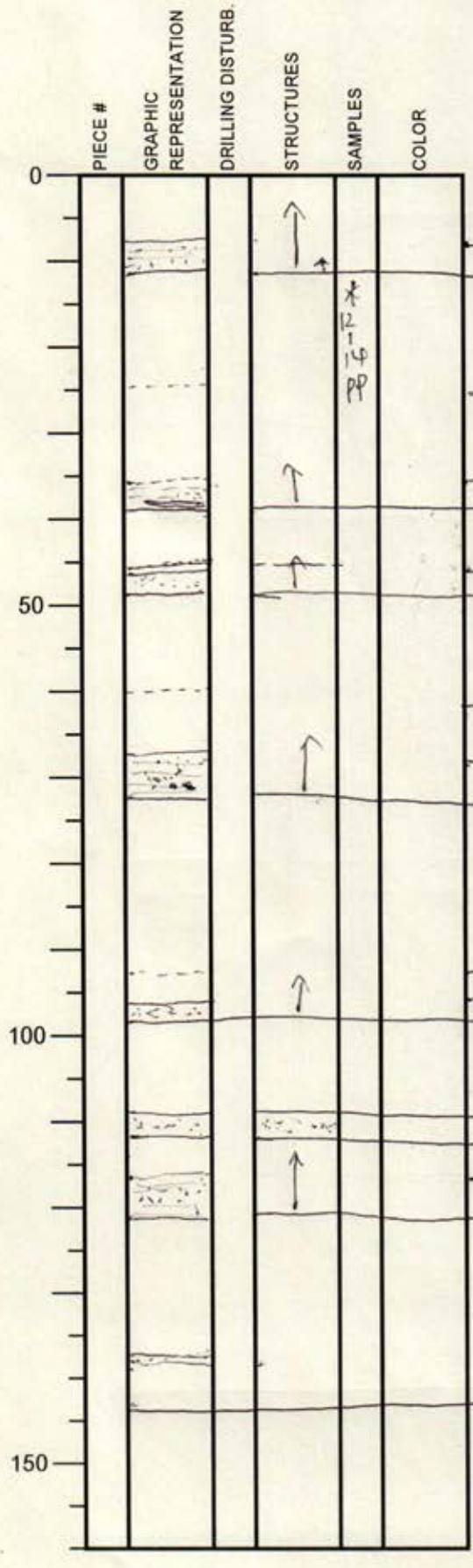

Cap -0.1 SECTION DESCRIPTION

7.5Y3/2 silt massive
8
7.5Y3/1 v.f.s-c.silt graded upper part paral. laminated
11.5 sharp
7.5Y3/2 silt biotu-b
23
7.5Y3/2 silt massive
36
39 7.5Y3/1 c.silt-v.f.s graded upper part paral. laminated
sharp
7.5Y3/2 silt biotub.
47.8
49.2 7.5Y3/1, v.f.s sharp
7.5Y 7/2 silt massive sponge spicule.
60
7.5Y 3/2 silt massive - with sandy laminae or burrows
68
72 7.5Y3/1, v.f.s paral. laminated pumice bearing
sharp
7.5Y4/2 silt biotub.
93.2
96.2 7.5Y3/2 silt massive
98.8 7.5Y3/1, c.silt-v.f.s. paral. laminated
sharp
7.5Y3/2 silt biotub.
109
112 7.5Y3/1, c.silt-v.f.s sharp top & base
117 7.5Y3/2 sandy silt paral laminated
121 7.5Y3/1, c.silt-v.f.s paral. laminated
sharp
7.5Y3/2 silt biotub.
137-138 7.5Y3/1, c.silt layer.
143
Cap 143.5

linear
140.5
patched.

International Ocean Discovery Program

Visual Core Description

NO.
DATE: 1/8/20
EXP.: 912
SITE/HOLE: C9035/B
CORE: 3H
SECTION: 7A
TOP DEPTH (m CSF): 6
2230.7 –
2359.5
3

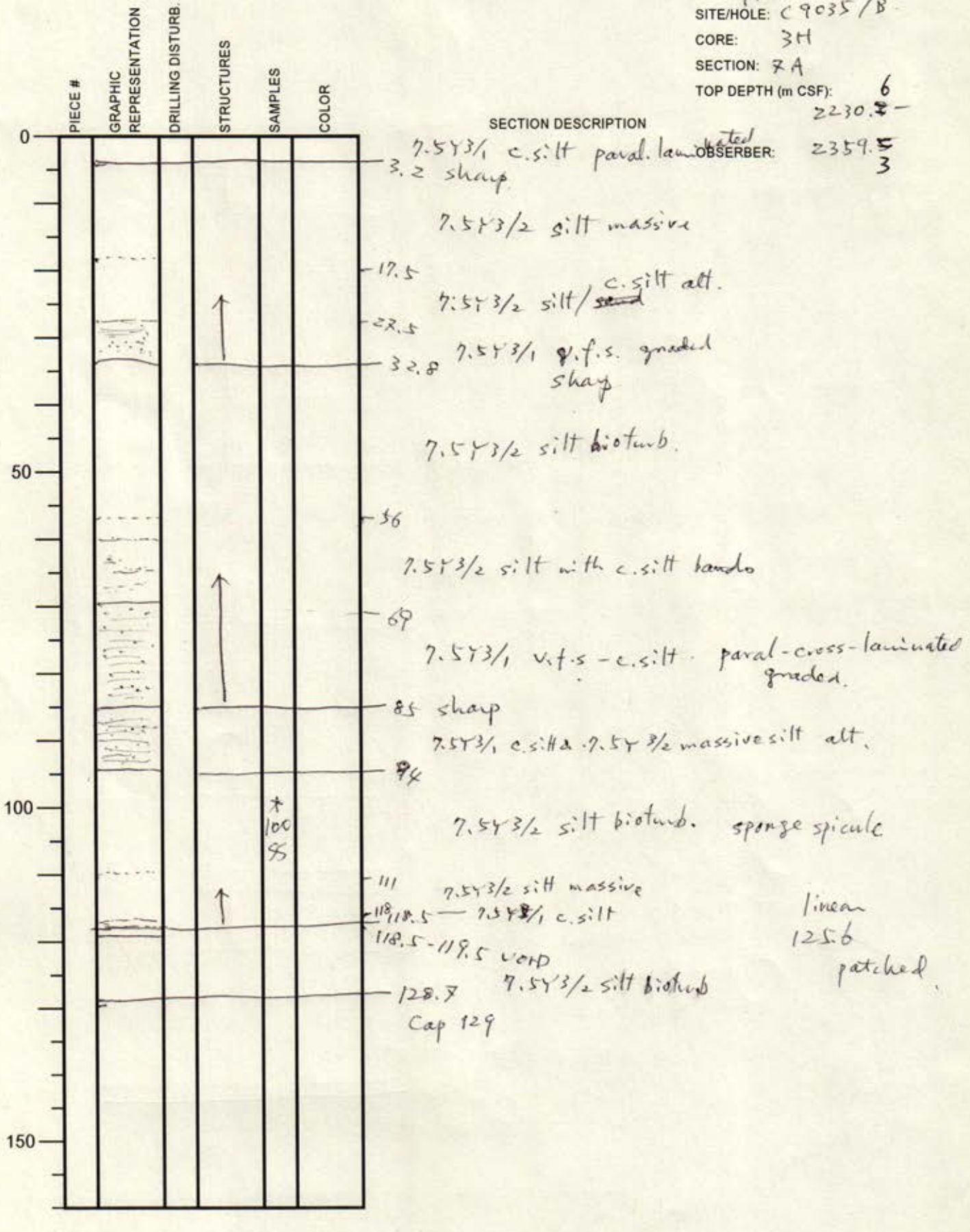

International Ocean Discovery Program

Visual Core Description

NO.
DATE: 1/8/20
EXP.: 912
SITE/HOLE: C9035/B
CORE: 3H
SECTION: CCA
TOP DEPTH (m CSF):

OBSERBER: 3
2359.5 –
2389.5
3

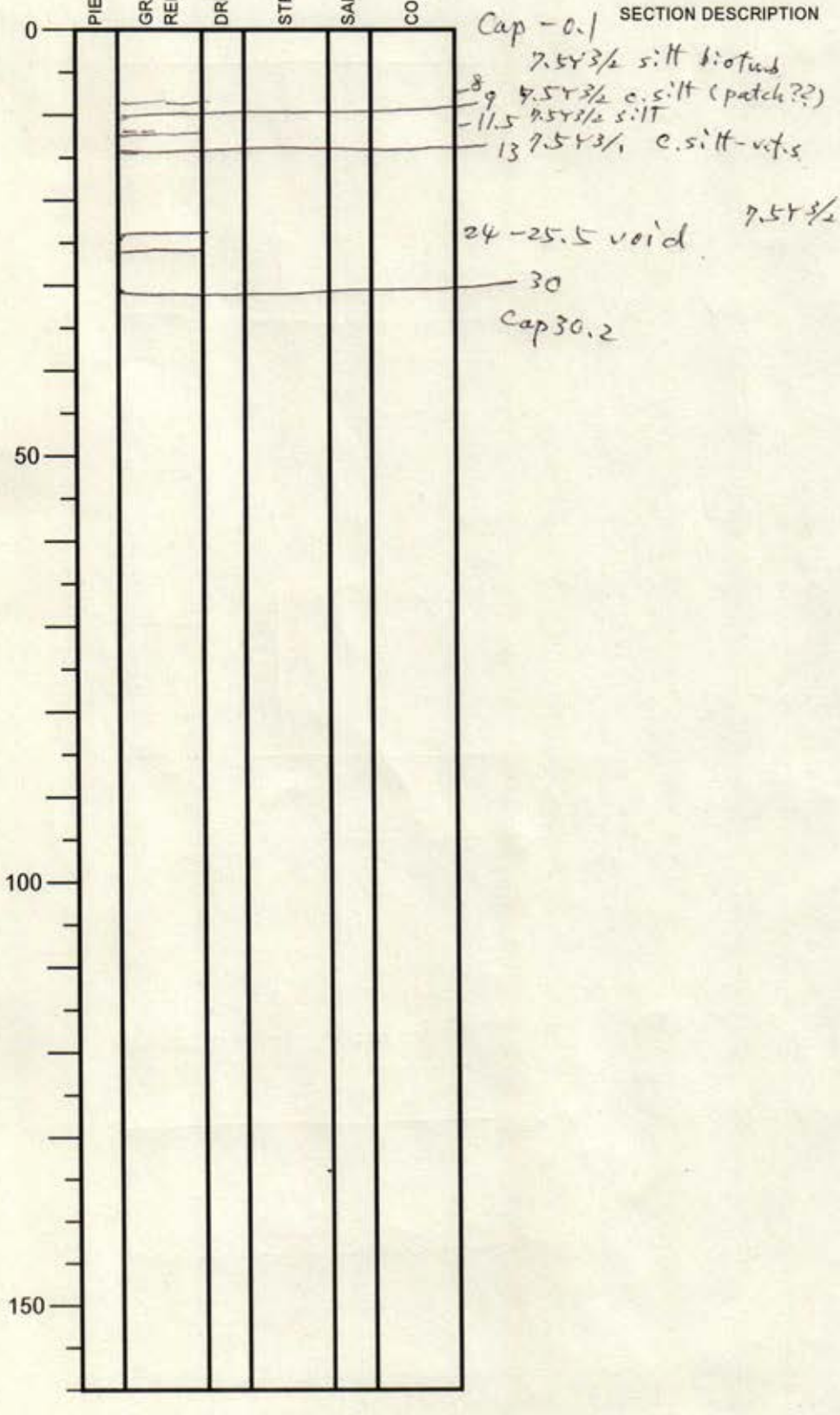

VCD_sheet_160629.xlsx

International Ocean Discovery Program

Visual Core Description

NO.
DATE: 1/8/20
EXP.: 912
SITE/HOLE: C9035 / B
CORE: 4H
SECTION: 1A
TOP DEPTH (m CSF): 3
2389.5 –
2401.4
OBSERBER: Z

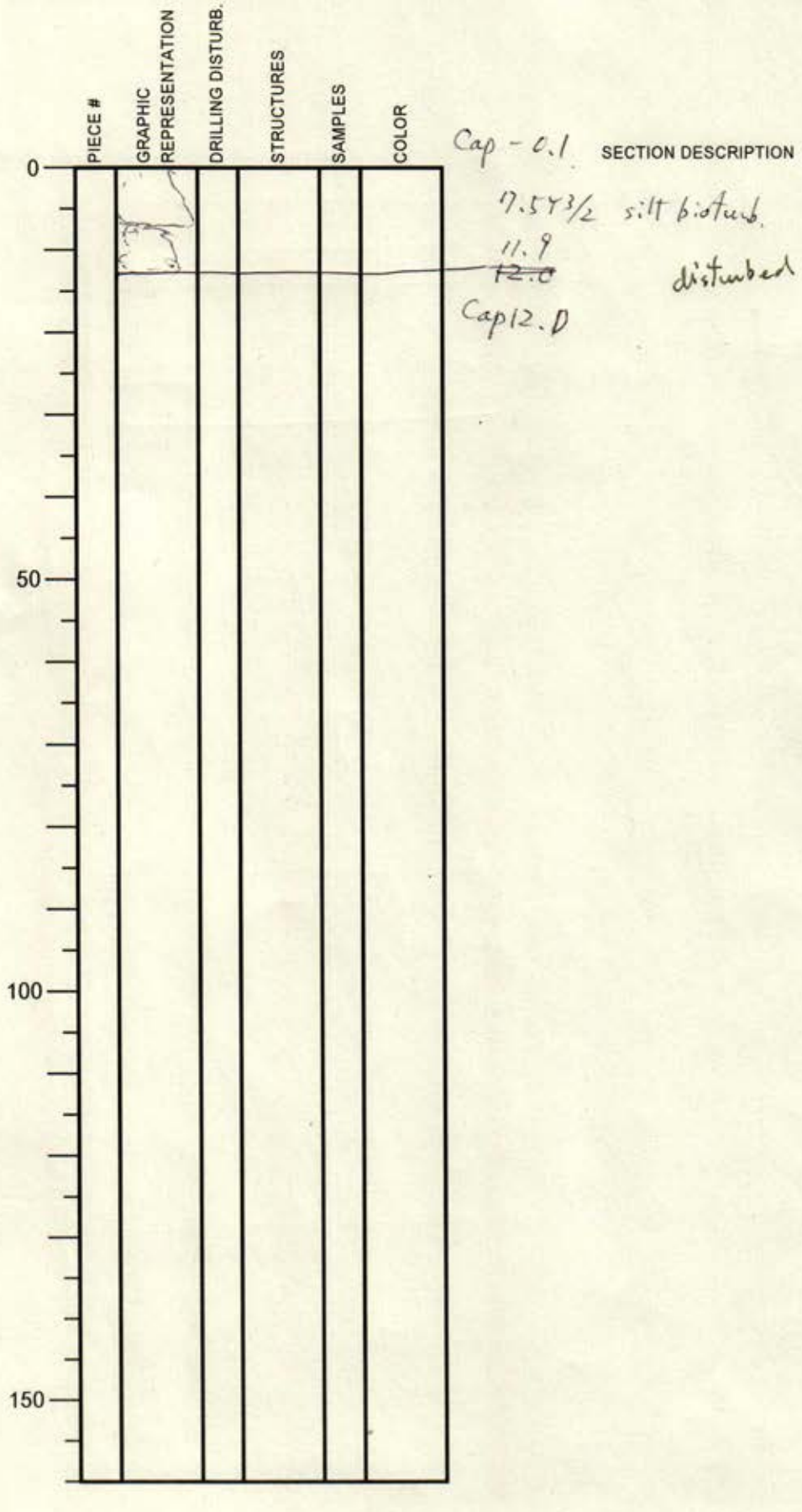

International Ocean Discovery Program

Visual Core Description

NO.
DATE: 1 / 8/20
EXP.: 912
SITE/HOLE: C9035 / B
CORE: 4H
SECTION: 2A
TOP DEPTH (m CSF): 2
2401.4 -
2541.4
OBSERBER:
2

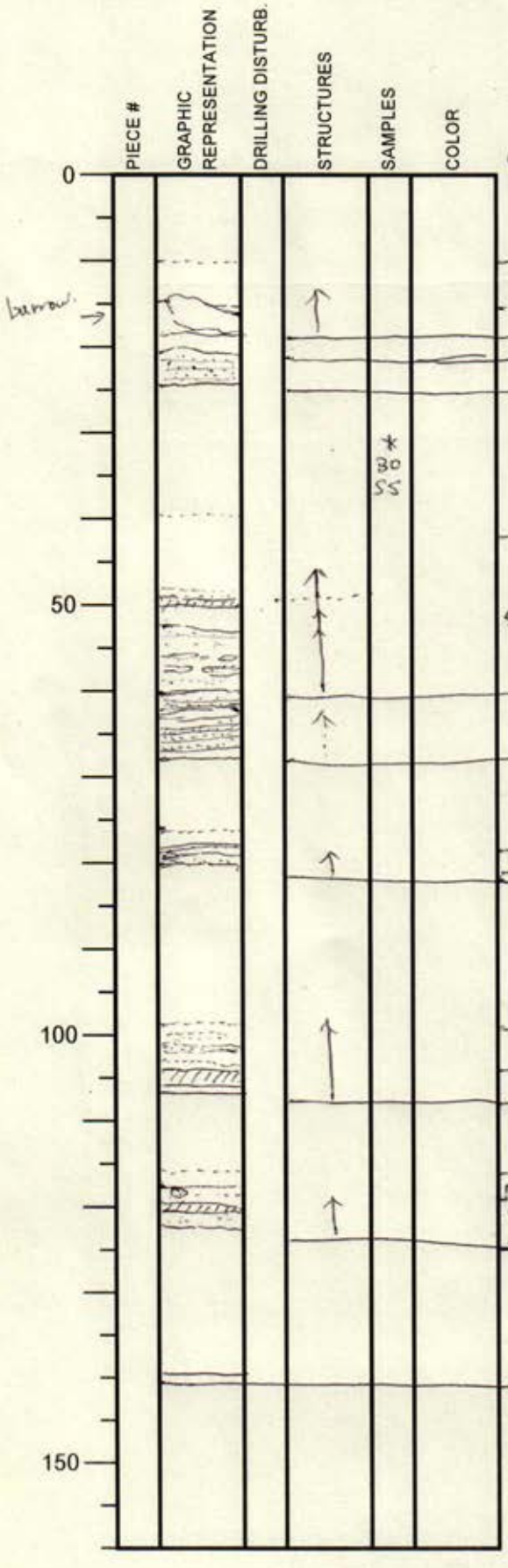

Cap -0.1 SECTION DESCRIPTION

7.5Y3/2 silt biotub

10?

7.5Y3/2 silt massive

14

7.5Y3/1 c. silt sharp

18

20 7.5Y3/2 silt biotub

24.5 7.5Y3/1 c. silt - v.f.s. paral. laminated sharp top & base

7.5Y3/2 silt biotub

39.5

7.5Y3/2 silt massive.

48-49 7.5Y3/2 v-c. silt

49-50 void.

7.5Y3/1 v.f.s-c. silt paral. laminated sharp

60

7.5Y3/1 c. silt & 7.5Y3/2 silt massive alt.

68

7.5Y3/2 silt biotub.

76.5

80 79.5 7.5Y3/2 c. silt sharp base

7.5Y3/2 silt biotub.

98

7.5Y3/2 silt massive with c. silt layers

102.5

104 - 105.5 void 7.5Y3/1 c. silt - v.f.s. graded sharp base

106

7.5Y3/2 silt biotub

116 118.5 7.5Y3/2 silt massive

119 -

120 void. 7.5Y3/1 c. silt graded. sharp base.

121.7

7.5Y3/2 silt biotub sponge spicules

139.5 - 140 void.

140.0

cap 140.1

International Ocean Discovery Program

Visual Core Description

NO.
DATE: 1/8/20
EXP.: 912
SITE/HOLE: c9035/B
CORE: 4H
SECTION: 3A
TOP DEPTH (m CSF): 2541.4 - 2681.5 2
OBSERBER:

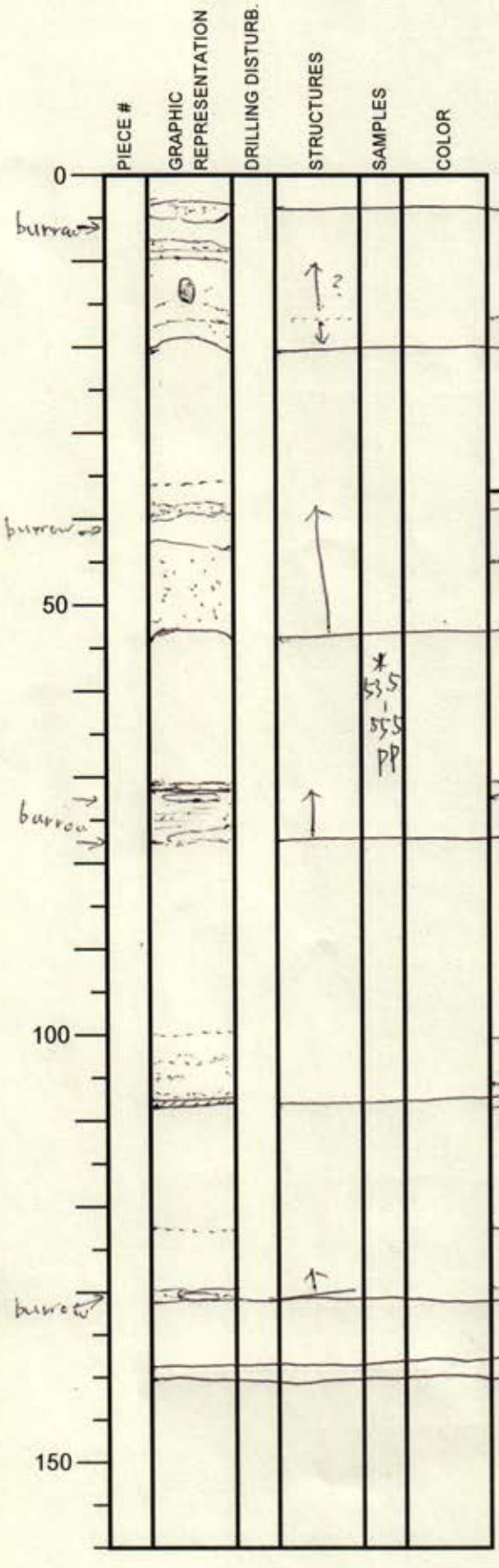

Cap -0.2 SECTION DESCRIPTION

7.5Y3/2 silt bioturb. 3.2

7.5Y3/1 v.f.s-c.silt with silt laminae (bedded)
shell frag bearing 13-15 wood
sharp top & base.
16 muddy
19

7.5Y3/2 silt bioturb
sponge spicule

35.5
37.5 7.5Y3/2 silt massive

~~37.5~~

7.5Y3/1 v.f.s-c.silt
sharp.
52

53.5
55.5
PP

7.5Y3/2 silt bioturb.

90.5
~~90.5~~ 91
98

7.5Y3/1 c.silt paral. laminated
sharp

7.5Y3/2 silt bioturb.

99
106
106.5
102 void

7.5Y3/1 c.silt well sorted sharp

7.5Y3/2 silt bioturb.

121.5
125.5
130.5

7.5Y3/2 silt massive
7.5Y3/2 c.silt sharp base

139.6 void
140

7.5Y3/2 silt bioturb.

Cap 140.4

International Ocean Discovery Program

Visual Core Description

NO.
DATE: 1/ 8/20
EXP.: 912
SITE/HOLE: C9035 / B
CORE: 4H
SECTION: 4A
TOP DEPTH (m CSF): 2681.2 ~ 2821.20
OBSERBER:

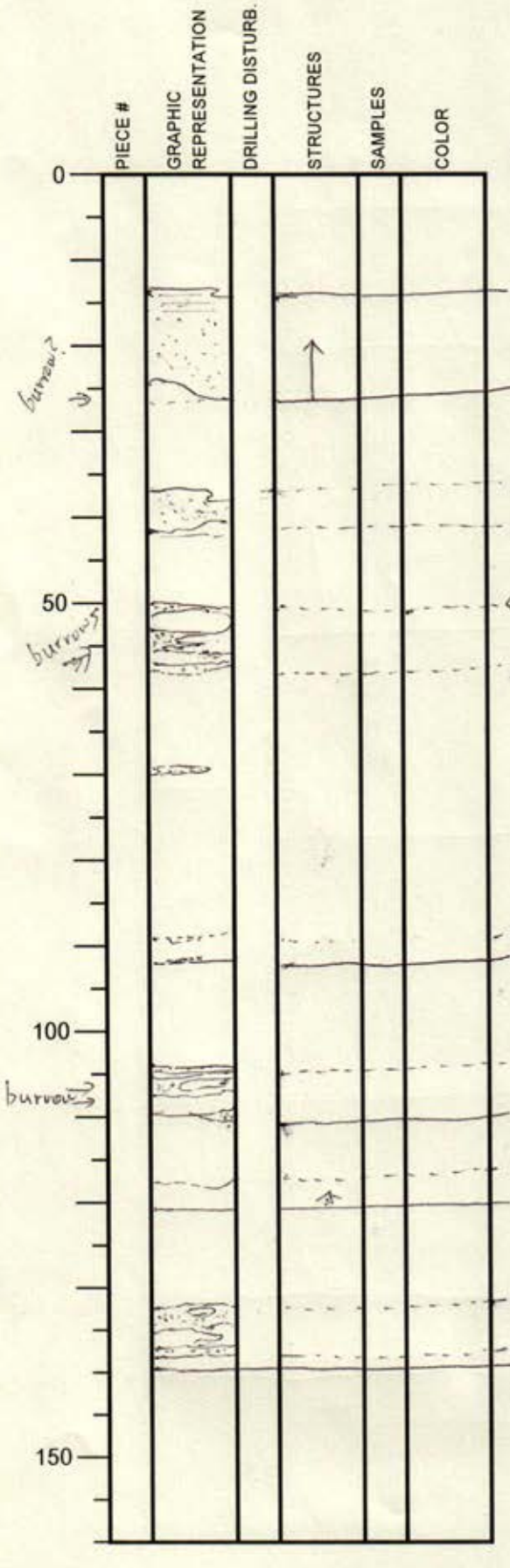

upper part parel. laminated
7.5Y3/1 v.f.s. sharp

7.5Y3/1 c.silt burrowed layer with distortion

7.5Y3/2 c.silt burrowed layer with distortion

7.5Y3/2 silt bioturb

7.5Y3/2 c.silt a burrowed bed? or thin layers

7.5Y 3/2 silt bioturb

7.5Y 3/2 c.silt a burrowed bed

7.5Y3/1 c.silt parel. laminated sharp base

7.5 3/2 silt bioturb.

7.5Y3/2 c.silt a burrowed bed

International Ocean Discovery Program

Visual Core Description

NO.
DATE: 1/8/20
EXP.: 912
SITE/HOLE: C9035/B
CORE: 4H
SECTION: 5A
TOP DEPTH (m CSF): 0
2821.5 –
2961.5
OBSERBER:
2

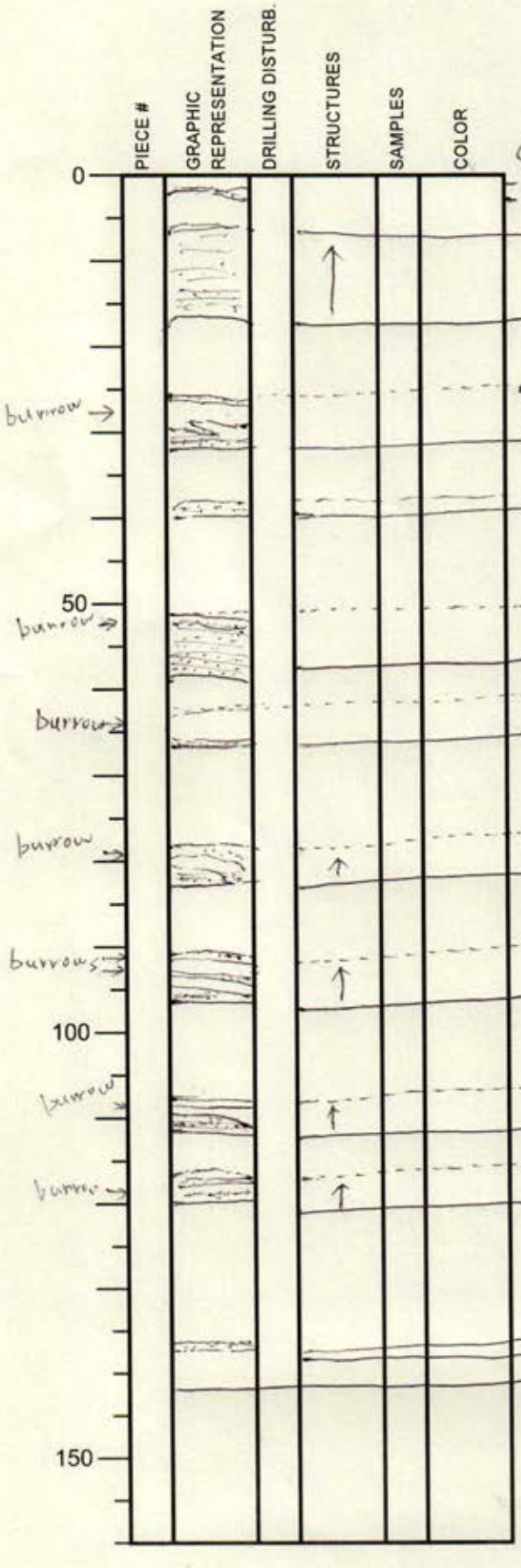

2.5Y3/2 c.silt burrowed
7.5Y3/2 silt bioturb
7.5Y3/1 c.silt paral. laminated
sharp top & base
7.5Y3/2 c.silt paral. laminated sharp
7.5Y3/2 c.silt paral. laminated sharp top & base
bioturb top
7.5Y5/1 c.silt paral. laminated
sharp
7.5Y3/1 v.f.s-c.silt burrowed
sharp base
7.5Y3/2 silt bioturb
7.5Y3/2 c.silt burrowed paral. laminated
sharp top & base
7.5Y3/1 c.silt-v.f.s paral. laminated
sharp burrowed.
7.5Y3/2 c.silt paral. laminated burrowed
sharp top & base
7.5Y3/1 c.silt-v.f.s paral. laminated burrowed
sharp top & base
7.5Y3/2 c.silt sharp top & base.

VCD_sheet_160629

International Ocean Discovery Program

Visual Core Description

NO.
DATE: 1 /8 /20
EXP.: 912
SITE/HOLE: C9035 /B
CORE: 4H
SECTION: 6A
TOP DEPTH (m CSF): 2961.2 - 3101.8
OBSERBER: B

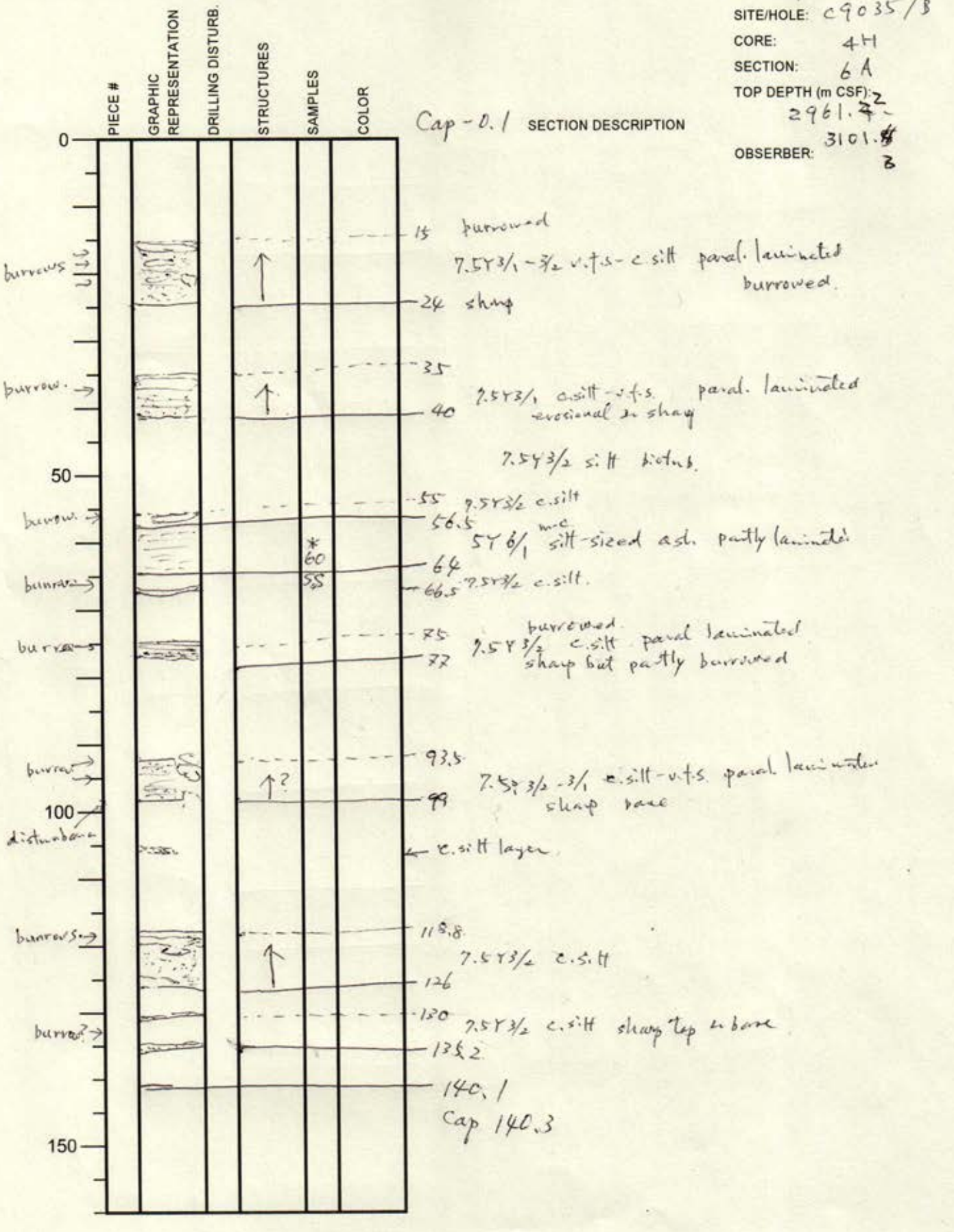

VCD_sheet_160629

International Ocean Discovery Program

Visual Core Description

NO.
DATE: 1/8/20
EXP.: 912
SITE/HOLE: C9305/B
CORE: 4H
SECTION: 2A
TOP DEPTH (m CSF): 3
3101.0 –
OBSERBER: 3241.6
4

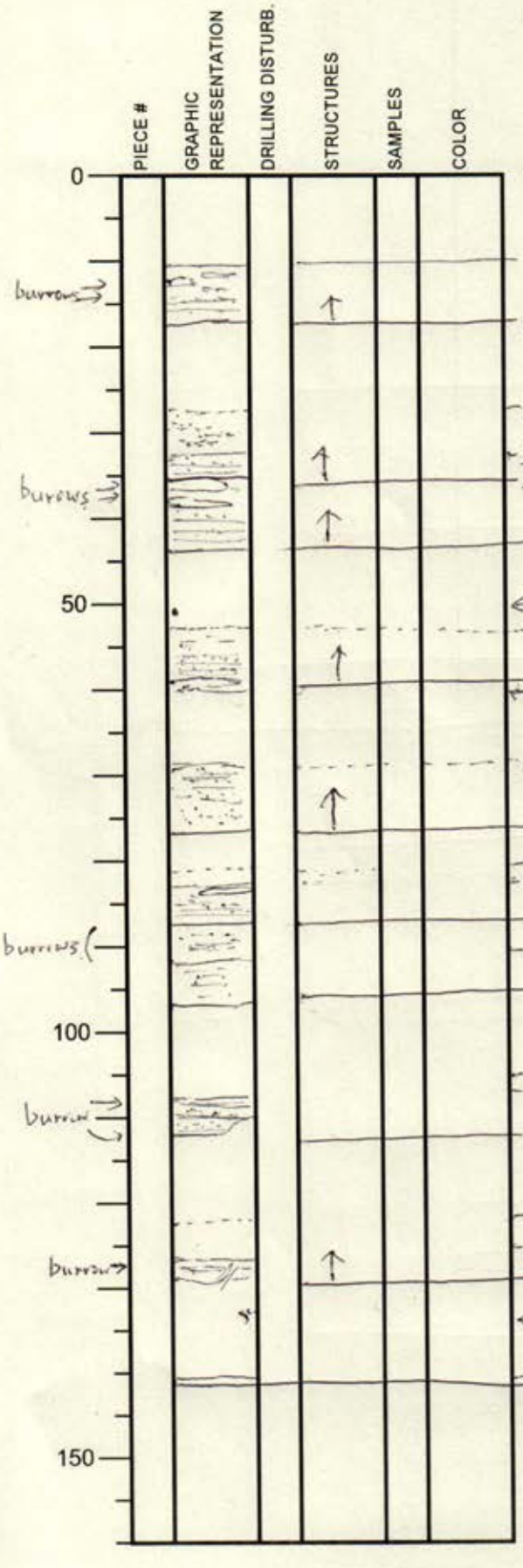

VCD_sheet_160629

International Ocean Discovery Program

Visual Core Description

NO.
DATE: 1/8/20
EXP.: 912
SITE/HOLE: C9035 / B
CORE: 4H
SECTION: 8A
TOP DEPTH (m CSF): 3241.t4
OBSERBER: 3363.4 2

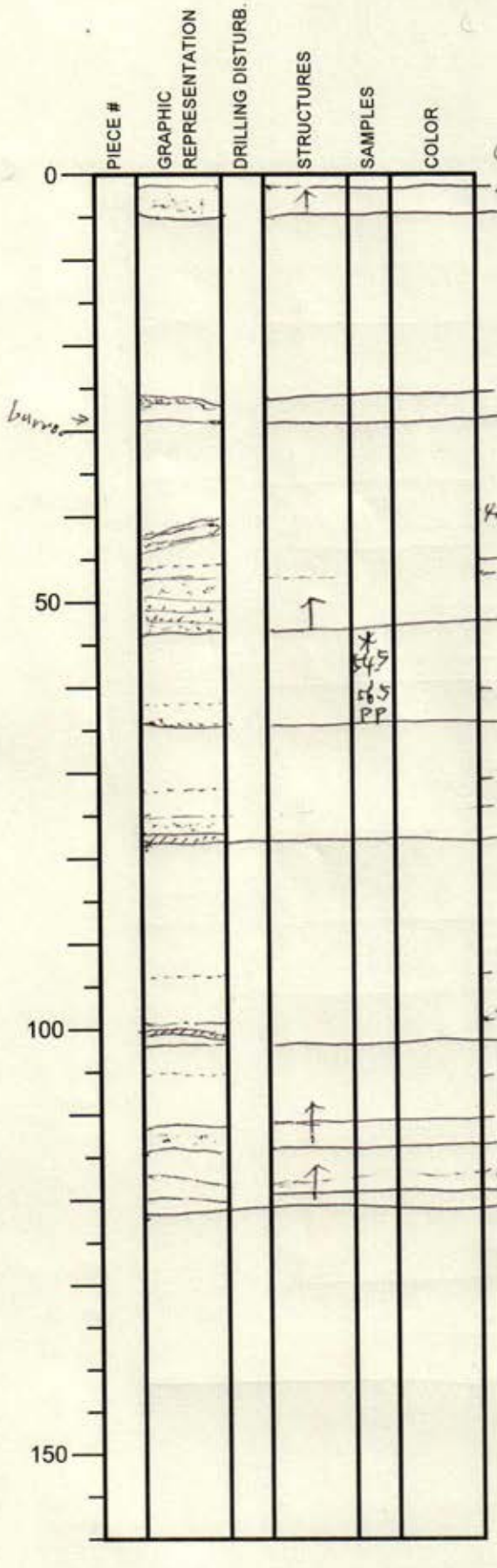

Cap - 0.2 SECTION DESCRIPTION

2
5 7.5Y3/2 c.silt paral laminated sharp but partly burrowed

26.5 sharp top
29 7.5Y3/1 c.silt pumice bearing burrowed base indistinct

40-42 — burrow? c.silt at wall

45.5
47 7.5Y3/2 cm-c.silt

52 7.5Y3/1 v.f.s-c.silt paral. laminated sharp base

54.5
55
PP

61.5
64.5 7.5Y3/1 cm silt layer

72 silt with c.silt layers
75
78 7.5Y3/1 c.silt-v.f.s. sharp base sharp.

77-78 void

94 silt with c.silt layers
99
101 7.5Y3/1 v.f.s-c.silt pumice bearing sharp
99.5-100.5 void
105

110.8
114.5 7.5Y3/2 c.silt massive

118
120 7.5Y3/1 c.silt paral laminated sharp
121.8

Cap 122.0

VCD_sheet_160629

International Ocean Discovery Program

Visual Core Description

NO.
DATE: 1/8/20
EXP.: 912
SITE/HOLE: C9035/B
CORE: 4H
SECTION: CC A
TOP DEPTH (m CSF): 2
3363.4-
OBSERBER: 3402 2.6

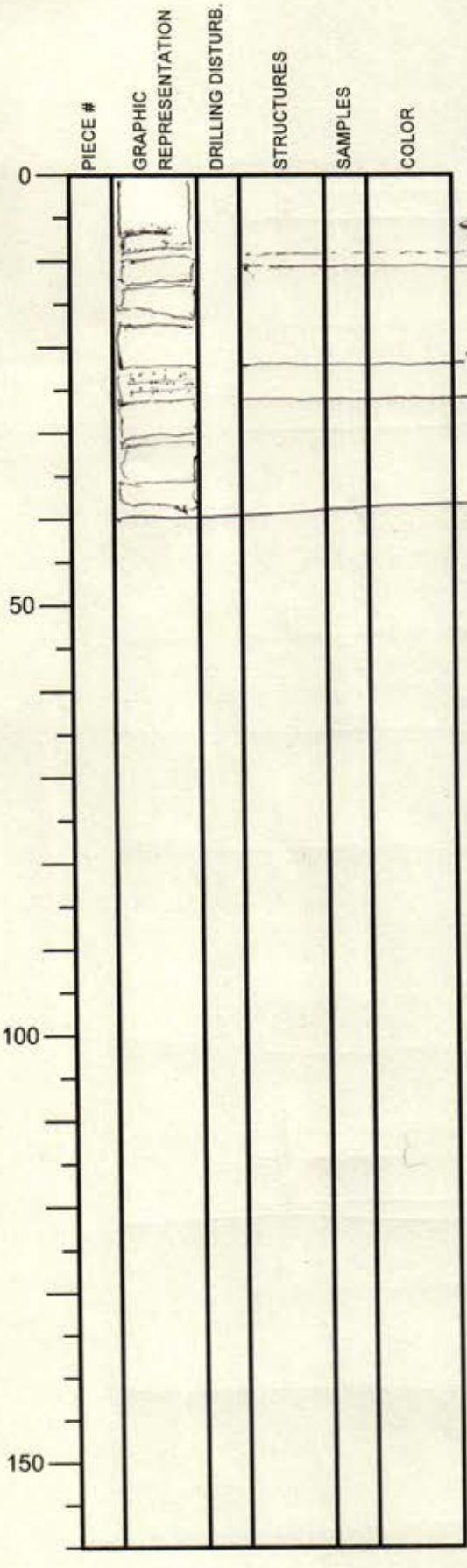

International Ocean Discovery Program

Visual Core Description

NO.
DATE: 1/8/20
EXP.: 912
SITE/HOLE: C9035/B
CORE: 5H
SECTION: 1A
TOP DEPTH (m CSF): 2.6
~~340~~ 354
OBSERBER: ~~350~~ 2.5

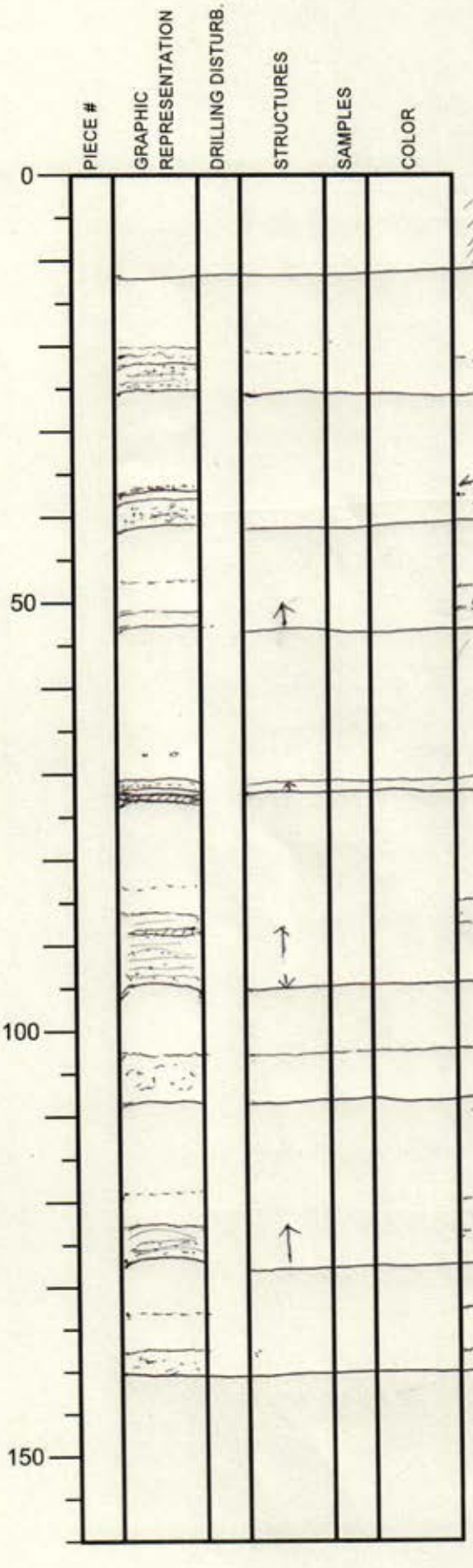

Cap - 0.1

7.5Y4/1 loose mud. Fall-in?

11.2

7.5Y3/2 silt bioturb

20

7.5Y3/2 c. silt upper part paral. laminated

25 sharp

36.5-37 c. silt layer.

38

40.3 7.5Y3/1 c. silt - v.f.s. sharp base & top

47 slightly coarser silt

50.5 7.5Y3/2 c. silt paral. laminated

52.7 sharp base

sponge spicules.

71.5 7.5Y3/1 v.f.s. sharp base & top

72.5-73.5 void.

83.5 slightly coarser silt

85.5 87.5-88 void.

7.5Y3/1 v.f.s. lower & upper paral. laminated

94.5 sharp base

103 7.5Y3/1 v.f.s. sharp top & base mud bundles?

107.5

118.5 slightly coarser.

121.5

126 7.5Y3/1 v.f.s-c. silt paral. laminated sharp

132 silt slightly coarser.

137

138.9 7.5Y3/1 v.f.s massive

140.0 cap

VCD_sheet_160629

International Ocean Discovery Program

Visual Core Description

NO.
DATE: 1/8/20
EXP.: 912
SITE/HOLE: C9035 / B
CORE: 5H
SECTION: 2A
TOP DEPTH (m CSF): 354 2.5 ~~2.0~~
OBSERBER: 368 ~~3.4~~ 2.9

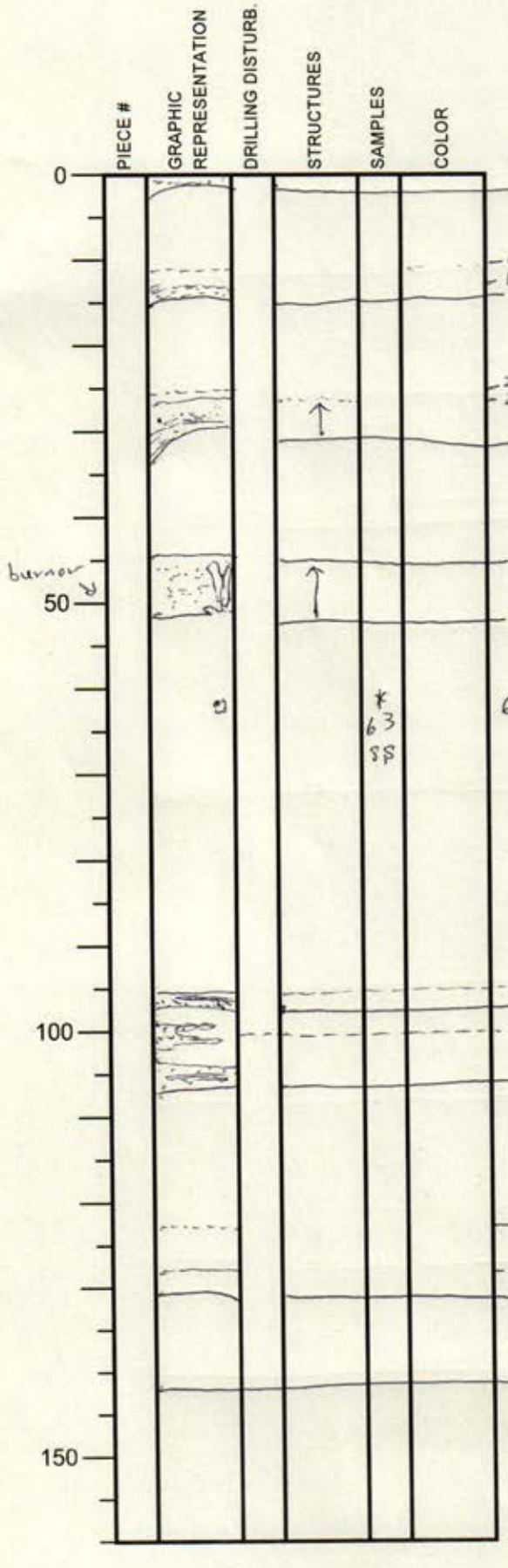

Cap -0.1 SECTION DESCRIPTION

1.5 7.5Y3/1 v.f.s massive sharp.

10.5 slightly coarser
12.8
14.2 7.5Y3/1 c.silt paral.lami sharp bse

7.5Y3/2 silt bioturb

25
25.8 slightly coarser
30.2 7.5Y3/1 v.f.s. cross laminated sharp but disturbed

44.8
7.5Y3/1 v.f.s-c.silt graded sharp top & base
51.2

62.5-63 7.5Y5/1 c.silt-sized ash spot ☆ biotite bearing??

96
98 7.5Y3/2 c.silt burrowed
101 top ?
7.5Y3/1 c.silt-v.f.s. burrowed
102 sharp base

122.5
128 slightly coarser.
130 7.5Y3/2 c.silt sharp

140.4
Cap 140.5

VCD_sheet_160629

International Ocean Discovery Program

Visual Core Description

NO.
DATE: 1/8/20
EXP.: 912
SITE/HOLE: C9035/B
CORE: 5H
SECTION: 3A
TOP DEPTH (m CSF): 29 – 368 ~~384~~ 382 ~~3~~ 29
OBSERBER:

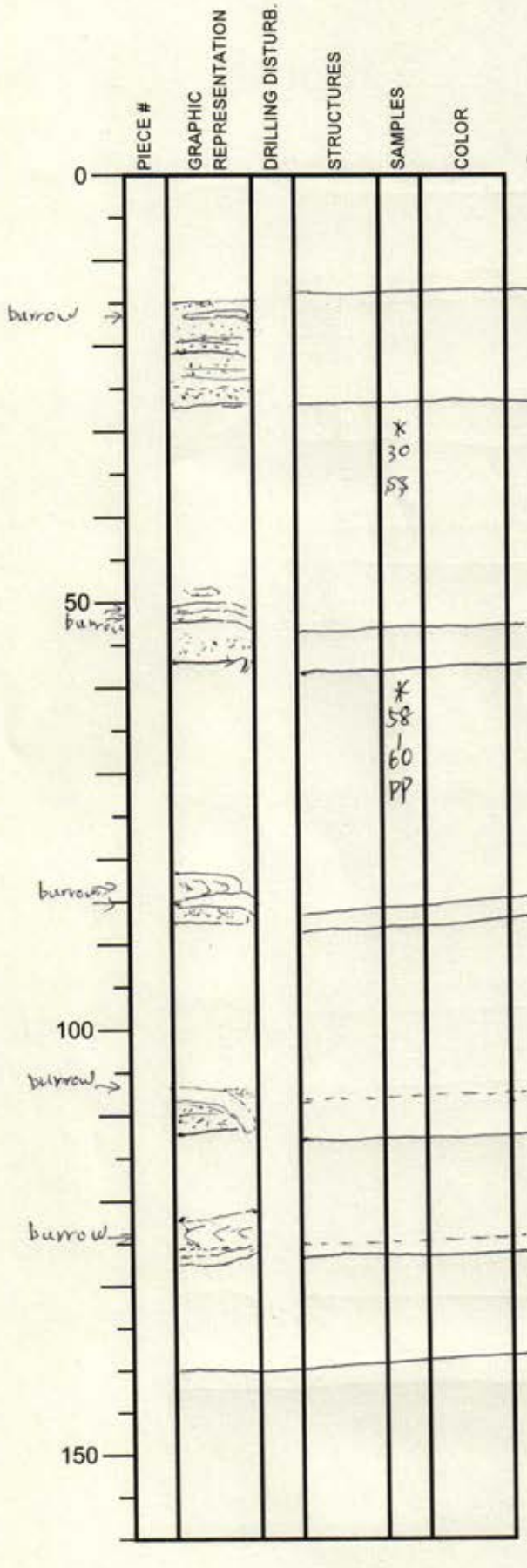

VCD_sheet_160629

International Ocean Discovery Program

Visual Core Description

NO.
DATE: 1/8/20
EXP.: 912
SITE/HOLE: C9035 / B
CORE: 5H
SECTION: 4A
TOP DEPTH (m CSF): 2.9
~~3825.4~~
OBSERBER: 396~~8.4~~
2.9

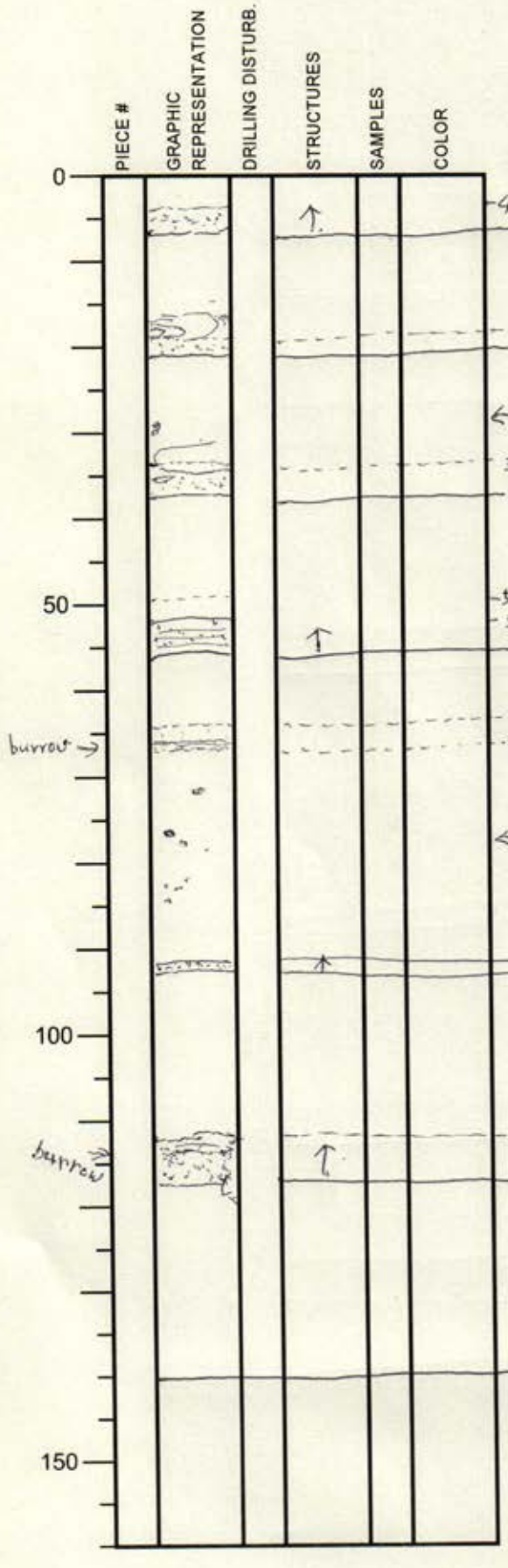

7.5Y3/2 silt
biotumb
sponge spicules

VCD_sheet_160629

International Ocean Discovery Program

Visual Core Description

NO.
DATE: 1/8/20
EXP.: 912
SITE/HOLE: C9035/B
CORE: 5H
SECTION: 5A
TOP DEPTH (m CSF): 2.9
3963.4 -
OBSERBER: 410 3.5

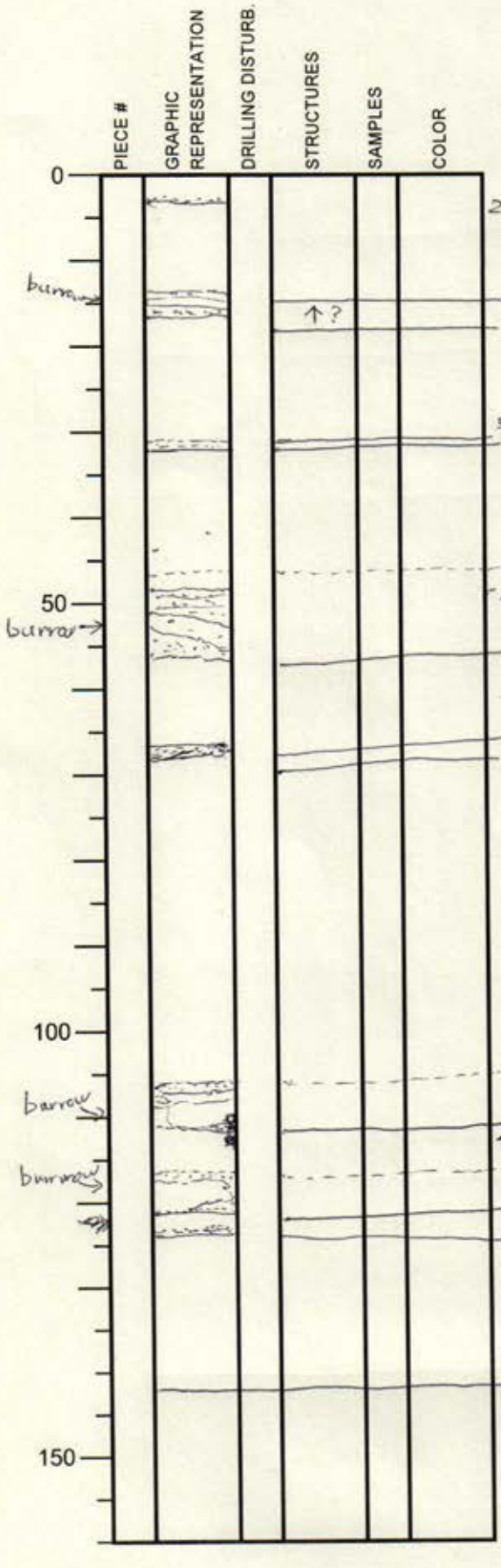

Cap -0.1 SECTION DESCRIPTION

2.2-2.5 c.silt layer

13.2
15.5 7.5Y3/2 c.silt burrowed. sharp base

30.5
31 7.5Y3/1 c.silt.

7.5Y3/2 silt biotub.

46
48
7.5Y3/1 c.silt burrowed upper part paral. laminated
55.5 sharp partly burrowed base

62.5
68.5 7.5Y3/1 c.silt sharp top & base.

105.1 7.5Y3/2 c.silt burrowed.
111
110 subangular pebble 1/cm ϕ.
116.5 7.5Y3/2 c.silt burrowed.
121.5
124.3 7.5Y3/1 c.silt (single layer or bottom of a burrowed layer)

140.6
Cap 140.8

VCD_sheet_160629

International Ocean Discovery Program

Visual Core Description

NO.
DATE: 1/8/20
EXP.: 912
SITE/HOLE: C9035/B
CORE: 5H
SECTION: 6A
TOP DEPTH (m CSF): 3.5
~~410~~
OBSERBER: ~~424~~ 3.5

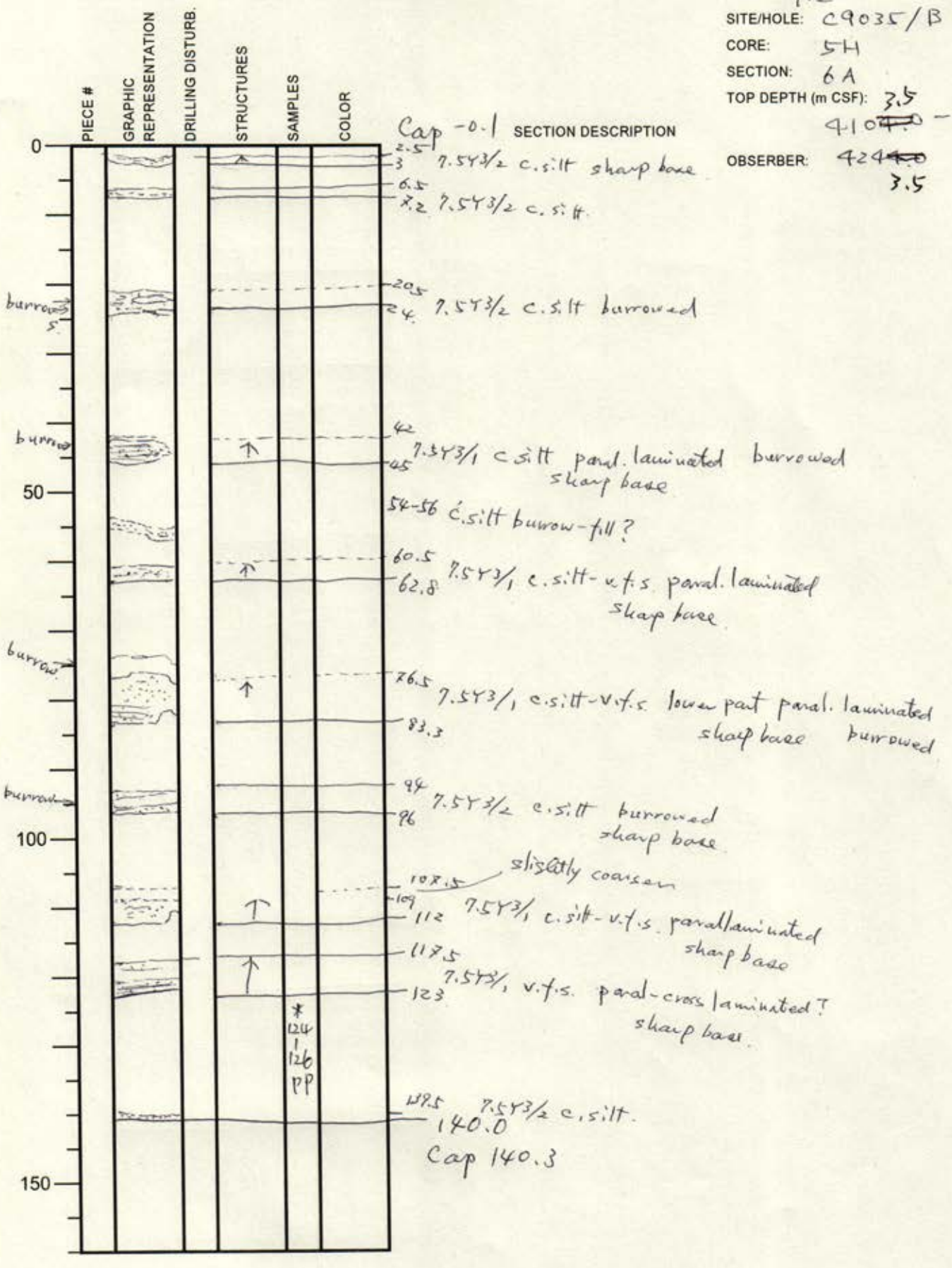

VCD_sheet_160629

International Ocean Discovery Program

Visual Core Description

NO.
DATE: 1 / 8 / 20
EXP.: 912
SITE/HOLE: C9035 / B
CORE: 5H
SECTION: 7A
TOP DEPTH (m CSF): 3.5
~~424~~ 43~~2.0~~
OBSERBER: RL.S

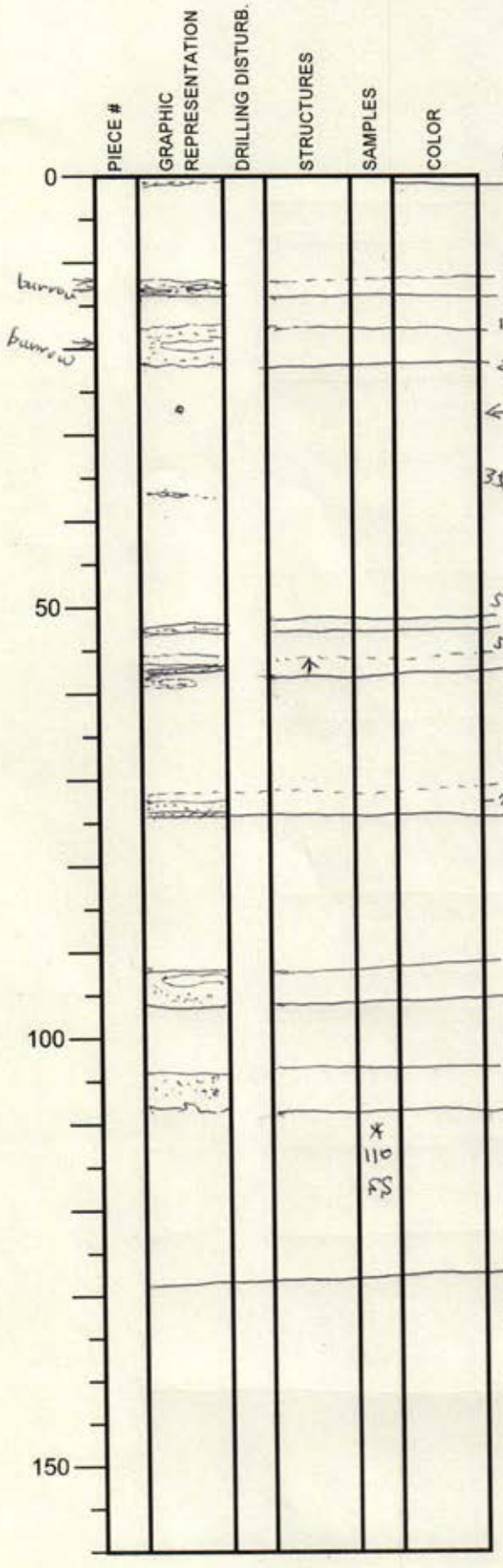

7.5Y3/2 silt biotub.

73.5-74.2 void

VCD_sheet_160629

International Ocean Discovery Program

Visual Core Description

NO.
DATE: 1/8/20
EXP.: 912
SITE/HOLE: C9035 / B
CORE: 5H
SECTION: cc A
TOP DEPTH (m CSF): 433 ~~1.5~~ -
OBSERBER: ~~440.8~~ 6.3

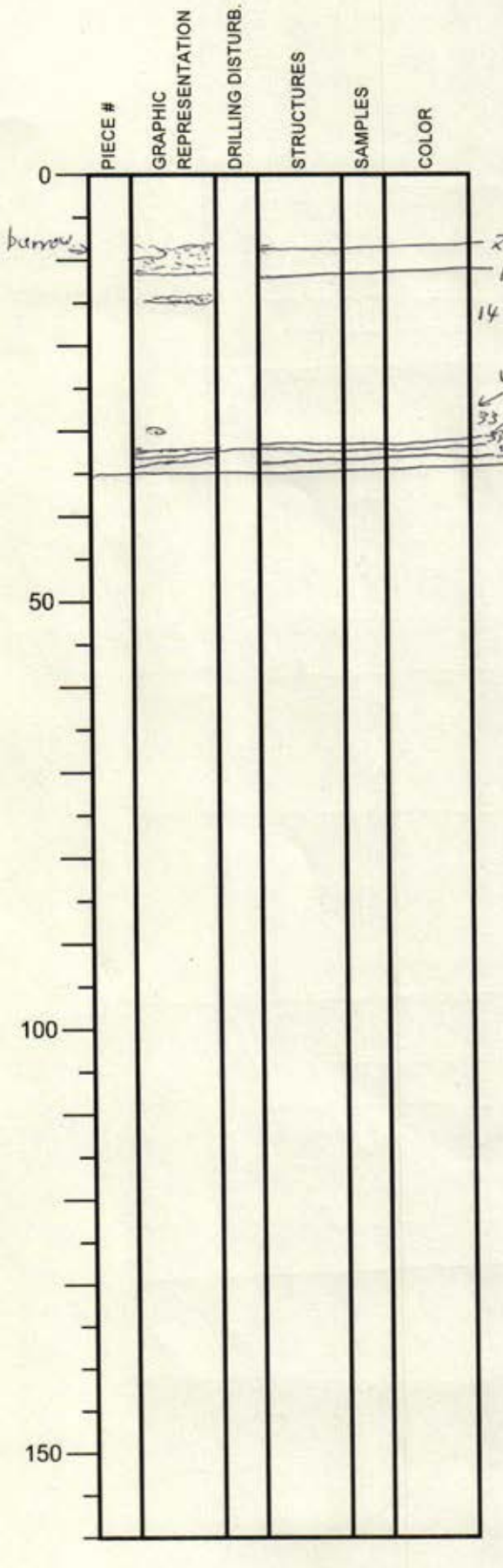

VCD_sheet_160629

International Ocean Discovery Program

Visual Core Description

NO.
DATE: 1/8/20
EXP.: 912
SITE/HOLE: C9035/B
CORE: 6H
SECTION: 1A
TOP DEPTH (m CSF): 4406.83 – 4546.74
OBSERBER:

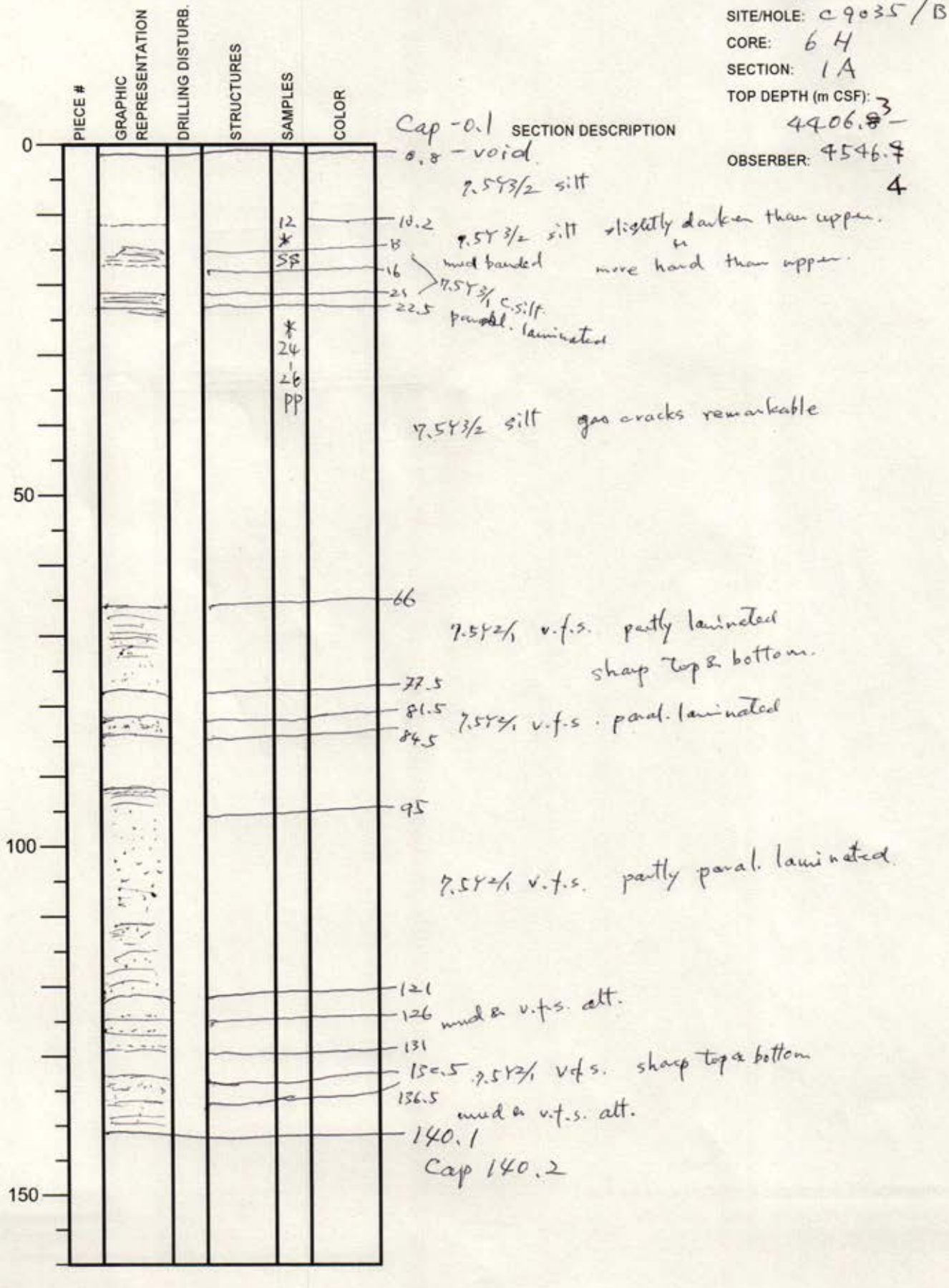

VCD_sheet_160629

International Ocean Discovery Program

Visual Core Description

NO.
DATE: 1/8/20
EXP.: 912
SITE/HOLE: C9035/B
CORE: 6H
SECTION: 2A
TOP DEPTH (m CSF): 4
4546.7-
OBSERBER: 4686.4
4

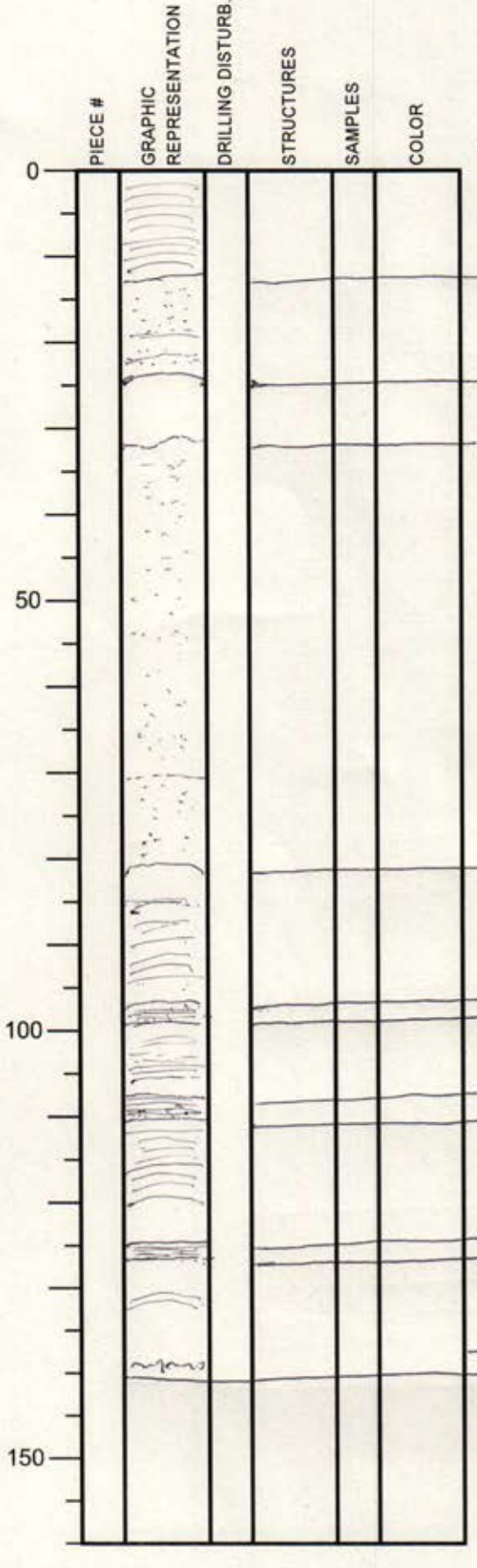

Cap -0.1 SECTION DESCRIPTION

banded mud & v.f.s.

13

7.5Y2/1 v.f.s.

23

7.5Y3/2 silt massive with a few v.f.s. layers

32

7.5Y2/1 v.f.s.

80

banded mud & v.f.s.

96

98.5 7.5Y2/1 v.f.s. para. laminated

banded mud & v.f.s.

107

110 7.5Y2/1, v.f.s para. laminated cross

banded mud & v.f.s.

124.5

126 7.5Y2/1 v.f.s. para-cross laminated

banded mud & v.f.s.

138

140.0 7.5Y4/1 silt. irregular boundary.

Cap 140.1

VCD_sheet_160629

International Ocean Discovery Program

Visual Core Description

NO.
DATE: 1/8/20
EXP.: 912
SITE/HOLE: C9035/B
CORE: 6H
SECTION: 3A
TOP DEPTH (m CSF): 4
4686.7-
OBSERBER: 482 ~~9.4~~ 8.9

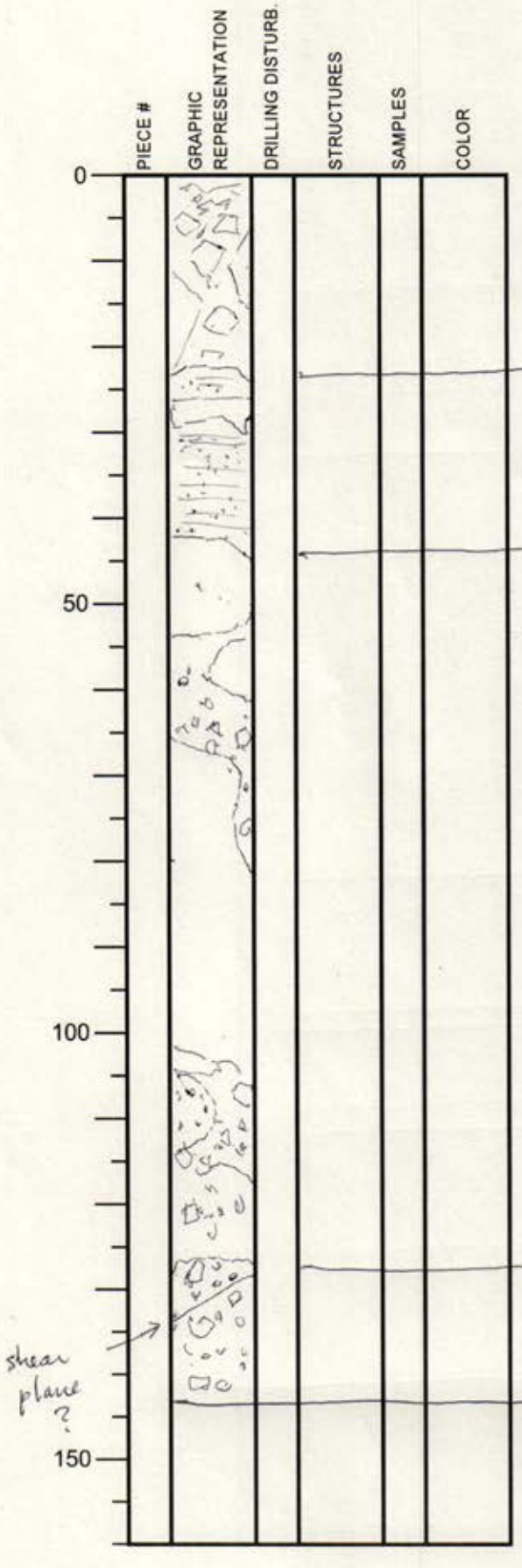

Cap-0.2 . SECTION DESCRIPTION

angular gravels. varicolored mudstone

23

7.5Y 2/1 v.f.s. para-cross laminated

42.5

large s.st gravels fill by matrix supported angular pebbles and f.s?

chaotic matrix-supported angular gravels

128

poorly sorted angular gravels. matrix rich.

142.5

Cap 142.8

VCD_sheet_160629

International Ocean Discovery Program

Visual Core Description

NO.
DATE: 1/8/20
EXP.: 912
SITE/HOLE: C9035/B
CORE: 6H
SECTION: 4A
TOP DEPTH (m CSF): 8.9 – 482~~9.4~~7 497~~3.3~~ 2.8
OBSERBER:

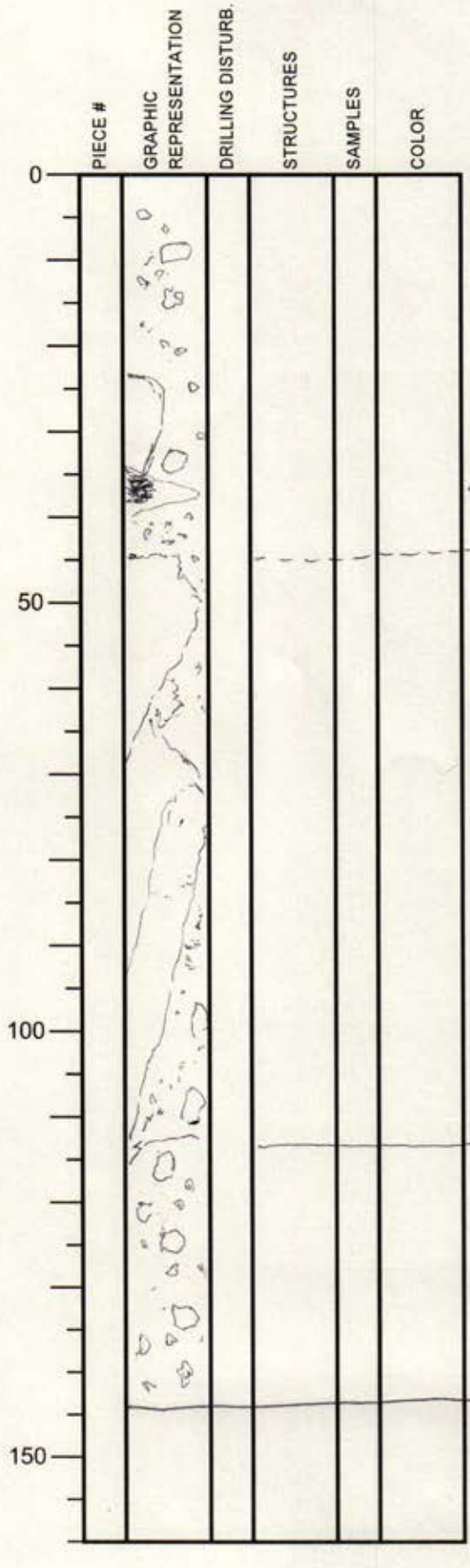

chaotic
angular gravel
matrix support.

140.1 patched

VCD_sheet_160629

International Ocean Discovery Program

Visual Core Description

NO.
DATE: 1/8/20
EXP.: 912
SITE/HOLE: C9035 / B
CORE: 6H
SECTION: 5A
TOP DEPTH (m CSF): 497 ~~2.8~~ 5113.7
OBSERBER: Z

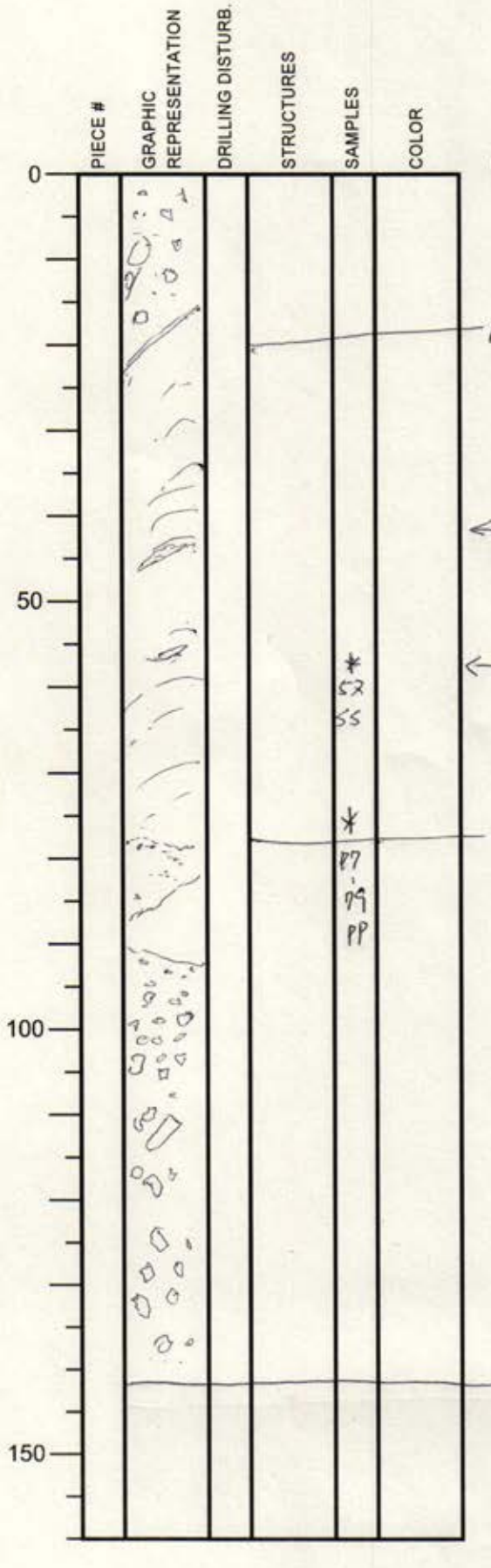

chaotic matrix supported angular gravel with distorted silt layer

136.3
Patch

VCD_sheet_160629

International Ocean Discovery Program

Visual Core Description

NO.
DATE: 1/8/20
EXP.: 912
SITE/HOLE: C9035/B
CORE: 6H
SECTION: 6A
TOP DEPTH (m CSF): 2
5113.7 -
OBSERBER: 52 ~~30.0~~ 29.5

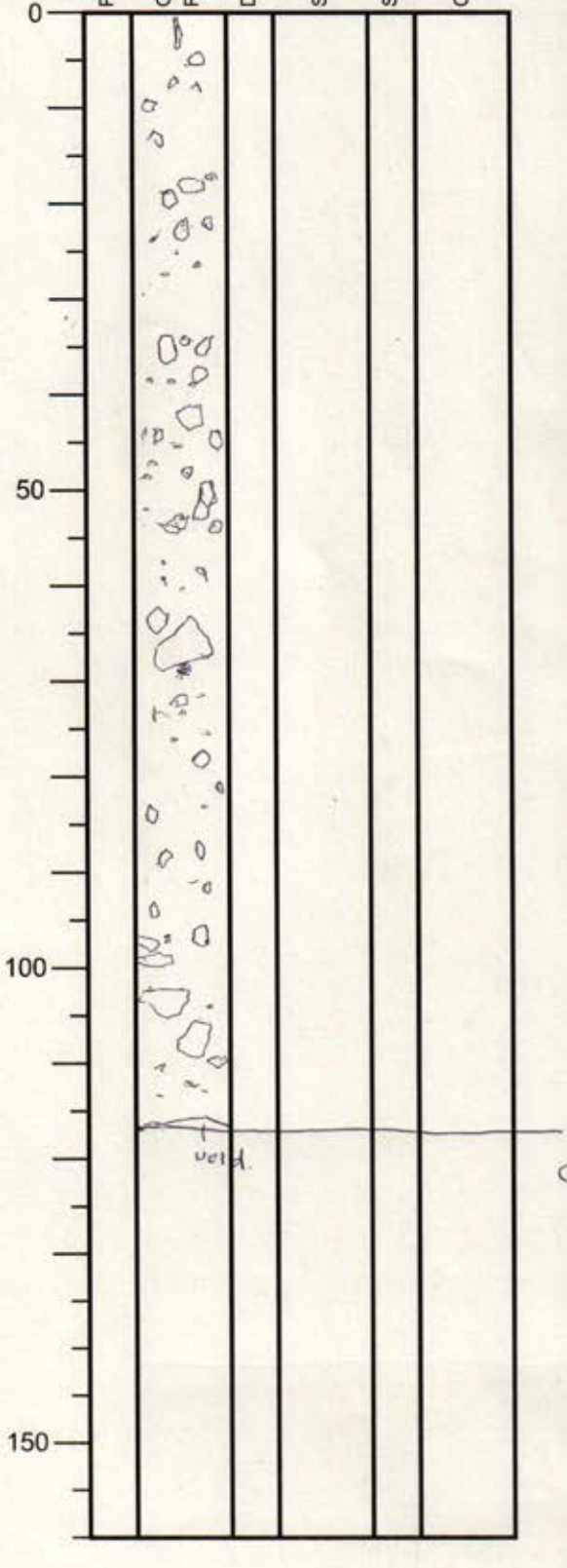

VCD_sheet_160629

International Ocean Discovery Program

Visual Core Description

NO.
DATE: 1/8/20
EXP.: 912
SITE/HOLE: C9035/B
CORE: 6H
SECTION: CC A
TOP DEPTH (m CSF): 295-
~~5238.0~~ 5259.7
OBSERBER:
matrix 2
7.5Y4/1 silt

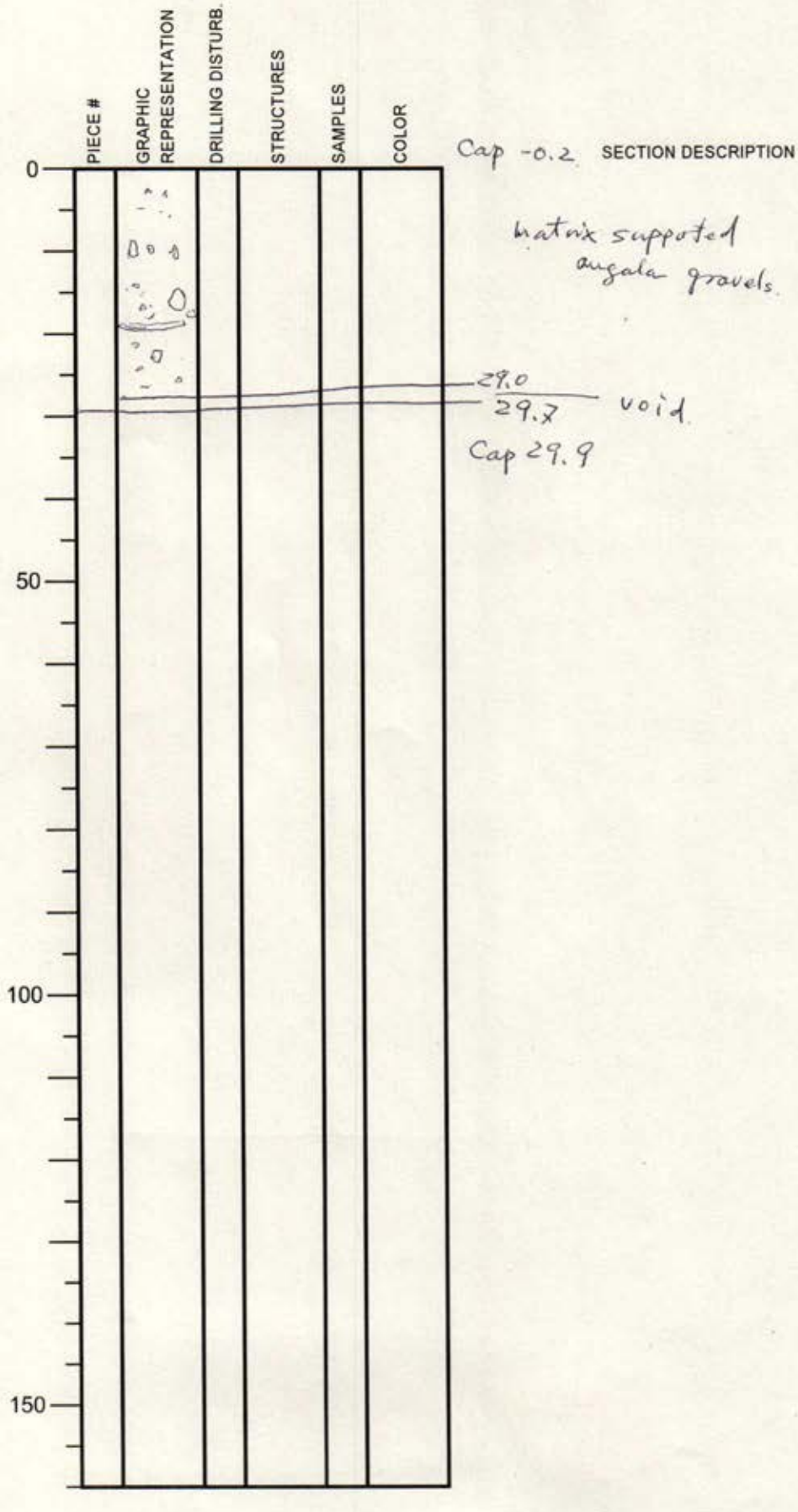

VCD_sheet_160629

International Ocean Discovery Program

Visual Core Description

NO.
DATE: 1/8/20
EXP.: 912
SITE/HOLE: C9035/B
CORE: 8H
SECTION: 1A
TOP DEPTH (m CSF): 5259.2
OBSERBER: 539 8.8

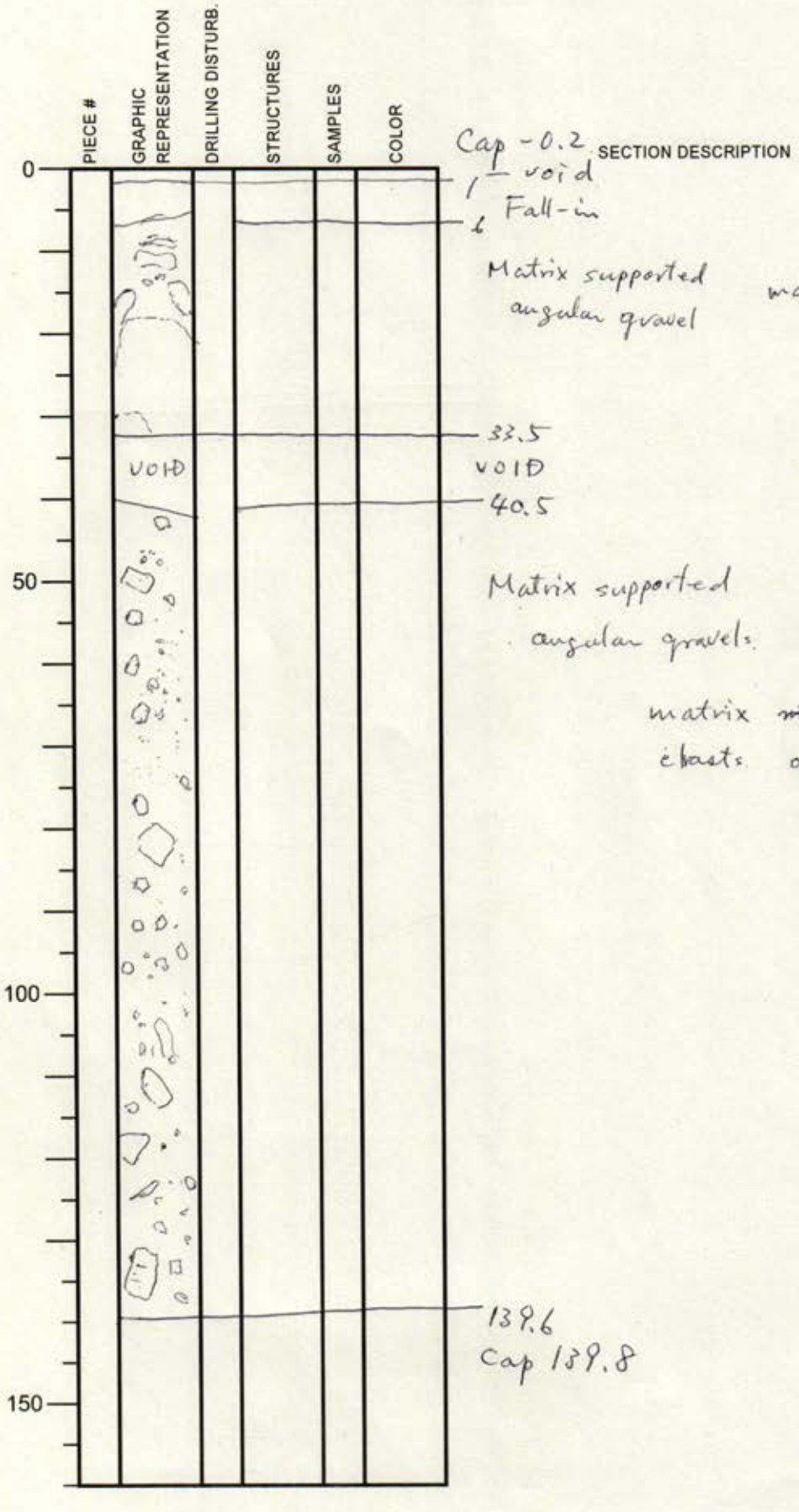

VCD_sheet_160629

International Ocean Discovery Program

Visual Core Description

NO.
DATE: 1/8/20
EXP.: 912
SITE/HOLE: C9035 / B
CORE: 7H
SECTION: 2A
TOP DEPTH (m CSF): 8.8 ~~539.3~~
OBSERBER: ~~554.0~~ 0.5

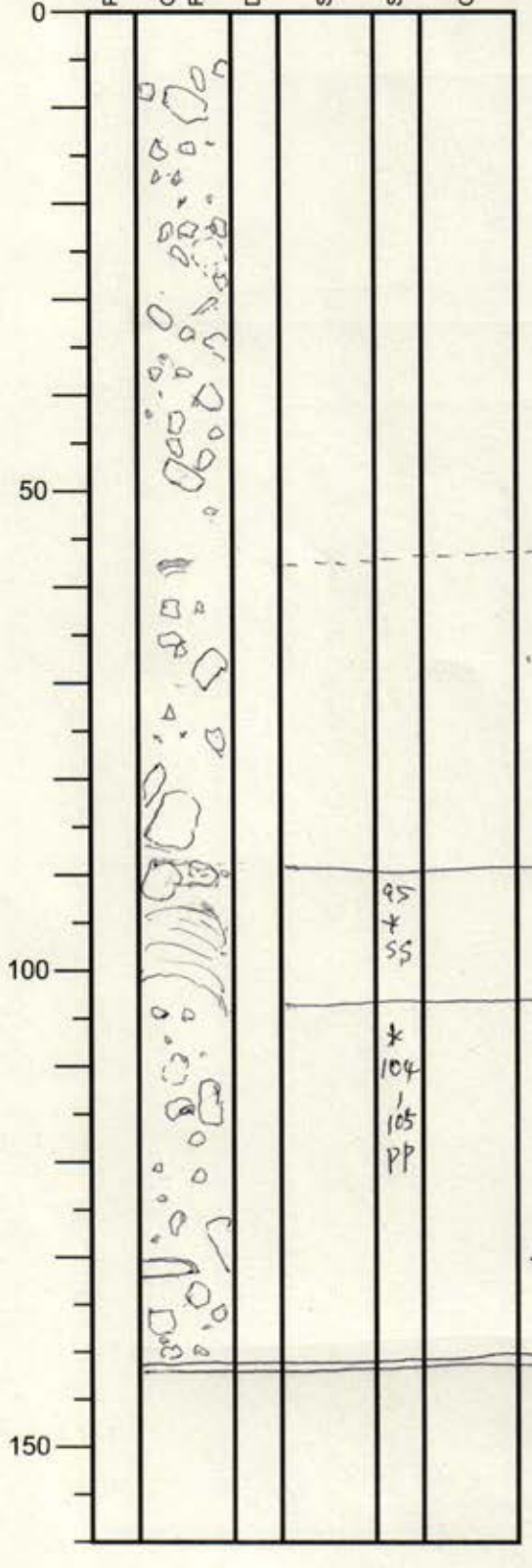

Matrix supported angular gravels.
matrix 5Y4/1 sandy mud.
clast mudstone.
most of them <1cm
max. 3-4cm

matrix rich

← clast ~4cm

distorted silt layer.
2.5Y4/1

Matrix supported angular gravels
matrix 5Y4/1 sandy mud
clast mudstone
most of them < 1cm
max. 3cm

← platy 4cm long.

void.

Cap 141.9

135.6cm patched

VCD_sheet_160629

International Ocean Discovery Program

Visual Core Description

NO.
DATE: 1/8/20
EXP.: 912
SITE/HOLE: C9035/B
CORE: 7H
SECTION: 3A
TOP DEPTH (m CSF): 554.5 - 563.5
OBSERBER: O

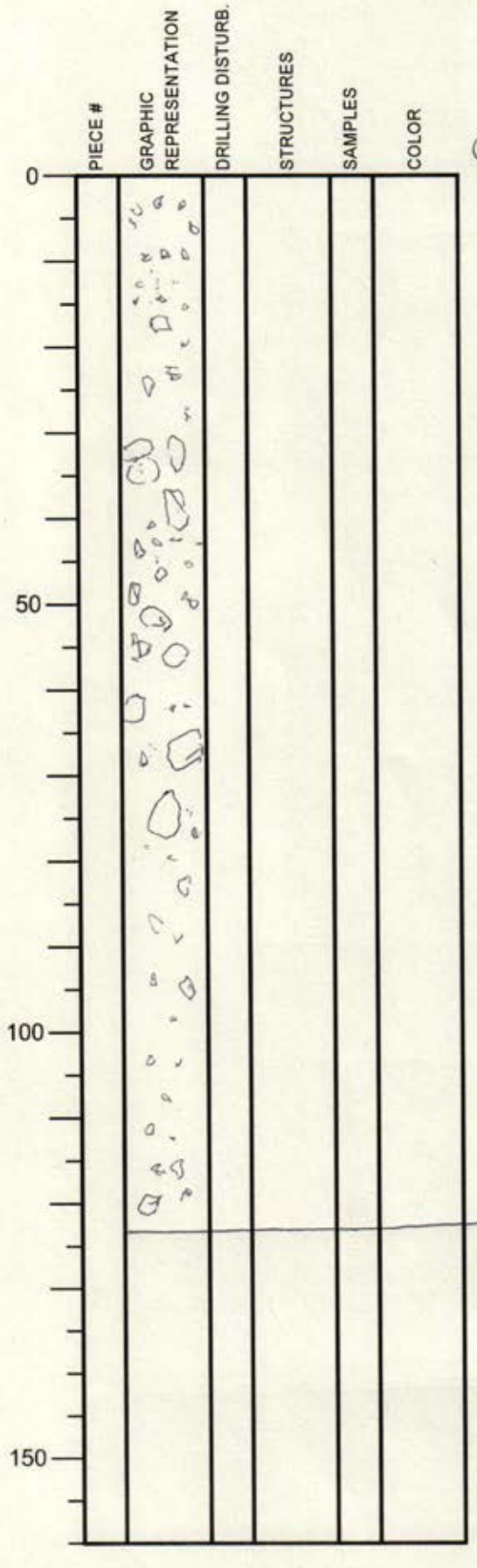

VCD_sheet_160629

International Ocean Discovery Program

Visual Core Description

NO.
DATE: 1 /2 / 20
EXP.: 912
SITE/HOLE: C9035 / B
CORE: 7H
SECTION: 4A
TOP DEPTH (m CSF): 0
5663.5 -
OBSERBER: ~~5784.3~~
5784.3

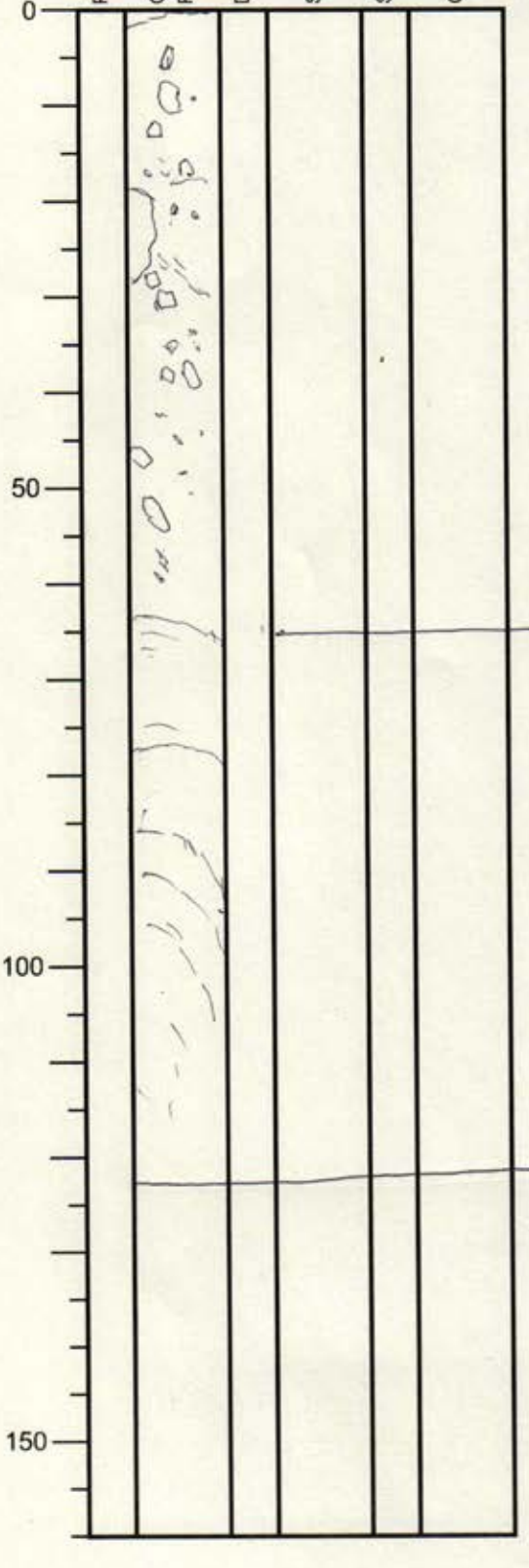

matrix supported
angular gravels.
matrix 5Y 4/1 silt
clast mudstone
< 1cm
max ~ 2cm.

distorted silt layer.
2.5Y 4/1

VCD_sheet_160629

International Ocean Discovery Program

Visual Core Description

NO.
DATE: 1/8/20
EXP.: 912
SITE/HOLE: C9035/B
CORE: 7H
SECTION: 5A
TOP DEPTH (m CSF): 5784.3 – 5909.8
OBSERBER:

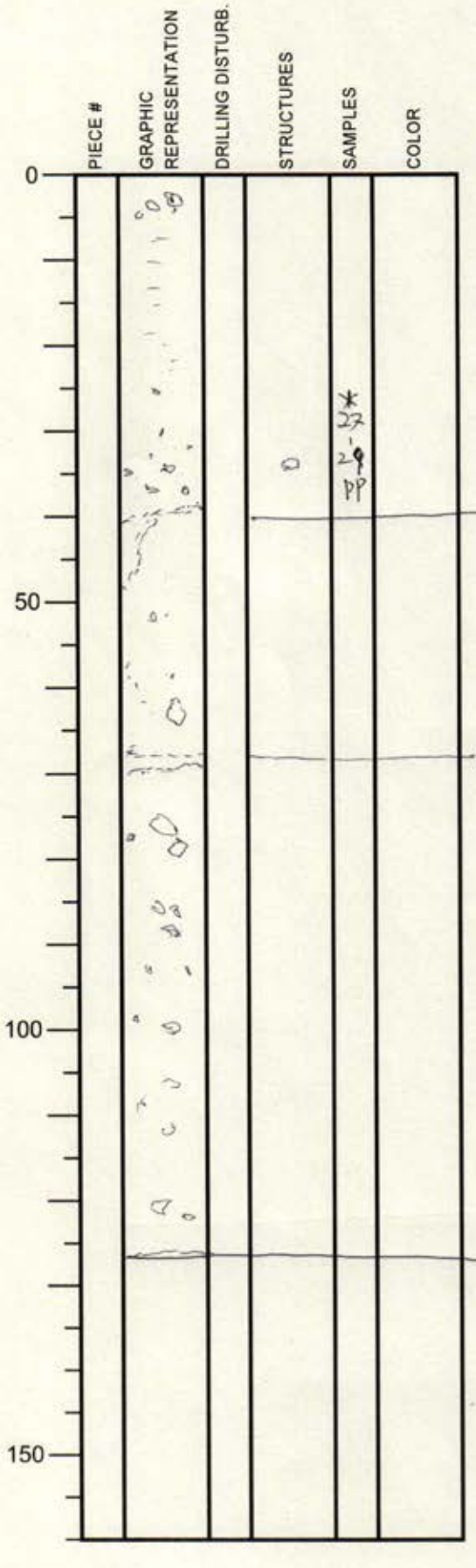

VCD_sheet_160629

International Ocean Discovery Program

Visual Core Description

NO.
DATE: 1/8/20
EXP.: 912
SITE/HOLE: C9035/B
CORE: 7H
SECTION: CCA
TOP DEPTH (m CSF): 5909.8-
OBSERBER: 5950.8.

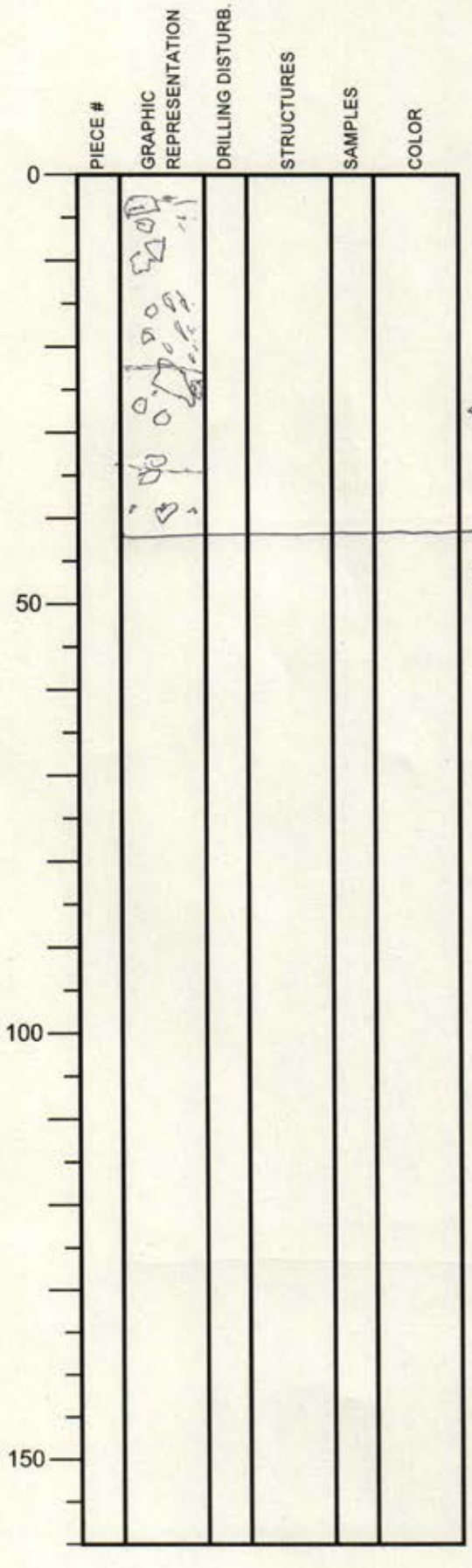

VCD_sheet_160629

International Ocean Discovery Program

Visual Core Description

NO.
DATE: 1/9/20
EXP.: 912
SITE/HOLE: C9035/B
CORE: 8H
SECTION: 1A
TOP DEPTH (m CSF): 5950.8 – 6023.6
OBSERBER:

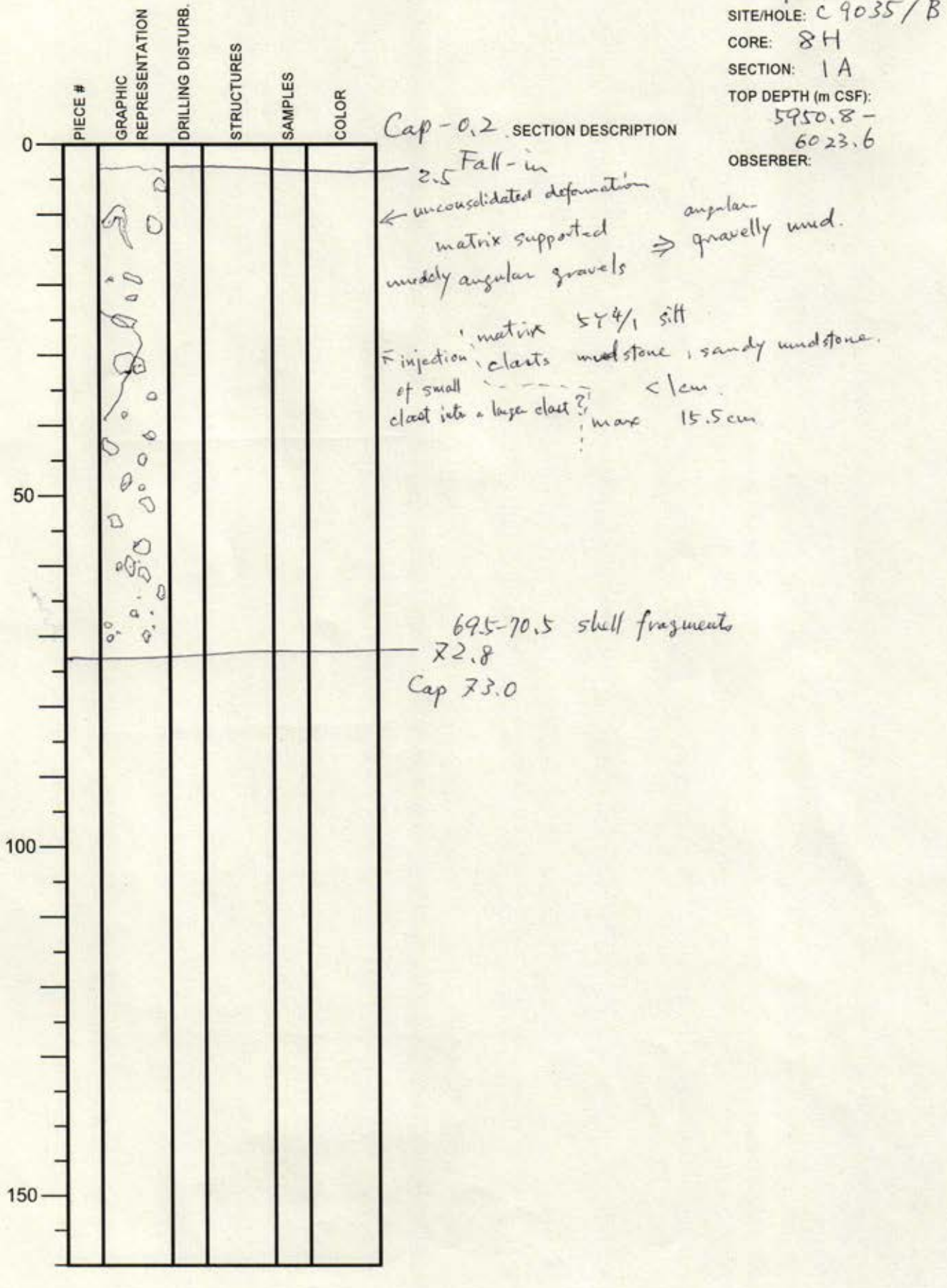

VCD_sheet_160629

International Ocean Discovery Program

Visual Core Description

NO.
DATE: 1/9/20
EXP.: 912
SITE/HOLE: C9035/B
CORE: 8H
SECTION: 2A
TOP DEPTH (m CSF): 6023.6 – 6163.4
OBSERBER:

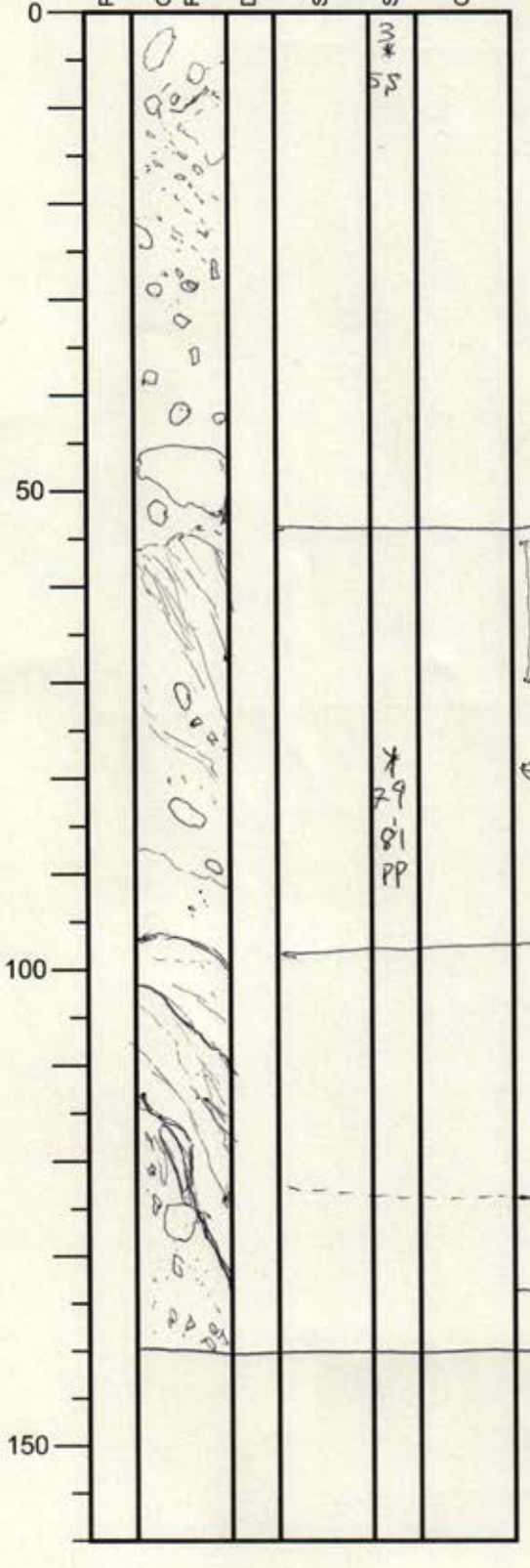

matrix supported
muddy angular gravels.
matrix 7.5Y4/1 silt
clast mudstone
< 1cm
max > ~ 8cm

53 distorted silt layer
matrix supported
muddy angular gravels with distorted silt layer
matrix 7.5Y4/1 silt
clast mudstone ~ <0.5cm
mak. 2cm.

← distorted silt layer.

97
7.5Y3/1 sheared mudstone (blocks)

125
matrix supported
muddy angular gravels.
matrix 7.5Y4/1 silt
clast mudstone <0.5cm
max. 2cm.
134
139.8
Cap 139.9

VCD_sheet_160629

International Ocean Discovery Program

Visual Core Description

NO.
DATE: 1/ 9/20
EXP.: 912
SITE/HOLE: C9035/B
CORE: 8H
SECTION: 3A
TOP DEPTH (m CSF): 6163.4 - 6381.9
OBSERBER: 1

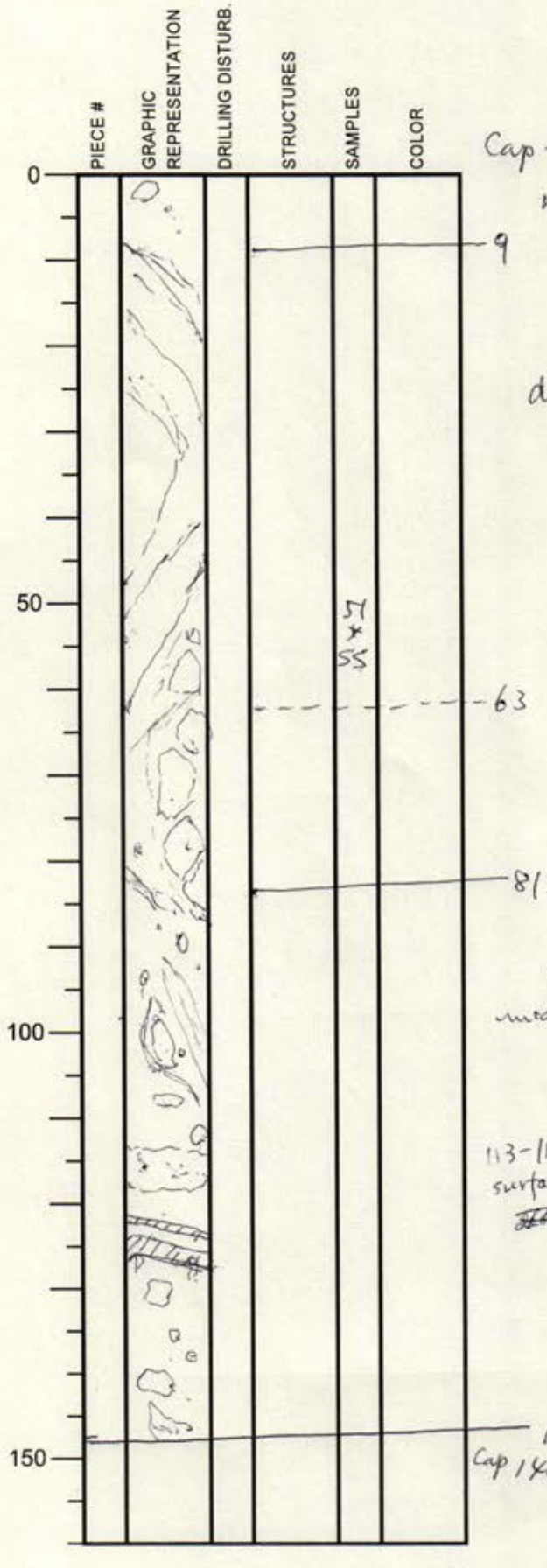

Cap -0.6

matrix supported angular gravels muddy

distorted silt layer
7.5YR 3/1
partly blocky.

51
x
55

matrix supported
muddy angular gravels
matrix 5Y4/1 silt.
clast · mudstone, muddy sandstone
<1cm.
max. ~3cm.

113-118
surface disturbed

122-123 void.
124.5-126.5 void

140.5
patched

Cap 148.1

VCD_sheet_160629

International Ocean Discovery Program

Visual Core Description

NO.
DATE: 1/9/20
EXP.: 912
SITE/HOLE: C9035/B
CORE: 8H
SECTION: 4A
TOP DEPTH (m CSF):
6~~4~~1.4 - ~~649~~.0
OBSERBER: 59

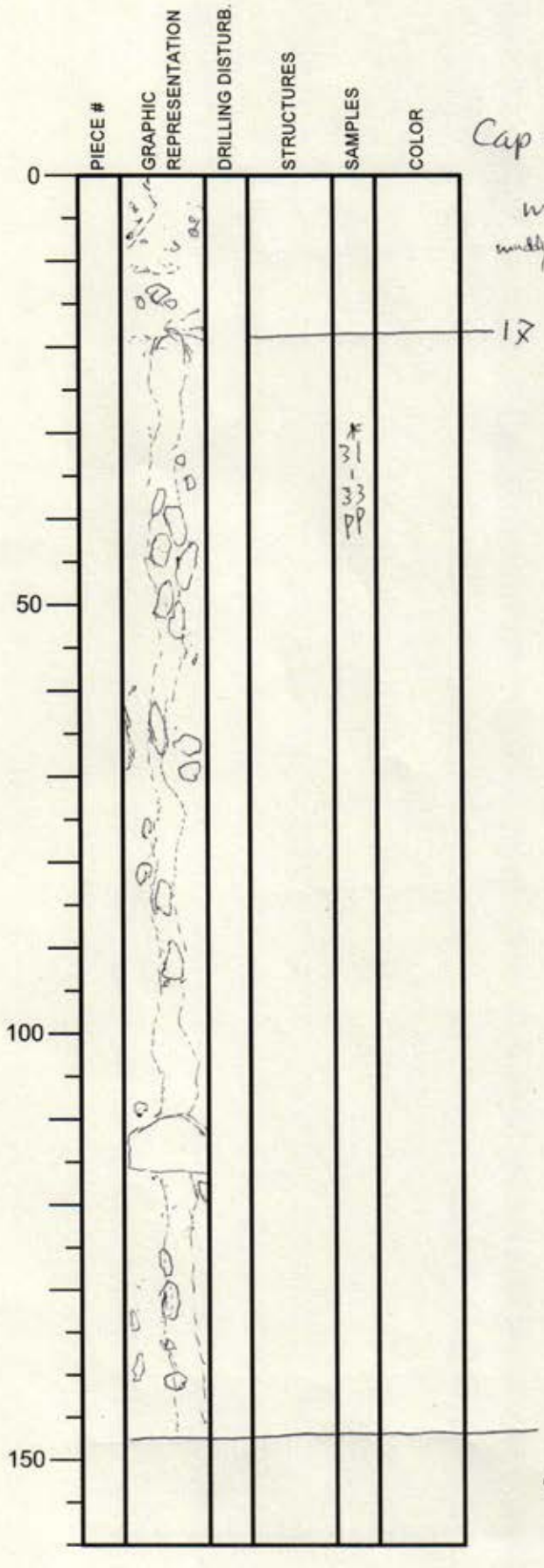

141.0
patched.

VCD_sheet_160629

International Ocean Discovery Program

Visual Core Description

NO.
DATE: 1/9/20
EXP.: 912
SITE/HOLE: C9035 / B
CORE: 8H
SECTION: 5A
TOP DEPTH (mbsf): 6449.0 – ~~6591.6~~ 6601.6
OBSERBER:

Cap - 1.1 SECTION DESCRIPTION

flow-in
matrix supported
muddy angular gravels

142.6
Cap 142.8.

linear 142.3

140.4
patched

VCD_sheet_160629

International Ocean Discovery Program

Visual Core Description

NO.
DATE: 11 9 20
EXP.: 912
SITE/HOLE: C9035 / B
CORE: 8H
SECTION: 6A
TOP DEPTH (m CSF): ~~6591.6~~ 6601.6 ~ 66~~55~~.1
OBSERBER: ~~95~~

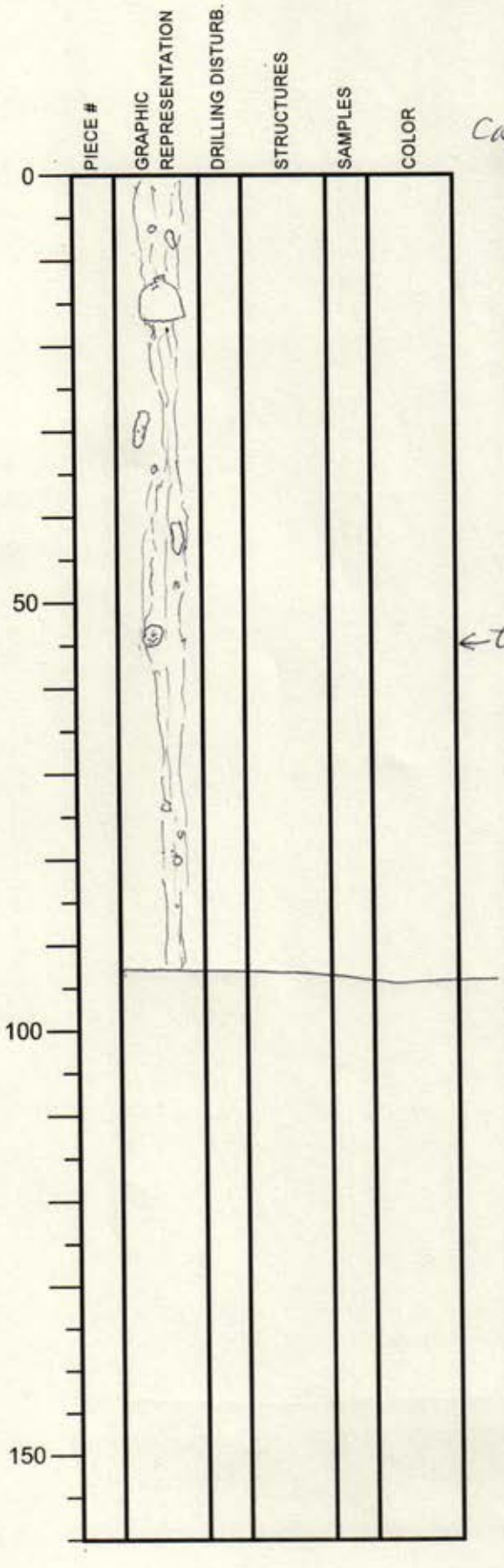

VCD_sheet_160629

International Ocean Discovery Program

Visual Core Description

NO.
DATE: 1/9/20
EXP.: 912
SITE/HOLE: C9035 / B
CORE: 8H
SECTION: CC A
TOP DEPTH (m CSF): 66~~6~~.95 / 67~~7~~.7
OBSERBER: ~~z~~9

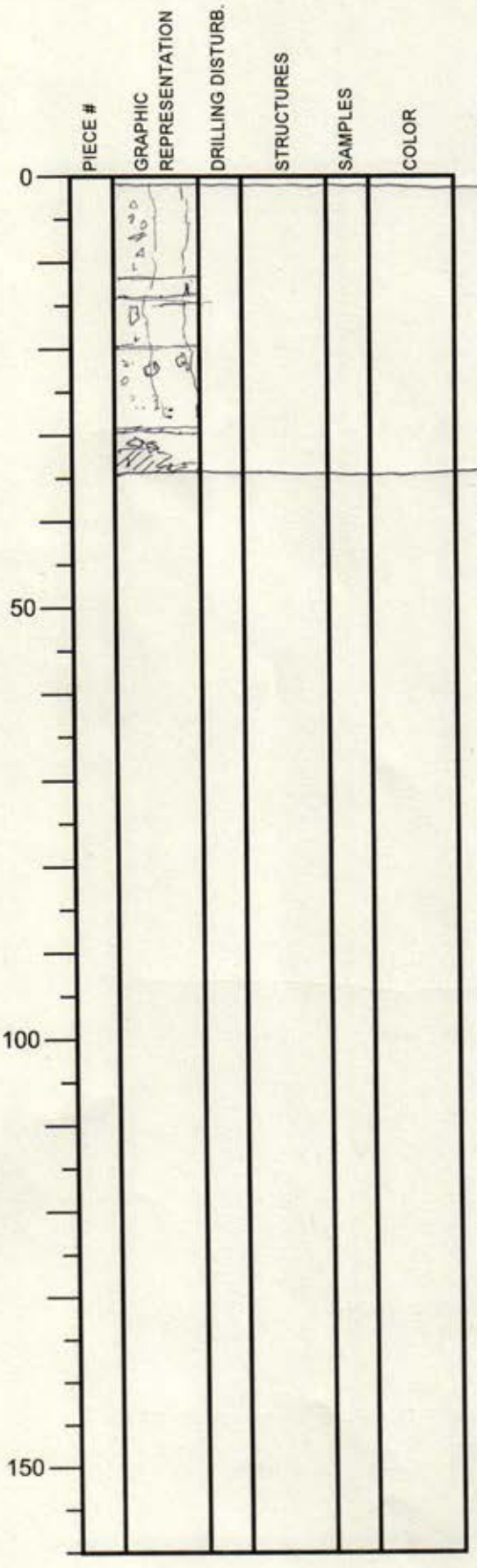

29.2 - 29.7 void

VCD_sheet_160629

International Ocean Discovery Program

Visual Core Description

NO.
DATE: 1/9/20
EXP.: 912
SITE/HOLE: C9035/B
CORE: 9H
SECTION: 1A
TOP DEPTH (m CSF):
~~67~~ 67.7 – 29
OBSERBER: 68~~50~~.0 60

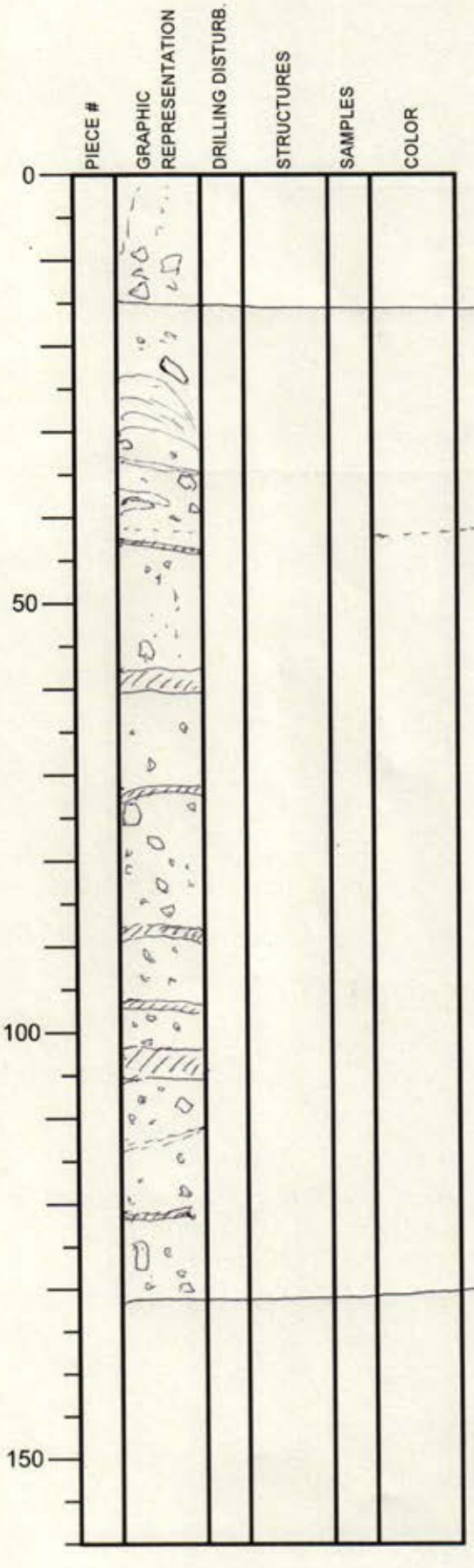

33 crack

43.5-44.5 void

57-60 void

70.5-71.5 void

88-89 void

95.7-96.7 void

102-106 void

111-113 cracks

121-122 void

VCD_sheet_160629

International Ocean Discovery Program

Visual Core Description

NO.
DATE: 1 / 9/20
EXP.: 912
SITE/HOLE: c9035 / B
CORE: 9H
SECTION: 2A
TOP DEPTH (m CSF):
68~~80~~.0 –
69~~80~~.3
OBSERBER: ~~80~~90

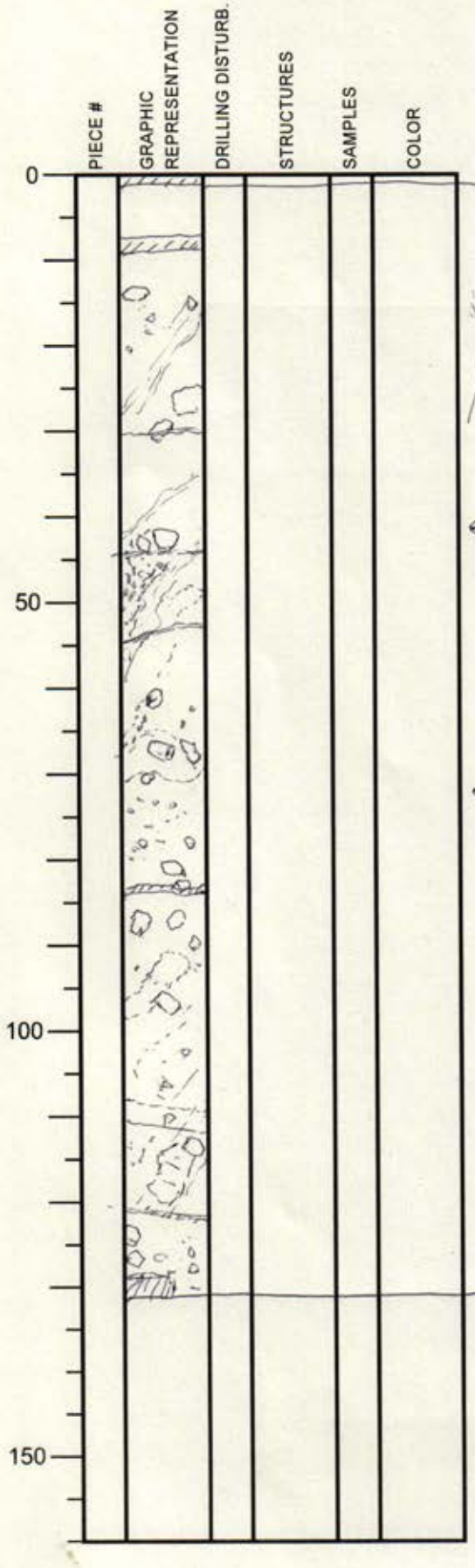

Cap -0.1

0.8

reddish.
matrix supported
muddy angular gravels
(gravelly mud)

matrix 7.5Y4/1 clayey silt

← black mudstones clast mudstone. <1cm max. 6cm.

bedded upper right to lower left??

greenish fine clasts

larger clasts.

130.3

Cap 130.4

0-0.8 void

7-9 void

30 crack

44 crack

53-55 crack

84-85 void

108 cracks

110 cracks

121-122 void

VCD_sheet_160629

International Ocean Discovery Program

Visual Core Description

NO.
DATE: 1/9/20
EXP.: 912
SITE/HOLE: C9035/B
CORE: 9H
SECTION: 3A
TOP DEPTH (m CSF): 69~~90~~3-~~7000.2~~ 7062.2
OBSERBER:

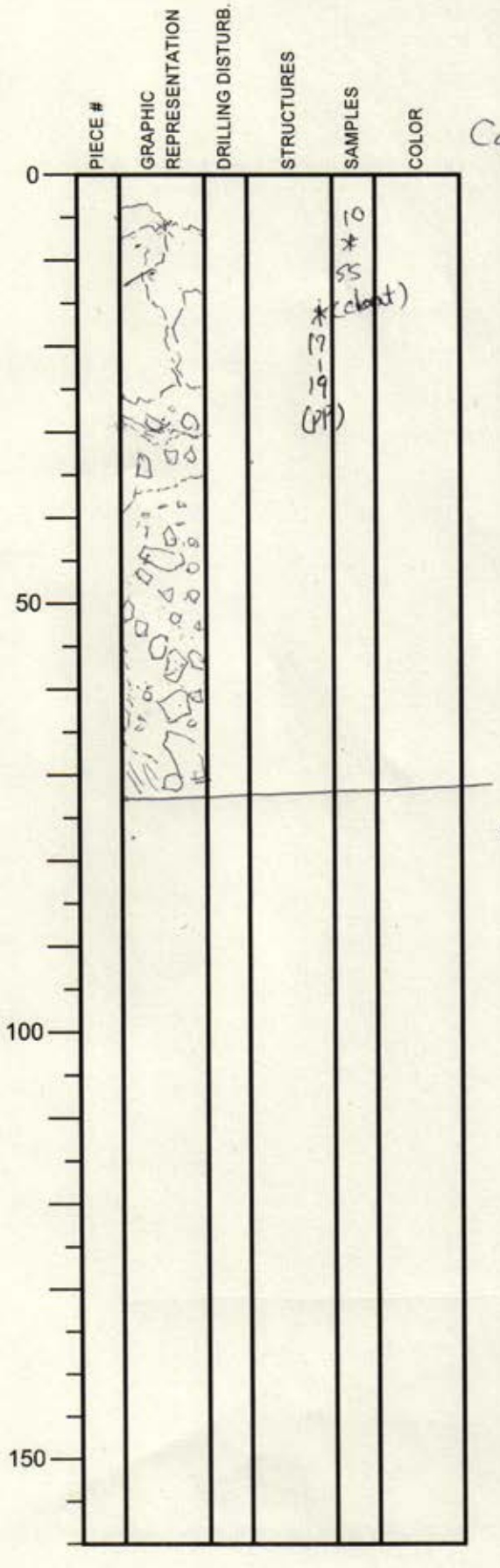

VCD_sheet_160629

International Ocean Discovery Program

Visual Core Description

NO.
DATE: 1/9/20
EXP.: 912
SITE/HOLE: C9035/B
CORE: 9H
SECTION: CCA
TOP DEPTH (m CSF):
~~2~~ 706.2 –
709.3
OBSERBER: ~~8~~

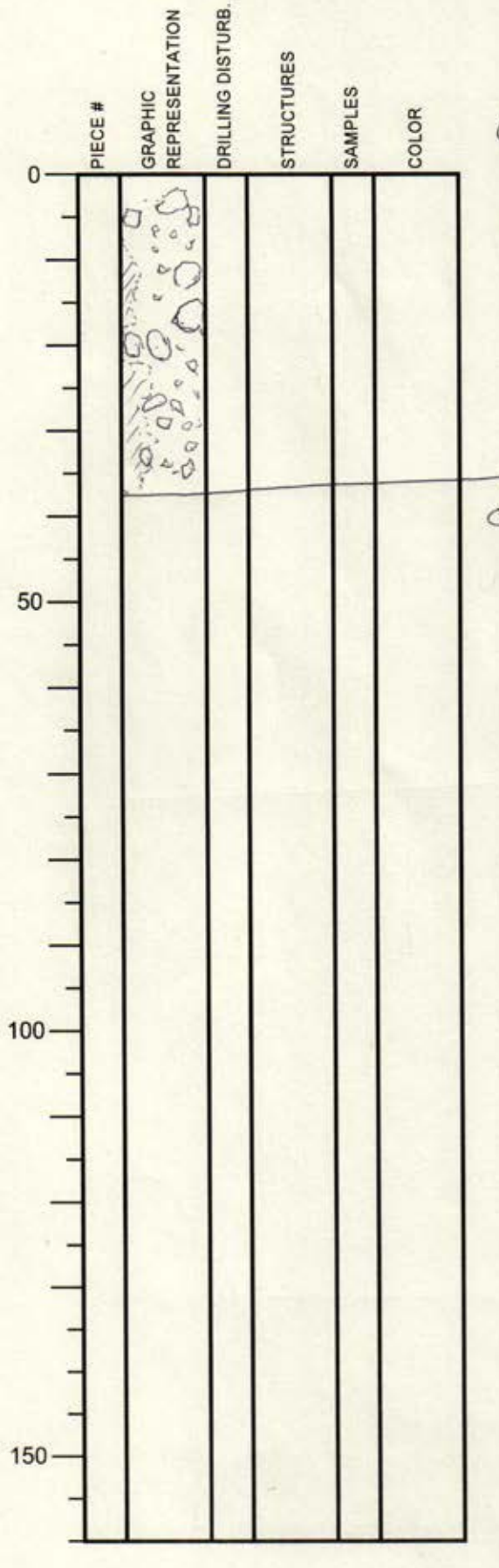

Cap – 0.2

SECTION DESCRIPTION

matrix supported
muddy angular gravels
(gravelly mud)
matrix 5Y 4/1 clayey silt
clast mudstone < 1cm
max. 3cm.

36.1
Cap 36.2

liner 36.0

VCD_sheet_160629

International Ocean Discovery Program

Visual Core Description

NO.
DATE: 1/9/20
EXP.: 912
SITE/HOLE: C9035/B
CORE: 10F
SECTION: 1A
TOP DEPTH (m CSF): ~~7096.3~~ 7137.9
OBSERBER: 9

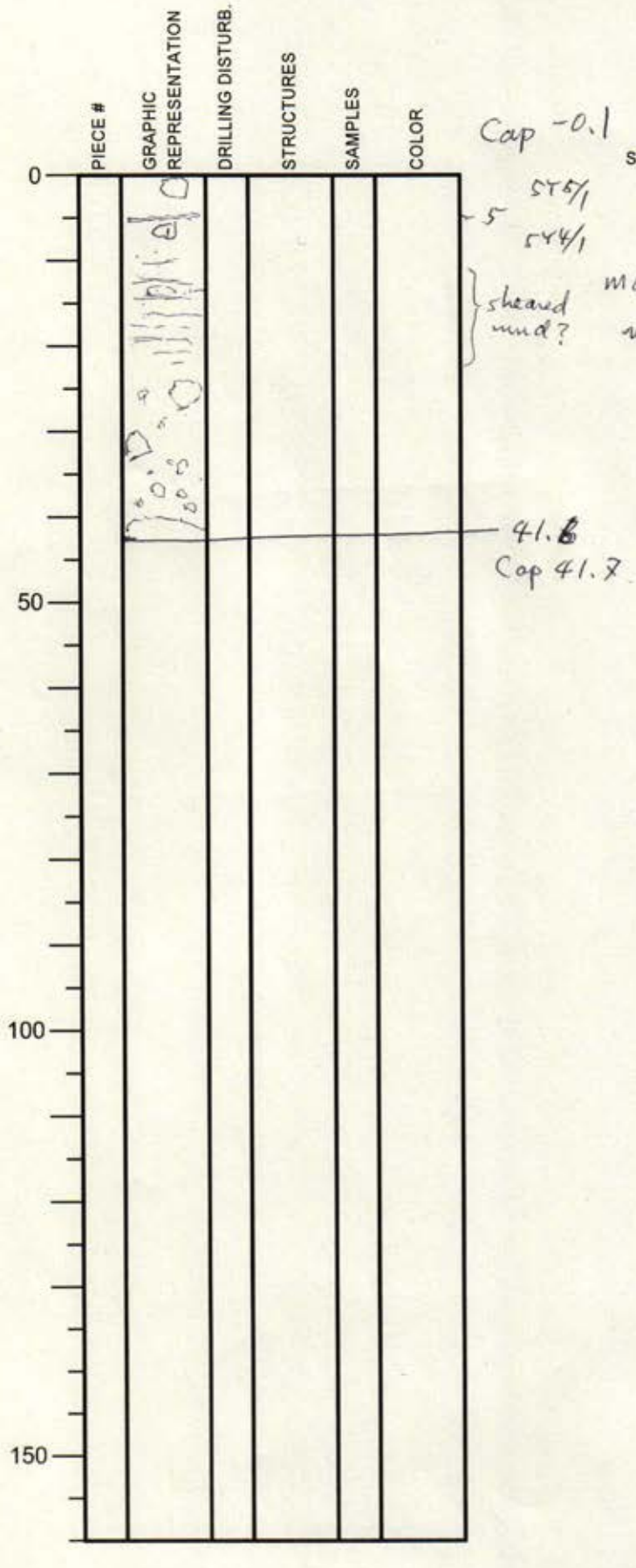

VCD_sheet_160629

International Ocean Discovery Program

Visual Core Description

NO.
DATE: 1/9/20
EXP.: 912
SITE/HOLE: C9035/B
CORE: 10F
SECTION: 2A
TOP DEPTH (m CSF): ~~X13~~9.9 – ~~X2~~72.4
OBSERBER: ~~80~~

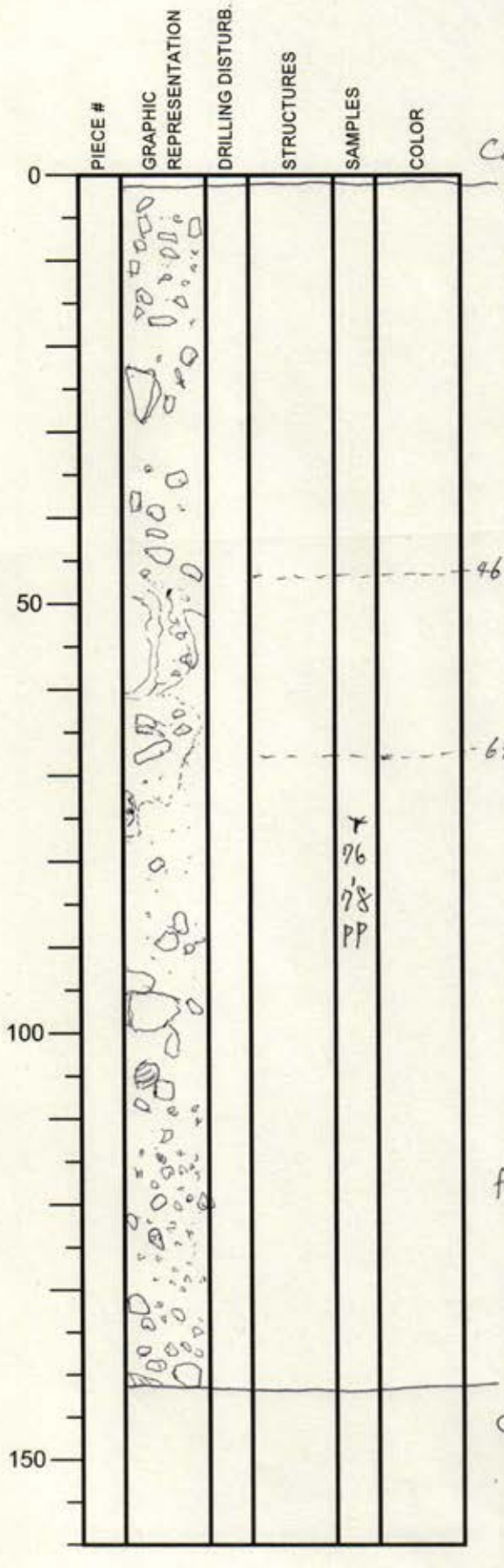

VCD_sheet_160629

International Ocean Discovery Program

Visual Core Description

NO.
DATE: 1/9/20
EXP.: 912
SITE/HOLE: C9035/B
CORE: 10F
SECTION: 3A
TOP DEPTH (m CSF): ~~80~~ 8274.4 - ~~80~~ 26 7427.4
OBSERBER:

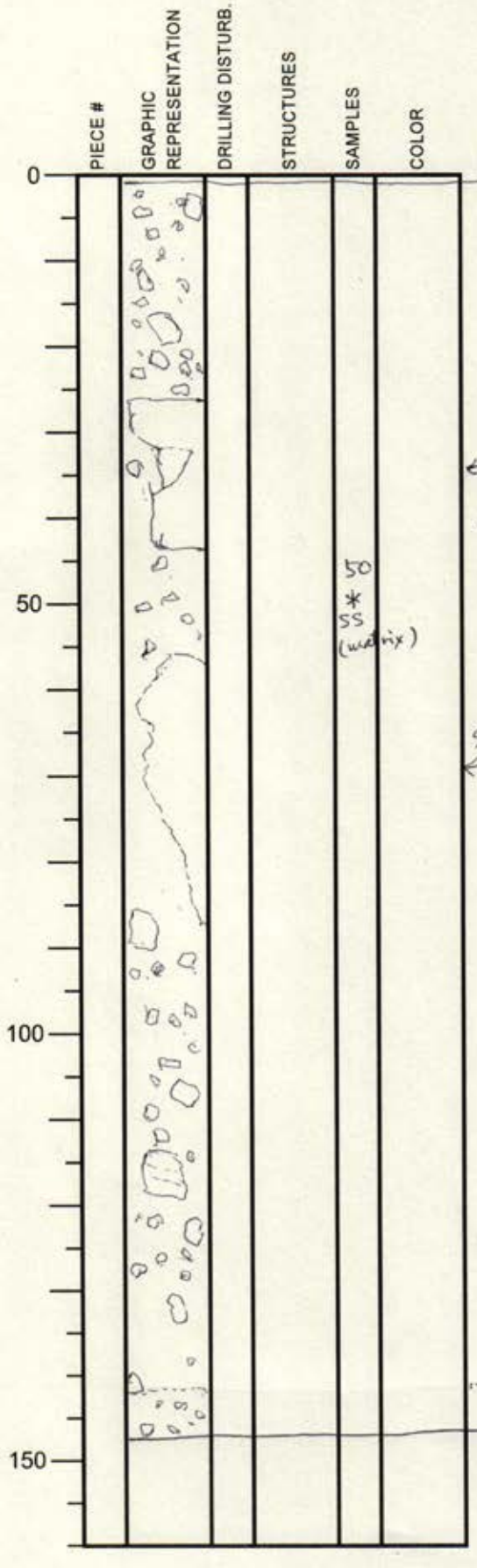

1.8 cm patched

141.9 cm patched

VCD_sheet_160629

International Ocean Discovery Program

Visual Core Description

NO.
DATE: 1/9/20
EXP.: 912
SITE/HOLE: C9035/B
CORE: 10F
SECTION: 4A
TOP DEPTH (m CSF):
~~74~~ ~~28~~.4 -
~~75~~ ~~55~~.8
OBSERBER: ~~SK~~ SK

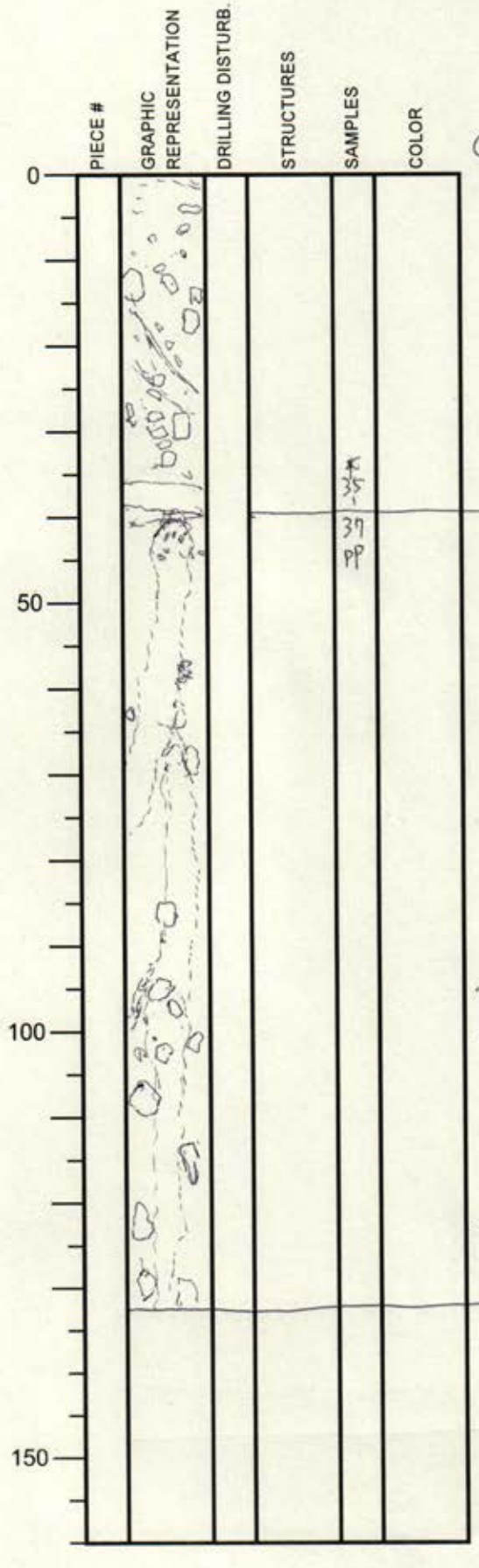

Cap - 0.2 SECTION DESCRIPTION

matrix supported
muddy angular gravels
(gravelly mud)
matrix 5Y4/1 clayey silt
clast mudstone, silty sandstone? <1cm
max ~2cm

40

flow-in
matrix supported
muddy angular gravels
(gravelly mud)

) silty sandstone? Carbonate coated??

← pumice?? or carbonate coated clast??

131.4
Cap 131.6

VCD_sheet_160629

International Ocean Discovery Program

Visual Core Description

NO.
DATE: 1/9/20
EXP.: 912
SITE/HOLE: C9035 / B
CORE: 10F
SECTION: CC A
TOP DEPTH (m CSF):
~~357~~.8 – 57~~75~~.5
OBSERBER: SG

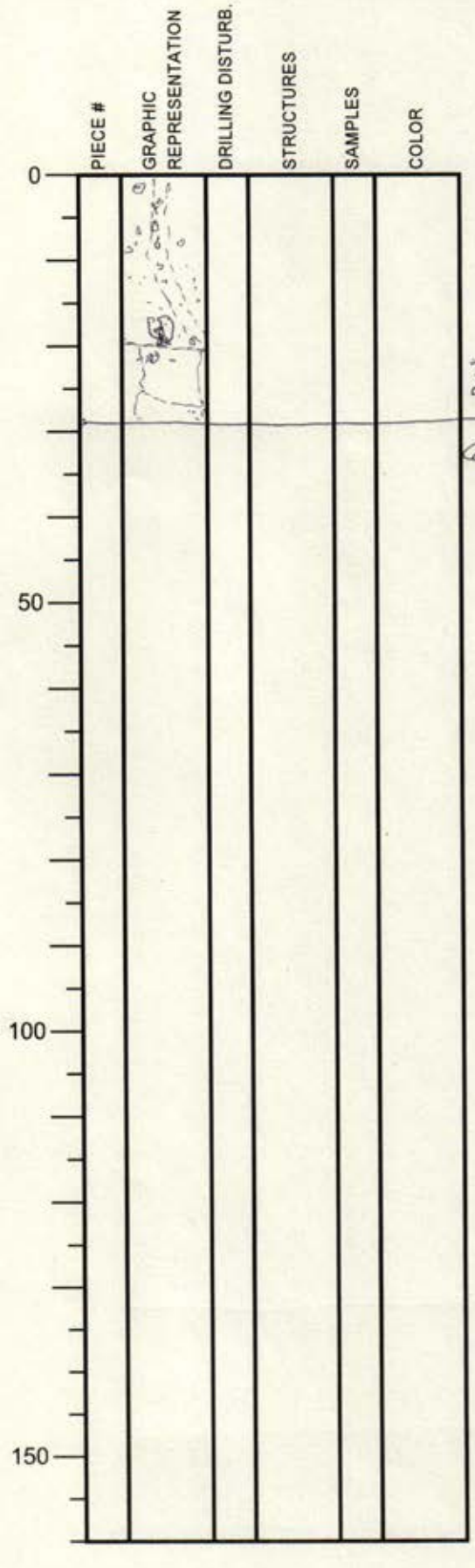

VCD_sheet_160629

International Ocean Discovery Program

Visual Core Description

NO.
DATE: 1/9/20
EXP.: 912
SITE/HOLE: C9035/B
CORE: 11F
SECTION: 1A
TOP DEPTH (m CSF):
7585.5 - 7736.9
OBSERBER: S

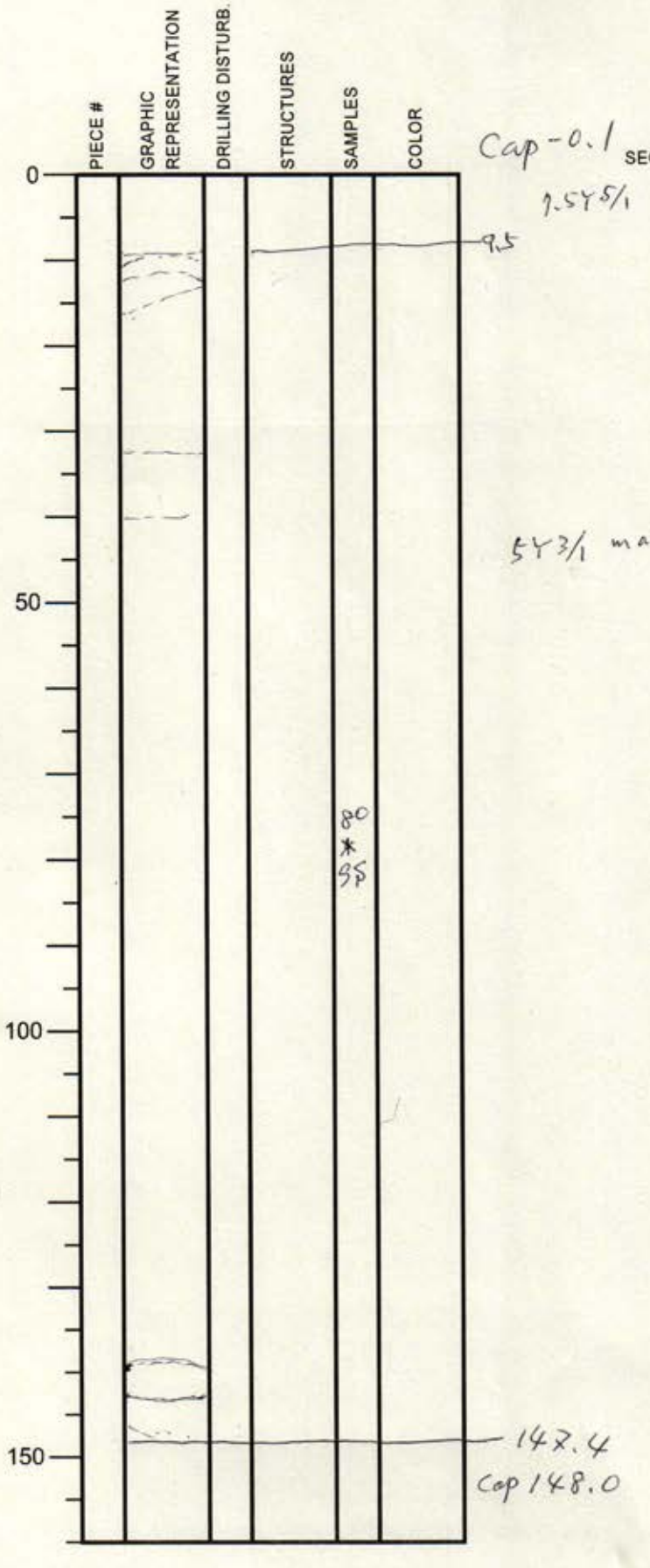

139.4 patched

VCD_sheet_160629

International Ocean Discovery Program

Visual Core Description

NO.
DATE: 1 /9 / 20
EXP.: 912
SITE/HOLE: C9035 / B
CORE: 11 F
SECTION: 2A
TOP DEPTH (m CSF):
~~7734~~ 3
7734.9 -
~~7878~~ 7878.2
OBSERBER: ~~SO~~

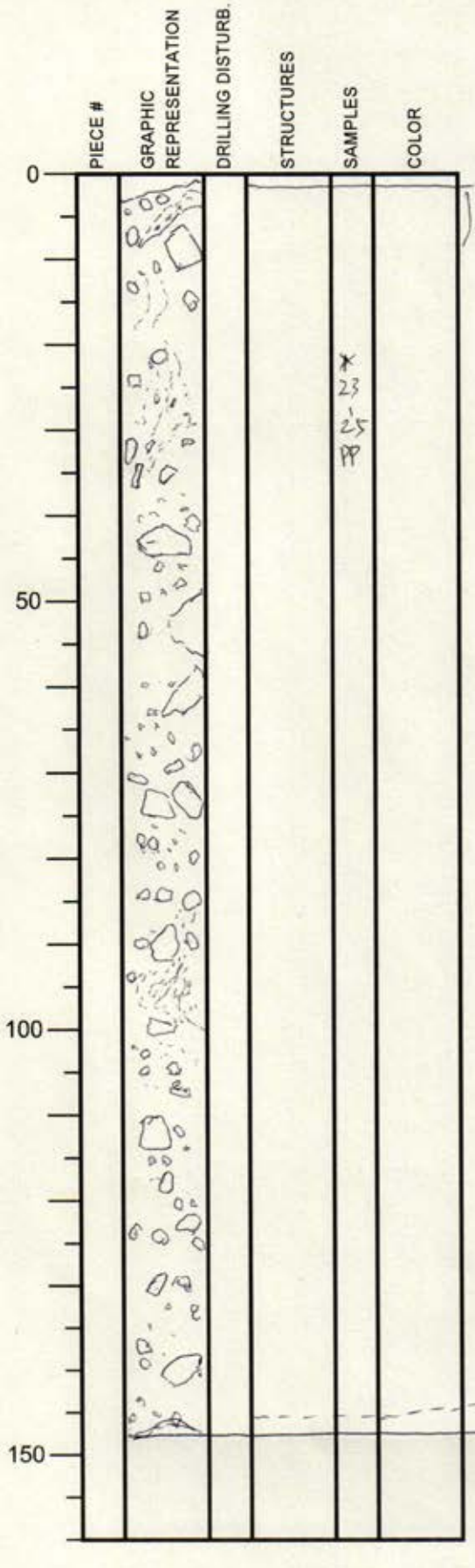

140.4
patched

VCD_sheet_160629

International Ocean Discovery Program

Visual Core Description

NO.
DATE: 1/9/20
EXP.: 912
SITE/HOLE: C9035/B
CORE: 11F
SECTION: 3A
TOP DEPTH (m CSF):
~~788~~.2 –
~~807~~.2
OBSERBER: 19

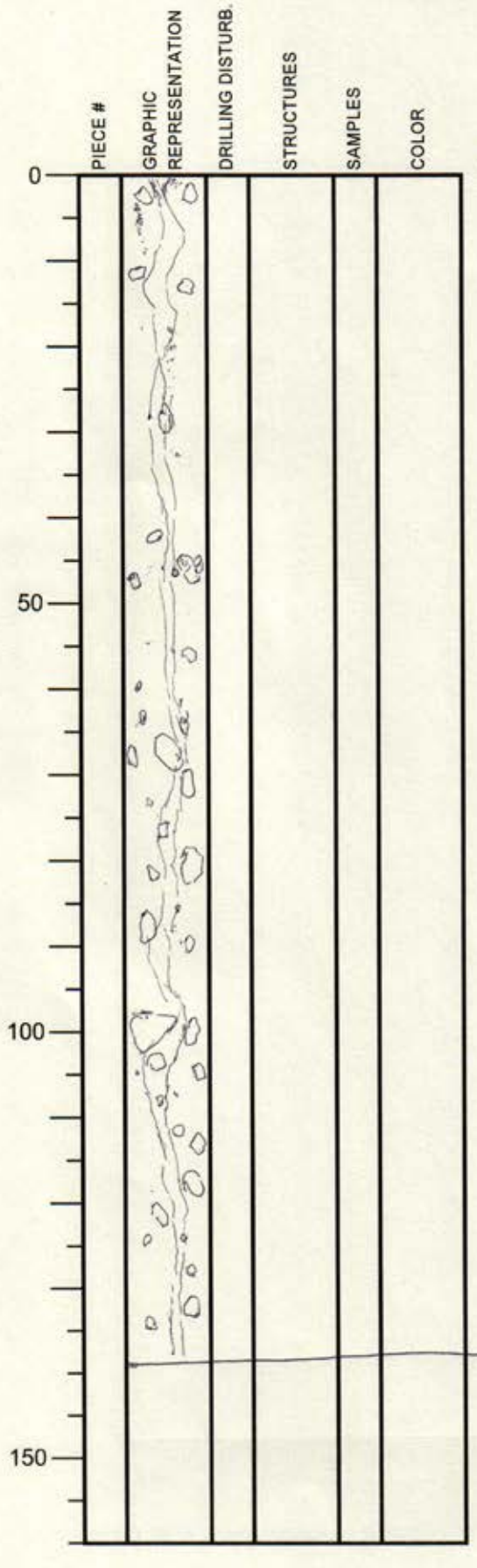

Cap -0.3 SECTION DESCRIPTION

flow-in
matrix supported
muddy angular gravels
(gravelly mud)
matrix 5Y4/1 clayey silt
clast mudstone silty sandstone

139.0
Cap 139.2

VCD_sheet_160629

International Ocean Discovery Program

Visual Core Description

NO.
DATE: 1/9/20
EXP.: 912
SITE/HOLE: C3095/B
CORE: 11F
SECTION: 4A
TOP DEPTH (m CSF): 8019.2 – 8058.2
OBSERBER: ?

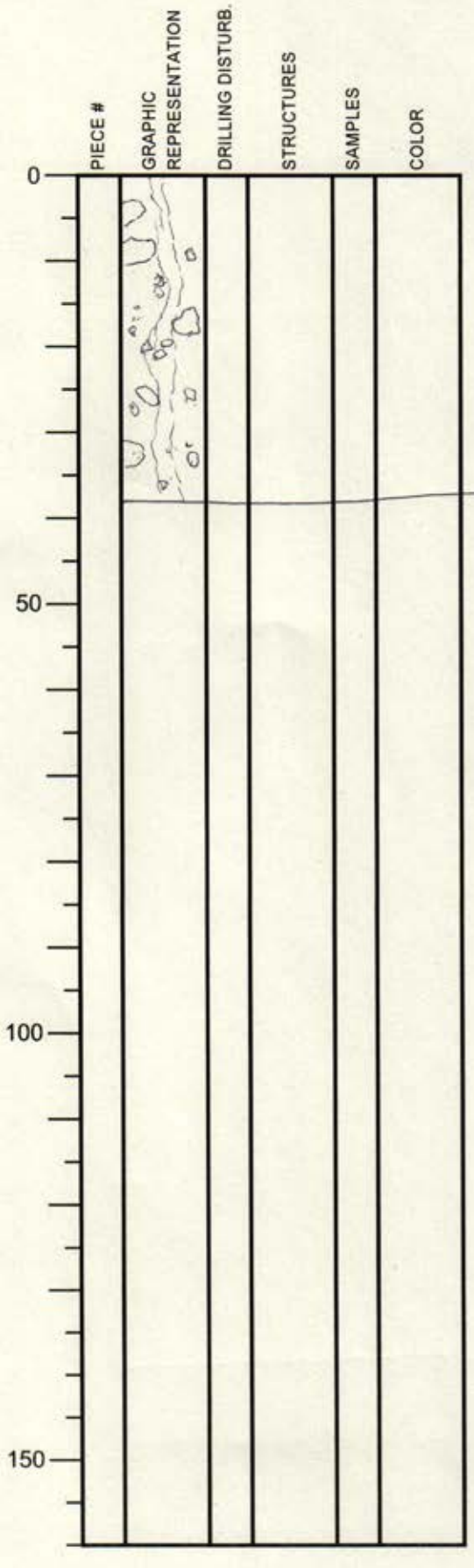

Cap -0.2 SECTION DESCRIPTION

flow-in
matrix supported
muddy angular gravels
(gravelly mud)
matrix
clast mudstone, silty sandstone
< 0.5cm
max > 3cm

38.0
Cap 38.2.

linear 37.6

VCD_sheet_160629

International Ocean Discovery Program

Visual Core Description

NO.
DATE: 11 9 20
EXP.: 912
SITE/HOLE: C9035/B
CORE: 11F
SECTION: CCA
TOP DEPTH (m CSF):
8058.2 –
8088.2
OBSERBER: 3

3.5-4.8 void

disturbed

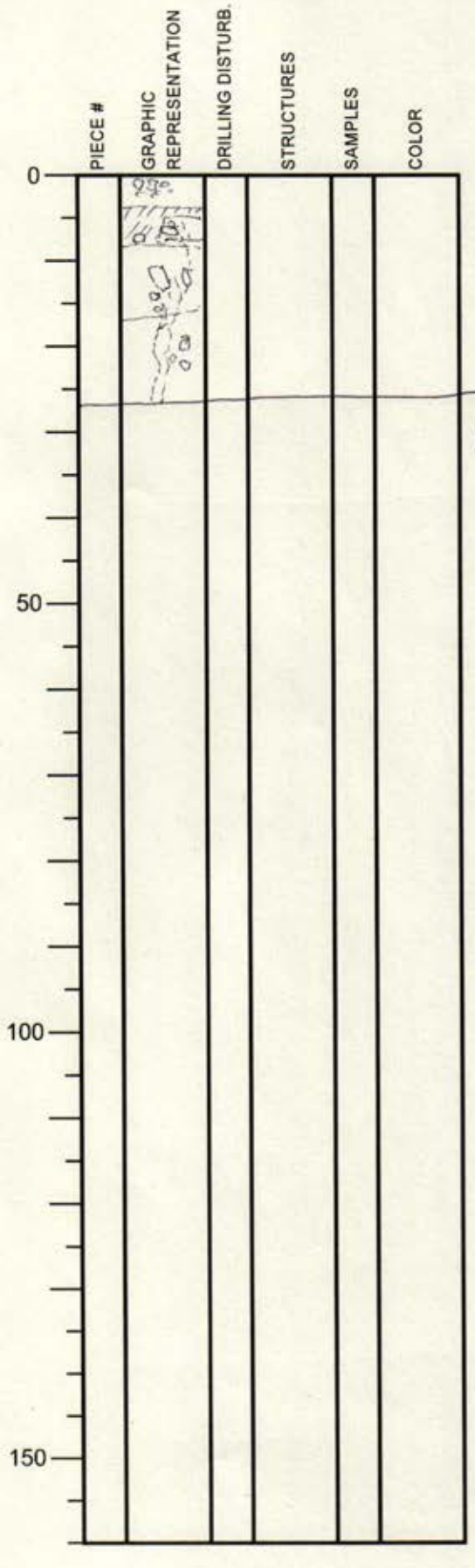

Cap -0.1 SECTION DESCRIPTION

flow-in
matrix supported
muddy angular gravels
(gravelly mud)
matrix
26.0 clast mudstone <1cm
cap 26.2 max 1.5cm.

VCD_sheet_160629

International Ocean Discovery Program

Visual Core Description

NO.
DATE: 1/9/20
EXP.: 912
SITE/HOLE: C9035 / B
CORE: 12 H
SECTION: 1 A
TOP DEPTH (m CSF):
8089.2 –
8188.7
OBSERBER:
YI

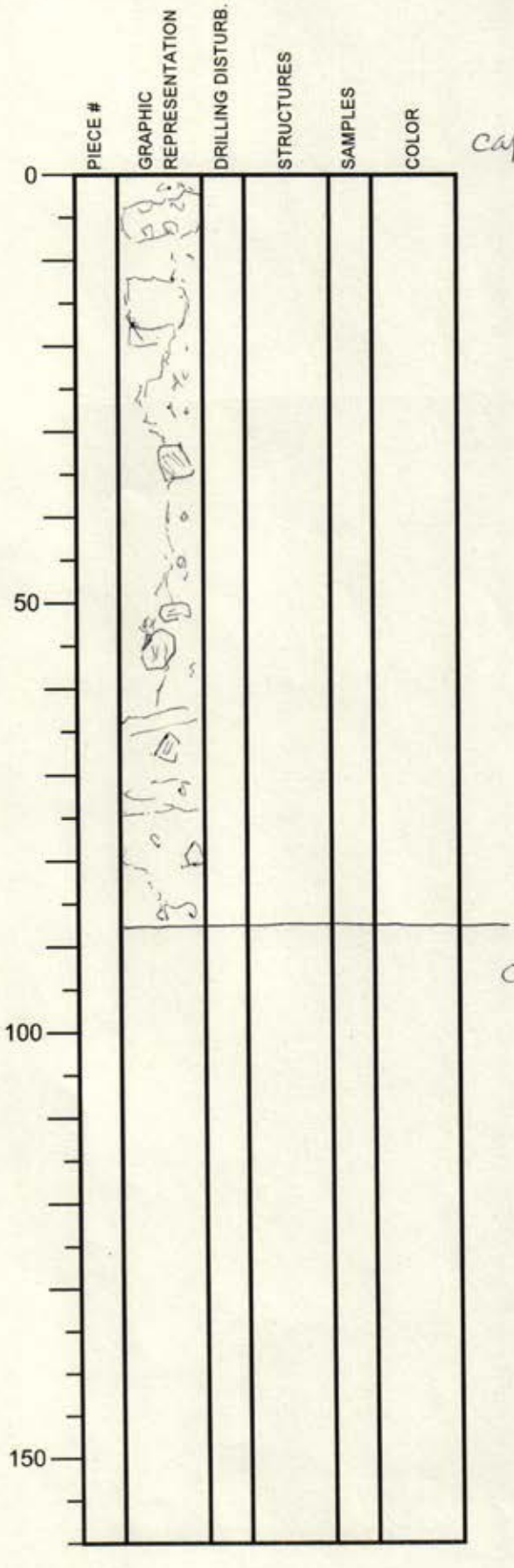

matrix supported
muddy angular gravels
(gravelly mud)

matrix 5Y4/1 sandy mud.
clast mudstone <1cm
max i3cm
some clasts have shear vains?
higlely distubed during core recovery.

VCD_sheet_160629

International Ocean Discovery Program

Visual Core Description

NO.
DATE: 1/9/20
EXP.: 912
SITE/HOLE: C9035 / B
CORE: 12H
SECTION: 2A
TOP DEPTH (m CSF):
8187.7 -
8227.0
OBSERBER: 2

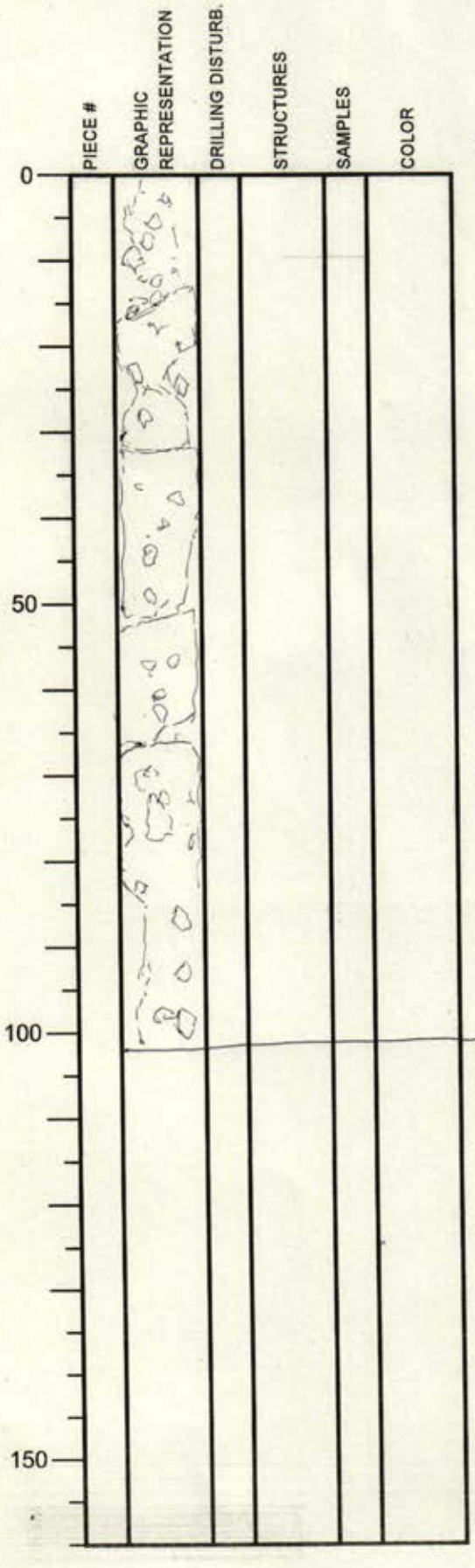

matrix supported
muddy angular gravels
(gravelly mud)
matrix 5Y4/1 sandy silt
clast mudstone <1cm
max ~2cm.
highly disturbed during core recovery

VCD_sheet_160629

International Ocean Discovery Program

Visual Core Description

NO.
DATE: 1/9/20
EXP.: 912
SITE/HOLE: C9035/B
CORE: 12H
SECTION: 3A
TOP DEPTH (mCSF): 8270.0 – 8370.4
OBSERBER: 2

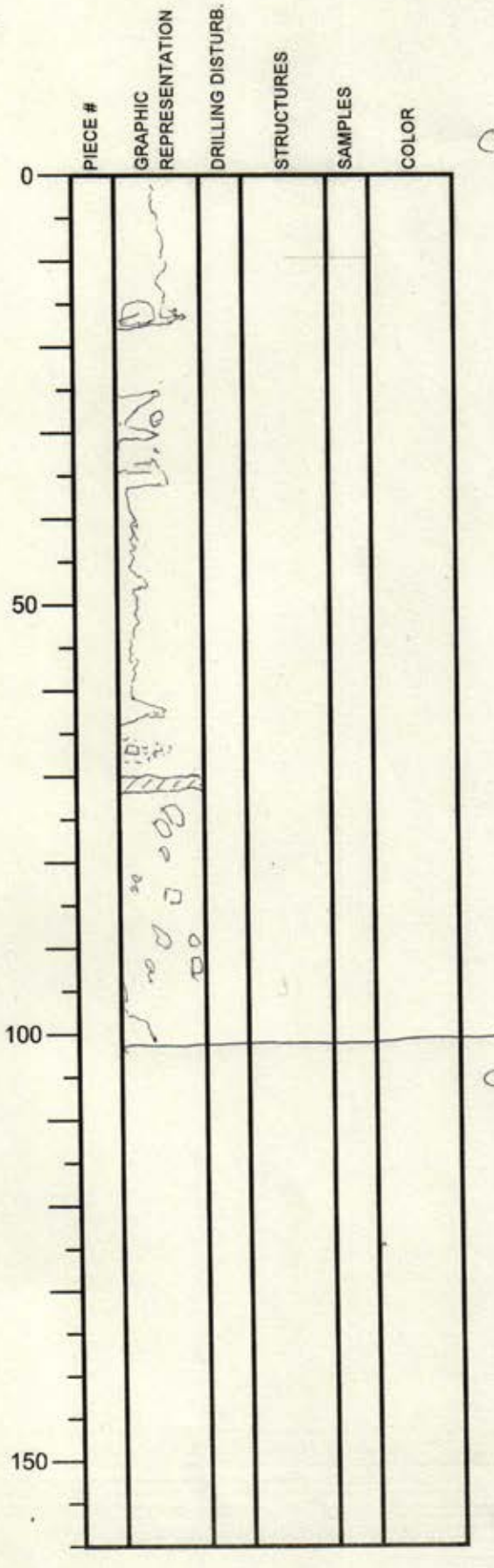

Cap -0.1 SECTION DESCRIPTION

matrix supported
muddy angular gravels
(gravelly mud)
matrix 5Y4/1 clayey silt
clast mudstone <1cm
less abundant than ~~the~~ other sections?

highly disturbed during core recovery.

70-72 void

100.4
Cap 100.5

VCD_sheet_160629

International Ocean Discovery Program

Visual Core Description

NO.
DATE: 1/9/20
EXP.: 912
SITE/HOLE: C9035/B
CORE: 12H
SECTION: cc A
TOP DEPTH (m CSF): 8378.4 – 8450.7
OBSERBER: 2

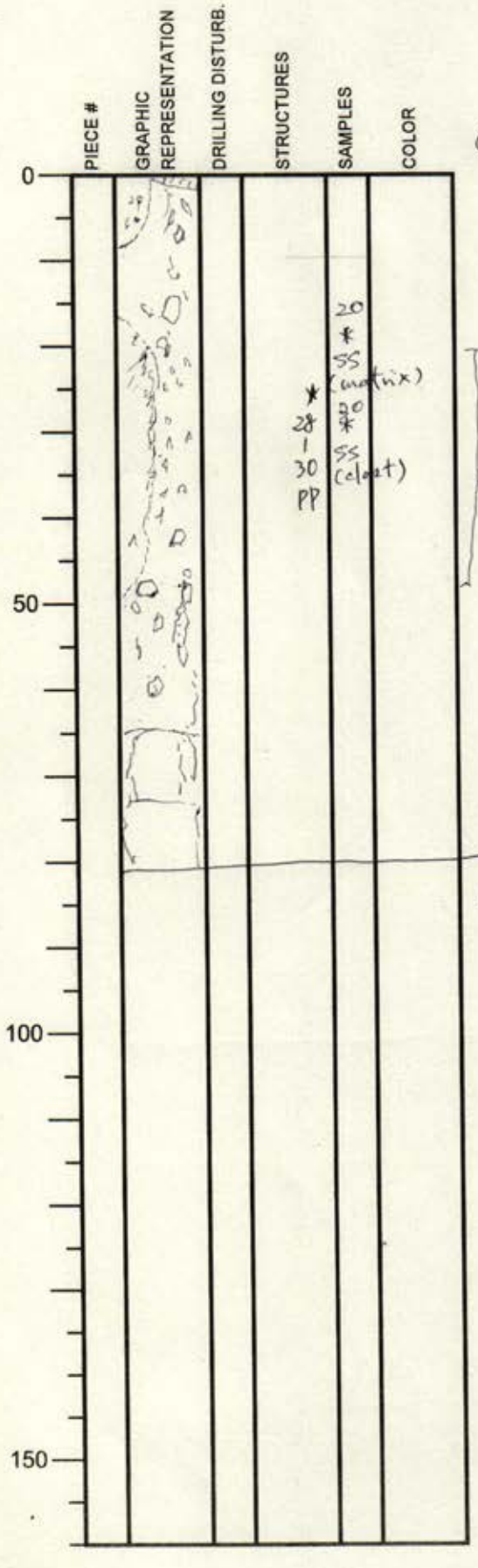

matrix supported muddy angular gravels (gravelly mud)

matrix 5Y4/1 clayey silt

clast mudstone

slightly disturbed

VCD_sheet_160629